UNIVERSITAT POLITÈCNICA DE CATALUNYA

Second Harmonic Generation in Photonic Crystals

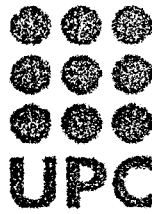TESIS DOCTORAL

Autor: José Francisco Trull Silvestre

Terrassa, 1999

UPC

UNIVERSITAT POLITECNICA DE CATALUNYA
Departament de Física i Enginyeria Nuclear

Second Harmonic Generation
in Photonic Crystals

Jose Francisco Trull Silvestre

A Carmen, Pablo y Miguel Angel.

Agradecimientos

La realización de este trabajo no hubiera sido posible sin el apoyo y confianza que han demostrado muchas personas. A ellos quiero expresar mi agradecimiento en estos momentos

Quiero agradecer en primer lugar a Jordi Martorell y a Ramón Vilaseca que aceptaran dirigir esta tesis. Sus acertadas observaciones e intuición científica han sabido abrir una puerta en aquellos momentos en que no encontraba salida. Si algo de bueno tiene este trabajo, sin duda alguna se lo debo a ellos. El rigor de su trabajo supone para mí un immejorable punto de referencia para mi labor investigadora en el futuro.

Carmen Nieves Afonso y Javier Solís Cespedes, del Consejo Superior de Investigaciones Científicas, fueron quienes me introdujeron en el mundo de la física experimental. De ellos aprendí el valor del trabajo bien hecho. Quiero agradecerles el que me contagiaran su entusiasmo y dedicación asi como todo el apoyo que me prestaron durante mi estancia alli.

A Crina Cojocaru, que ha compartido el laboratorio conmigo los últimos años y a la que debo el placer de provechosas charlas acerca de las estructuras con las que trabajamos, y en general a los miembros del grupo de Optica No Lineal por hacer tan agradable el ambiente de trabajo.

A mis amigos Victor Grau y Montse Corbalán con los que he compartido durante años los buenos y malos momentos quiero agradecerles su apoyo constante.

A mis compañeros de la Escuela quiero agradecerles las facilidades que me han prestado durante todos estos años.

A Quico, por enseñarme a valorar las cosas de otro modo y por su amistad.

Muy especialmente quiero agradecer a mi mujer y a mis hijos el esfuerzo que han realizado para que pueda acabar esta tesis. Su apoyo constante ha sido siempre para mí la mejor ayuda con la que he podidio contar.

Quiero dedicar este trabajo tambien a mi familia que con su cariño siempre me han animado en mi trabajo.

Contents

Preface

Photonic crystals emerged at the end of the last decade as a new frame to control the interaction between radiation and matter. The 3-D distribution in an ordered lattice of dielectric particles, with dimensions comparable to the wavelength of visible light, can lead to an extensive control of radiation phenomena, such as for example, the inhibition or enhancement of spontaneous emission. The potential advances that such structures could report in photonics technology has lead to an increasing research focused on the implementation of photonic crystals possessing full photonic band gaps, hindering the fact that more simple structures, possessing band gaps in selected directions of space, may also provide strong control of the electromagnetic radiation leading to the observation of many new interesting phenomena. In fact, the scope of this control is not limited to a linear interaction and can be extended to nonlinear interactions of any order.

In this work we present an experimental and theoretical study of the second order nonlinear interaction from nonlinear organic molecules placed within two different types of photonic crystals. First, we will discuss in detail the enhancement and inhibition of the radiation at the second-harmonic frequency of a sheet of dipoles embedded in a 1D photonic crystal, consisting of a set of dielectric layers with alternating indices and thickness, with- a defect introduced in the central period. The introduction of defects in the photonic crystal results in the appearance of localized states within the photonic band gap of the structure. The experimentally observed reflected second-harmonic intensity as a function of the angle of incidence shows sharp resonances corresponding to the excitation of the SH field in a local mode within the forbidden band in the structure, which position depends on the size of the defect, and additional resonance at the high angular band edge, arising as a consequence of the bending of the electromagnetic wave dispersion curve provided by the periodicity of the structure, which position is independent of the size of the defect. Comparison among these results and the SH intensity reflected by the same monolayer in free space (which presents a bell shaped radiation pattern as a function of the angle of incidence), shows

an enhancement of the radiation at the resonances, and strong inhibition of the radiation at other angles within the gap. Theoretical simulation of the experiment shows a good agreement with the experimental results.

A detailed analysis of the enhancement and inhibition phenomena occurring in these structures shows a clear dependence of the resulting intensity with the position of the monolayer within the defect and with the dipole orientation. The change in phase difference between the oscillating dipoles and the field at the SH frequency at the monolayer as it is moved within the defect is found to play a determining role in the final energy transfer to the second-harmonic field. The resulting enhancement and inhibition of the radiation may be studied in terms of a nonsymmetric contribution of the different components of the field to the energy transfer process.

The second configuration studied in the present work consider the experimental demonstration of second-harmonic generation in a 3-dimensional macroscopically centrosymmetric lattice formed by spherical particles of optical dimensions. In such photonic crystals, the surface separating each dielectric particle from the surrounding material provides a local breaking of the inversion symmetry, which allows for the existence of a nonvanishing second order interaction through the bulk of the entire crystal, enhanced by the adsorption of highly nonlinear organic molecule layer on the surface of each spherical particle constituting the photonic crystal. The growth of the SH radiation is provided by the phase-matching mechanism caused by the bending of the photon dispersion curve near the Bragg reflection bands of this photonic crystal. Experimental evidence of this phase-matching mechanism, inherent of such crystals, is reported in this work. The second-harmonic generation measured shows that SH radiation is peaked at the smaller angle side of its Bragg reflection band, where the change in the effective index of refraction introduced by the periodicity of the photonic crystal is sufficient to overcome the phase lag between the fundamental and second-harmonic beams. By measuring the SH intensity radiated from several crystals with different concentrations, thus having the Bragg reflection band at different angular positions, we obtained the angular dependence of this type of emission and confirmed the surface character of the nonlinear interaction. A simplified theoretical model based on the substitution of each crystal plane by a dielectric slab with nonlinear layers at each side can explain the most relevant features of this type of interaction, showing very

good agreement with the experimental results. It is important to notice that in this mechanism of SHG, the nonlinearity of the molecule is independent of the phase-matching mechanism, that is inherent to the periodicity of the crystal.

In conclusion, the results obtained show a clear influence of the photonic crystals in the radiated intensity at the second harmonic frequency, resulting in enhancement and inhibition of the dipoles radiation. Enhancement of SHG in defect modes could become particularly useful in the implementation of frequency doubler in vertical cavity surface emitting lasers. On the other hand, the observation of SHG from the surface of spherical particles ordered in a three-dimensional lattice may open numerous applications in the development of new nonlinear devices as well as possibilities for research in the basic field of scattering media.

Chapter 1

Introduction

1.   Photonic crystals

1.1.   Photonic crystals: general perspectives

The extraordinary improvement in electronic devices and communication systems in the last 50 years, resulting in the achievement of high-performance and considerable miniaturization of integrated electronic circuits, is directly related to the development of the semiconductor technology, which opened the possibility of controlling the propagation of electrons within a crystal. In a semiconductor, the Bragg-like diffraction suffered by the electrons in the conduction band caused by the periodicity of the structure results in the alteration of their propagating properties which leads to the formation of energy gaps for which the electron is forbidden to propagate inside the crystal. However, this miniaturization results in increasing resistance and power dissipation in circuits and higher speed operation leads to the necessity of signal synchronization. In order to avoid these problems there has been an increasing effort in the development of materials which use light as the information carrier instead of electrons.

Traditionally, the control of light beams was limited to devices based on the mechanism of total internal reflection or refraction, or to the use of electronic devices for which previous conversion of the light into an electronic signal was needed. The use of photons offers several advantages to electrons such as its greater speed, its higher bandwidth and the absence of interaction between photons which reduces energy losses. At present, some hybrid optoelectronic devices have contributed to the achievement of higher performances in electronic circuits, but the fabrication of devices based on all-optical signal processing is still a matter under research. The fabrication of a device capable of controlling the photons in the desired way is of paramount importance and should lead to a very great expansion in this field.

In 1987, it was proposed by Yablonovitch [Yab87] and independently by John [John87] that periodic arrangements of dielectric material conveniently designed could be used to control the propagation and radiation properties of light, creating a range of forbidden frequencies, called photonic band gaps, for which photons are not allowed to propagate, being highly reflected in close resemblance to the electronic behaviour in solid state physics. A difference of practical importance is that, in the case of electrons nature provides the periodic arrangement in common solids, while in the optical domain these structures need to be artificially fabricated so one can study these kind of processes. Such structures are known with the generic name of *photonic crystals*.

Since their proposal as potential structures to control the properties of photons within them, there has been an increasing interest in this field [Bow93][Kur94][Joann]. The possibility of molding the flow of light through these structures justifies its potential interest in many fields of physics as quantum electrodynamics [Kwe95] or nonlinear optics. The first structures acting as photonic crystals with a full photonic band gap were proposed by Yablonovitch [Yab89] and were mechanically constructed by drilling holes in a dielectric material, obtaining a photonic crystal with gap in the infrared. Since then, many different structures have been proposed to obtain photonic gaps, in one, two and three dimensions. Experimentally, the fabrication of photonic crystals for wavelengths in the visible spectrum is a difficult task, since the period for these structures should be of the order of the optical wavelength. Recent results show some progress in this direction [Ros96] [Che95][Fan94][Özb94]. The photonic crystal in one or two·dimensions is much easier to obtain. In fact, the analog of the 1-D photonic crystal is the well known multilayer film widely used in nowadays technology.

To obtain a photonic bandgap in a 3- dimensional periodic structure certain conditions for the index contrast and filling ratios are necessary in order to achieve a forbidden band in every direction in space. First studies of photonic crystals assumed an scalar model for the electromagnetic wave [John88][Eco89][Hui93] but soon it was seen that a vector model for the wave was necessary since different polarization modes present different gap widths thus appearing certain zones where pseudo gaps (gaps for one of the polarization modes) exist, but not corresponding to true gaps. For structures with periodicity in 2 dimensions or 1 dimension the necessary conditions to find a gap are less restrictive until the point that any 1-dimensional periodic structures exhibits a

photonic band gap in the structure irrespective of its refractive index contrast. An extension of a 1-dimensional (scalar) model to a three dimensional domain by considering a completely isotropic medium was considered by John to study some properties of atomic systems within those structures [John90]. This treatment gave some qualitative understanding of certain processes, but a complete and detailed study of the band theory for such structures requires a full vector calculation [Sat90][Ho90] [Leu90][Pla91][Zha90].

The study of the propagation of electromagnetic waves in periodic structures begins with the resolution of Maxwell equations for the structure. Let us consider propagation of electromagnetic radiation in a three dimensional periodic distribution of dielectric material. We will assume a lossless medium in which the dielectric constant may be treated as a real variable. The periodicity of the structure is taken into account in the periodicity of the dielectric constant of the structure:

$$\nabla \mathbf{D} = \nabla(\varepsilon(\mathbf{r})\mathbf{E}) = 0 \qquad\qquad 1.1.$$

$$\nabla \times \mathbf{E} = -\frac{\partial \mathbf{B}}{\partial t} \qquad\qquad 1.2.$$

$$\nabla \mathbf{B} = 0 \qquad\qquad 1.3.$$

$$\nabla \times \mathbf{H} = \frac{1}{c^2}\frac{\partial \mathbf{D}}{\partial t} \qquad\qquad 1.4.$$

where the periodicity of the dielectric constant is written as $\varepsilon(\mathbf{r}) = \varepsilon(\mathbf{r} + \mathbf{R})$, R being a vector of the periodic lattice which runs over the lattice points generated by the unit cell basis vectors $\vec{\mathbf{R}} = m\hat{\mathbf{a}}_1 + n\hat{\mathbf{a}}_2 + l\hat{\mathbf{a}}_3$. These equations remain unchanged under a translation of the coordinate system by a quantity R.

By combining Eq. 1.2. and 1.4. we obtain the wave equation for the electric field and a similar equation can be written for the magnetic induction

$$\nabla \times (\nabla \times \mathbf{E}) = -\mu_o \frac{\varepsilon(\mathbf{r})}{c^2}\frac{\partial^2 \mathbf{E}}{\partial t^2} \qquad\qquad 1.5.$$

The normal modes, solutions of this equation can be written in the form of Bloch type solutions as it is well known from the theory of periodic systems [Ash82]:

$$\vec{E}(\vec{r},t) = \hat{e} E_K(\vec{r}) \exp(i\vec{K}\vec{r}) \exp(-i\omega t) \qquad 1.6.$$

where the particular mode is labeled by the Bloch wavevector, K, and the function $E_K(r)$ is periodic with R, that is $E_K(r+R) = E_K(r)$. In order to find the amplitudes of the modes and the Bloch wavevectors for a given frequency we can expand the periodic functions in terms of the reciprocal lattice vectors of the periodic structure

$$\varepsilon(r) = \sum_G \varepsilon_G \exp(iGr) \qquad 1.7.$$

and

$$E_K(r) = \sum_{G'} E_{K+G'} \exp(iG'r) \qquad 1.8.$$

where the vectors G run over the reciprocal lattice vectors given by the relation $b_i a_j = 2\pi \delta_{ij}$, where b_i and a_j stand for the basis vectors of G and R respectively. After introducing these substitutions in the wave equation 1.5. we obtain an equation for the Fourier components of the field:

$$\sum_{G'} \hat{e} \left\{ (K+G') \times (K+G') \times E_{K+G'} - \omega^2 \mu_o \sum_G \varepsilon_G E_{K+G-G'} \right\} \exp(i(K+G')r) = 0 \qquad 1.9.$$

From this equation a solution for the eigenmodes and dispersion relation can be obtained giving the photonic band structure for the material. Those regions with real Bloch wavevector correspond to propagating modes within the structure, while those frequency regions where the corresponding wavevector becomes imaginary gives rise to evanescent solutions which amplitude decays exponentially as they propagate. These regions of frequency with imaginary Bloch vectors, are the photonic band gaps of the structure. Additionally, the bending of the wave dispersion curve at the band edges results in a change in the effective phasae velocity as well as in the group velocity. As we will see in the following chapters, these changes are highly relevant when a nonlinear interaction is considered within a 1-D as well as in a 3-D photonic crystal.

Calculation of PBG has been the subject of intensive theoretical study during the last decade to characterize a large amount of structures, periodic either in two or three dimensions . An experimental effort leading to the fabrication of structures possessing a full photonic band gap in the optical domain should be necessary in order to take advantage of all the possibilities of such kind of structures.

Although the construction of a periodic structure possessing a band gap in all directions in space should become a very desirable objective to be reached, the use of structures which does not posses a full photonic band gap, but that show a forbidden gap in selected directions of space, as it is the case for 1-dimensional or 2-dimensional photonic crystals, present a great deal of interest since the presence of such gaps may cause strong alteration of the properties of a light beam being incident on them [Sca95][Sca96], such as changes in the reflection and transmission coefficients, in the effective refractive index or in general the wave propagation velocity inside the structure, and enhancement or inhibition of nonlinear phenomena within such structures (as has been shown experimentally in the present work) among others. A significant number of research groups have studied the effects of combining the use of periodic structures together with optical nonlinearities [Hat97] [Has95][Ber97][Tru95][Tru98] [Tru99][Mar97][Mar94] and its potential utility to construct optoelectronic devices [Gibbs][Ste96][Sca94] [Sca97][Coj99]. The effect of these structures on the resulting radiation emission may be studied in terms of the interference effects due to the coherent superposition of the different fields present in the structure and in terms of the local alteration in the density of states introduced by the presence of the structure. The use of these structures to control the radiative properties of atoms embedded within them has also attracted much interest during last years. In particular experimental evidence of inhibition of the spontaneous emission of a dye solution in a photonic crystal has been reported [Mar90].

1.2   Defect modes in photonic crystals

If the perfect translational periodicity of the structure is broken in some way, localized states appear into the forbidden gaps for which light propagation is possible. Again this fact has its analogy in solid state physics, where the introduction of impurities within a

perfect periodic lattice results in the existence of localized states with energy in the gap region at the bottom of the conduction band or at the top of the valence band of the solid. The drastic effect of this kind of states on the conducting properties of the solid is well known in semiconductor physics. It was first pointed out by Yablonovitch et al. [Yab91] that localized states appear into the gap of a photonic crystal if the perfect periodicity of the structure is broken by introducing some kind of defect within it. These defects can be introduced for instance by removing part of the dielectric material or adding material to one of the sites of the structure. The effect of this variation in the dielectric composition at the structure is the same as the impurity atoms introduced in a solid. The removal of dielectric material results in the appearance of localized modes within the gap emerging from the lower frequency band edge and moving towards the center of the gap ("acceptor modes"). In the same way if extra material is added to the structure, the localized states appear from the bottom of the high frequency edge within the gap ("donor modes").

Localization phenomena have been a subject of active research since the first works by Anderson [And58], centered in the localization of electrons in solids. This effect arises as a consequence of the strong variations of the potential that the electron sees in a strong disordered medium (such as in glasses). For strong enough potentials the electron may be trapped in the region close to the initial one, thus preventing the electron to diffuse away from its sites being localized in space. The effect of localization is not a particular property of the electronic systems and can be studied also in any kind of wave phenomena [Sheng], [Abr79], [Koh83], [Kra93].

In particular, the possibility of obtaining localization of electromagnetic waves, in the sense that photons propagating in a material can be trapped within it, has been proposed by using photonic crystals with defects. Localization effects in electromagnetic waves are entirely due to the coherent superposition of the multiple scattered waves at the material sites. Localization phenomena may be found in two opposite regimes, either in a collection of random scattering sites or in a periodic distribution of scatterers [John91]. The study of localization in electromagnetic waves propagating in strong disordered structures has been a very active field in the last years [John84], [Ete86],[Ary86]. As pointed out by John, for structures with a correlation distance of disorder comparable to the wavelength, localized states may appear as a consequence

of the superposition of the multiply scattered waves in the disordered potential. Within this regime, the transport properties of waves are altered thus conducting to a redefinition of certain parameters such as the diffusion length. The degree of disorder and index contrast necessaries to the observation of such localization effects makes difficult their experimental observation. Related phenomena associated to a regime of weak light localization, such as backscattering of light (a process in which light is reflected back from the structure in opposite direction to the incident wave) has been experimentally measured [Sheng] [Alb85][Wolf85].

Photonic crystals have been proposed as potential structures to obtain light localization in ordered media. The electric field distribution within such photonic crystals when a defect is introduced, is strongly confined at the defect sites and its amplitude decays exponentially as we move away from the defect. The high energy density of these localized states has been measured in a two dimensional periodic structure in the infrared domain [Smi93].

The introduction of defects in photonic crystals offers new possibilities to their potential use to control light beams and atomic radiative properties. A point defect into a photonic crystal could act as a microcavity, a line defect like a waveguide, and a planar defect like a perfect mirror. The nonlinear radiation generated within such microcavities will be strongly influenced by the environmental conditions as will be seen in following chapters.

2. Nonlinear Optics

2.1 General aspects of nonlinear interactions

The response of a given material to an incident electromagnetic wave may be characterized by the study of the induced polarization of the medium. The classical linear response of a medium to an incident electromagnetic wave is only valid whenever the incident radiation is weak and out of any resonance of the medium. As the intensity of the input light is increased, the polarization of the medium is no longer linear. Out of resonance, the relation between the polarization and the incident field may be expressed as a Taylor expansion of the field and nonlinear terms proportional to the square of the

field and so on appear in the induced polarization. The processes involved at the field intensities where these terms are significant are included within the generic field of nonlinear optics [Shen][Bloe][Boyd].

The birth of nonlinear optics is considered to coincide with the appearance of the laser since it represents the powerful light source needed to study these processes, although theoretical work on nonlinear dynamical properties of atoms were taken before this date. Nonlinear optical processes may be roughly divided as parametric and non parametric, all of these presenting a potential field of study of new physical aspects for electromagnetic theory. Roughly speaking, parametric interactions involve processes in which the final state of the atom doesn't change and include those which give rise to an exchange of energy between a number of different electromagnetic fields of different frequencies, such as harmonic generation, parametric amplification, self-focusing, light squeezing and cascading processes. Nonparametric interactions involve processes for which a change in the level populations of atoms occur. This happens when the frequencies of radiation are close to material resonances of the medium giving rise to strong interaction between the field and the atom. Saturable absorption, Stimulated Raman scattering, Stimulated Brillouin scattering, optical bistability, laser theory should be included within these kind of processes and clearly denote the importance of these kind of nonlinear phenomena.

The starting point for the study of nonlinear interactions is the response of a given material to an incident electromagnetic field. We can write such relation as:

$$P_i(\mathbf{r},\omega) = \varepsilon_o \left[\chi_{ij}^{(1)} E_j + \chi_{ijk}^{(2)} : E_j E_k + \chi_{ijkl}^{(3)} : E_j E_k E_l + ... \right] \qquad 1.10.$$

where the terms $E_i = E_i(r, \omega)$ represent the ith component (i=x,y,z) of the Fourier components of the field and we assume that the the electric field and polarization vector may be written as a superposition of plane waves of different frequencies, in the form:

$$\mathbf{E}(\mathbf{r},t) = \sum_{\omega} \mathbf{E}^{\omega}(\mathbf{r}) \exp{-i\omega t} \qquad 1.11.$$

$$\mathbf{P}_{NL}(\mathbf{r},t) = \sum_{\omega} \mathbf{P}_{NL}^{\omega}(\mathbf{r}) \exp{-i\omega t} \qquad 1.12.$$

where a spatially local relation is assumed between the induced polarization and the incident field. This relation accounts for nonlinear processes in the dipole approximation. A nonlocal relation should be considered to include other terms such as quadrupolar terms, etc..

The first term in Eq. 1.10. is the linear relation between the field and the polarization given by classical optics and accounts for the index of refraction of the medium. Second order processes such as SHG, sum frequency generation or parametric amplification are given by the quadratic term in the expansion of the induced polarization. The third term is responsible of processes such as third harmonic generation, phase conjugation, self focusing or self phase modulation provided by an intensity dependent refractive index. Usually third order terms may be neglected if second order are present, since for typical nonlinear materials, third order nonlinearities are much lower than second order terms. By symmetry considerations one can see that for materials with inversion symmetry second order processes are not possible. On the other hand, some of the main aspects of third order processes, such as intensity dependence of the refractive index, may be obtained through cascading second order nonlinearities. The study of these processes has opened the possibility of new advances in the implementation of all optical devices or soliton propagation, among other interesting effects.[Jeos] [Ste96].

The present work will be centered in the particular nonlinear process of second-harmonic generation (SHG). Our main purpose is to study both experimentally and theoretically, the SHG in periodic structures (photonic crystals). In the following sections I shall give a brief review on the theory of second-harmonic generation and I will consider its study in surfaces and monolayers in order to give a first insight into the problems that will be treated in the following chapters.

2.2   Second Harmonic Generation

Soon after the birth of nonlinear optics 35 years ago, the relative strength of second order nonlinear interactions prompted the development of mechanisms capable of generating new frequencies using lasers of moderately high intensity. In particular, the doubling of that laser frequency, known as second-harmonic generation (SHG), is one of the most widespread applications of quadratic nonlinear interactions. This type of

interaction occurs between an incident field and a given medium with a nonvanishing second order susceptibility $\chi^{(2)}$, and is described by Maxwell equations 1.1-1.4 when the polarization term posses a quadratic nonlinear part. From these equations, we can obtain the wave equation for the electric field:

$$\nabla \times \left(\nabla \times \mathbf{E}(\mathbf{r},t)\right) + \frac{\varepsilon}{c^2}\frac{\partial^2 \mathbf{E}}{\partial t^2} = -\mu_o\frac{\partial^2 \mathbf{P}_{NL}}{\partial t^2} \qquad 1.13.$$

where the nonlinear part of the polarization vector has been separated from the linear part. It is clear from this equation that the nonlinear polarization acts as a driven source for the electric field.

When the expressions 1.11 and 1.12 are substituted in equation 1.13, it decouples into a set of coupled equations for each given frequency component of the field. In this set of equations the nonlinear components of the polarization act as the coupling terms which are responsible of the energy transfer between the different components of the field at different frequencies. This coupling is at the origin of several interesting nonlinear phenomena such as second order processes (sum frequency generation, parametric amplification, down conversion) or third order processes (third harmonic generation, self-focusing). A detailed explanation of these and several other nonlinear processes may be found in several reviews on nonlinear optics [Boyd][Shen][Bloe][Zer].

In the process of second-harmonic generation, only two equations involving the field at the fundamental,ω, and second-harmonic, 2ω, frequencies need to be considered.:

$$\nabla \times \left(\nabla \times \mathbf{E}_{2\omega}\right) - \frac{\varepsilon_{2\omega}(2\omega)^2}{c^2}\mathbf{E}_{2\omega} = \mu_o(2\omega)^2\mathbf{P}_{NL}^{2\omega} \qquad 1.14.$$

$$\nabla \times \left(\nabla \times \mathbf{E}_{\omega}\right) - \frac{\varepsilon_{\omega}\omega^2}{c^2}\mathbf{E}_{\omega} = \mu_o\omega^2\mathbf{P}_{NL}^{\omega} \qquad 1.15.$$

where ε_ω and $\varepsilon_{2\omega}$ are the dielectric susceptibility of the medium at the fundamental and second-harmonic frequency respectively, and $\mathbf{P}_{NL}^{\omega}$ and $\mathbf{P}_{NL}^{2\omega}$ are the nonlinear terms of the polarization vector at each frequency resulting from the contraction of the nonlinear

susceptibility tensor $\chi^{(2)}$ with the corresponding fields in each case. These nonlinear terms couple both equations and its solution gives the energy exchange between both waves. In general, this coupling depends on the initial conditions of the fields, on the characteristics of the nonlinear material, and on the particular geometry chosen for the interaction. In general, one needs to match the velocities of the SH generated wave and of the polarization wave at the SH frequency which forces the oscillation of the dipoles for an effective process of second harmonic generation to take place. This condition, known as phase-matching may be obtained in a number of different ways as will be seen later.

Unfortunately, a general solution of this nonlinear system for a general source term is not possible and some simplifying assumptions must be made in order to get solutions of the equations. Between the most used assumptions we found the slowly-varying amplitude approximation, the infinite plane wave approximation and the constant-pump intensity approximation.

The use of a plane-wave expansion of the fields allows to consider fields propagating in different directions inside the material and in particular, to properly account for reflections when boundaries are present (which will be our case). The effect of considering plane waves in the expansion of the fields in Eq 1-13 assumes a constant field in the transverse plane, perpendicular to the propagation direction. Since any real field is of finite extent in space, it presents a dependence on the transverse coordinates which must be taken into account in certain circumstances. The net effect is that the distance within the material along which the beam can be focused depends on the beam profile and reduces the interaction length for the nonlinear process, consequently reducing the efficiency of the process. The use of diffraction-limited beams and waveguide geometries has proven to be a good way of achieving the best results. This fact, however is not crucial if the length of the crystal is not very large. For our particular case in which we will be concerned with monolayers of nonlinear materials, the use of the plane wave approximation is well justified, since the extent of the beam is at least 1000 times higher than the length.

The most used approximation to treat the process of SHG in bulk media is obtained by using the slowly varying envelope approximation, which is based on the assumption

that the amplitude variations of the fields take place along distances longer than the wavelength. This fact allow us to neglect the second derivative terms in the propagation direction, resulting in a coupled system of first order differential equations for the fundamental and second harmonic fields in the medium. This approximation may be used to derive the resulting power conversion to a field at the SH frequency in a bulk crystal for which propagation in the forward direction is considered. The resulting equations, replacing Eq. 1.14 and 1.15 may be written in the form:

$$\frac{dE_\omega}{dz} = i\kappa E_{2\omega} E_\omega^* \exp{-i\Delta kz} \qquad\qquad 1.16.$$

$$\frac{dE_{2\omega}}{dz} = i\kappa E_\omega E_\omega \exp{i\Delta kz} \qquad\qquad 1.17.$$

where the term Δk, known as the phase mismatch wavevector is given by:

$$\Delta k = k_{2\omega} - 2k_\omega \qquad\qquad 1.18.$$

When the amount of generated radiation at the second-harmonic frequency is not very large, we can assume that the fundamental incident beam will not be depleted significantly during the process and we can take it as a constant in order to solve for the second-harmonic field. This approximation, known as the constant intensity pump approximation is justified in the case considered since the coupling term in Eq. 1.16 will be much lower than the corresponding term of Eq. 1.17 (since we are assuming that the second-harmonic field is weaker than the fundamental field). For the cases in which this approximation is possible, we are left with one equation, which may be integrated to give the resultant second-harmonic field generated at the crystal. The solution for the resulting second harmonic output power ($P_{2\omega}$) is written as:

$$P_{2\omega}(z) = \frac{32\pi^3 \omega^2}{c^3 \varepsilon_\omega \sqrt{\varepsilon_{2\omega}}} \left| \hat{e}_{2\omega} \cdot \chi^{(2)} : \hat{e}_\omega \hat{e}_\omega \right|^2 z^2 \frac{\sin^2(\Delta kz/2)}{(\Delta kz/2)^2} \frac{P_\omega^2(0)}{A} \qquad 1.19.$$

From this equation we may see that the efficiency of the second harmonic frequency depends very strongly on the phase mismatch to the point that it goes to zero for certain crystal lengths given by the condition

$$z_o = n\frac{2\pi}{\Delta k}$$
$$\text{1.20.}$$

which with the aid of 1.18 may be written as

$$z_o = n\frac{\lambda}{2(n_{2\omega} - n_\omega)}$$
$$\text{1.21.}$$

This is consequence of the fact that the beams at the fundamental and second harmonic frequencies travel at different speeds within the crystal, and as a consequence the SH field generated at a given point in the medium by the driven source, becomes dephased with respect to the field at the SH frequency at the same point coming from previous planes of the crystal.

In order to obtain a continuous growth of the second harmonic generation, phase matching (Δk=0) is required [Eck84]. This is not achieved in the most general case since any material presents dispersion. However, phase-matching may be obtained by the two most commonly used mechanisms:

i)   A birrefringent material may be used to achieve phase-matching by a suitable choice of incident polarizations of the beams and incidence angles [Gio62] [Mak62]

ii)   A change in the sign of the nonlinearity after each coherence length of the crystal may be used to obtain a continuous growth of the second harmonic signal [Arm62]. This process known as quasi-phase matching has been developed during the last decades to the point that practical construction of such dispositives is possible [Fej92].

A third mechanism of phase-matching, proposed by Bloembergen and Sievers [Blo62] and experimentally demonstrated by van der Ziel [Zie76], uses a periodical distribution of dielectric material to induce a bending of the photon dispersion curve near the second-harmonic frequency. More recently, numerical results showed that this

mechanism could also be used in periodic multilayer structures with a defect breaking the perfect periodicity [Mar94]. As we shall see in later chapters this mechanism becomes of the utmost importance when the nonlinear interaction occur within a photonic crystal. We will show experimentally that the intrinsic periodicity built in a 3-D photonic crystal provides the necessary phase-matching mechanism. This constitutes the first experimental demonstration of long range phase-matching using this third mechanism.

In the case in which reflecting boundaries are present, the SVEA approximation cannot be used and second order derivatives should be kept in order to take into account all reflections at the interfaces. In that case, the plane-wave approximation provides in addition to a full description of the nonlinear interaction at the boundary, a complete description of the changes in the wave propagation phase velocity leading to the proper phase-matching mechanism.

2.3 Surface second harmonic generation

Although bulk inorganic crystals have proven to be very suitable materials to obtain a high power conversion to the SH field, nonlinear quadratic processes may be studied in other systems such as organic molecular crystals [Prasad]. For these materials the optical nonlinearity is associated to the molecular structures [Dul78].

When interfaces separating different media are present additional effects arise in the second harmonic process, the most significant is the existence of a reflected second-harmonic wave at the interface (Figure 1.1). This process, known since the early days of nonlinear optics [Blo68][Jha65][Jha67], is always present at the surface of a bulk material, being generated by a portion of material close to the interface, since contributions to the reflected wave from material placed at longer distances from the surface cancel out due to the absence of phase-matching. This surface second harmonic generation, which is not important in the case of SHG from bulk materials, has appeared as a new phenomena which has focused much attention due to its potential applications in the study of surfaces [She94][Guo86] and monolayer orientation of monolayer adsorbates [Hei83].
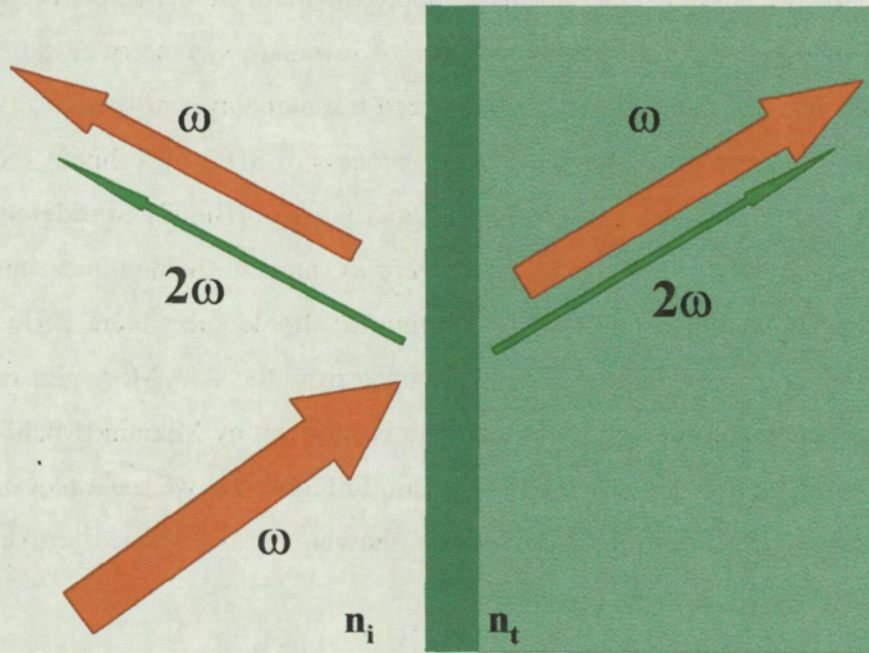
Figure 1.1 Surface SHG at the interface between two homogeneous media.
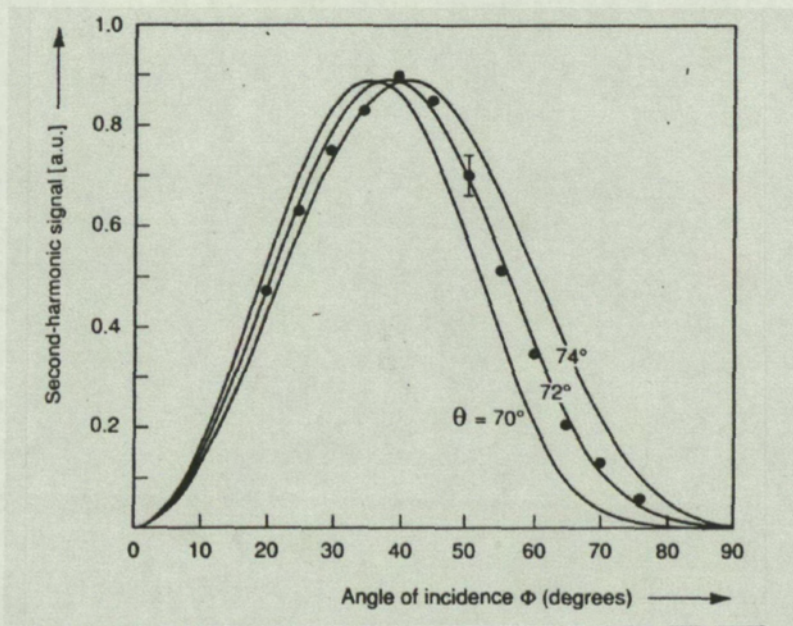
Figure 1.2 Angle of incidence dependence of TM polarized SH signal under TM polarized excitation fro different molecular orientations. This figure corresponds to a paper by Hollering et al. [Hol90].

SHG is always possible, in the dipole approximation, at the interface between two different media due to the intrinsic absence of inversion symmetry at the surface. This SH emission at the interface may be enhanced if a monolayer of nonlinear molecules is adsorbed at the interface. The study of the process of SHG by a dipole sheet has been treated in a number of ways. Bloembergen and Pershan [Blo62] considered a nonlinear slab of material of thickness approaching zero to simulate the nonlinear monolayer and the existing boundary conditions for a nonlinear dipole sheet were derived by Heinz [Heinz] in order to obtain the SH emitted power from the slab. More general treatments of surface second harmonic generation have been given by Mizrahi [Miz88] or by Sipe [Sip87] based on a Green-function formalism. In Figure 1.2 we see a plot of the surface second-harmonic radiation by a monolayer, showing the bell shaped form characteristic of these surface phenomena [Hol90].

Chapter 2

Second Harmonic Generation in Local Modes of 1-dimensional truncated periodic structures

The use of 1-dimensional periodic structures to control the properties of the electromagnetic radiation is well known and extensively used in nowadays technology. Dielectric mirrors, antireflection coatings, filters, DFB lasers and many other components are based in the properties of the 1-D periodic structures. As a consequence, in recent years, the study of electromagnetic wave propagation within such structures has been extensively studied in the literature [Yariv][Beth89][Leod]. The use of these kind of structures has been extended to the study of nonlinear phenomena such as optical diodes [Sca94], second-harmonic generation[Mar97], solitons, fiber optics [Fer99][Kni97] and others.

In this chapter we will consider SHG from a NL monolayer placed within the defect of a 1-dimensional photonic crystal both, experimentally and theoretically. Our main purpose is to study the modification of the SHG induced by the presence of this structure and in particular how this radiation may be enhanced or inhibited depending on the conditions present in the experiment. The most simple photonic crystal consists of a set of dielectric layers with alternating refractive indices and thickness. These structures are shown to present band gaps or certain frequency windows for which electromagnetic radiation is strongly reflected. The band gaps in our experiments will be considered for a fixed frequency and as a function of the angle of incidence. We will present the theoretical model of these effects in the angular domain.

When a defect is placed within this structure, localized states appear within the band gaps as explained in section 1.2 of chapter 1. The radiative properties at the second-harmonic frequency of the monolayer of nonlinear molecules, adsorbed at the defect site of the structure, driven by a field at the fundamental frequency are changed by the
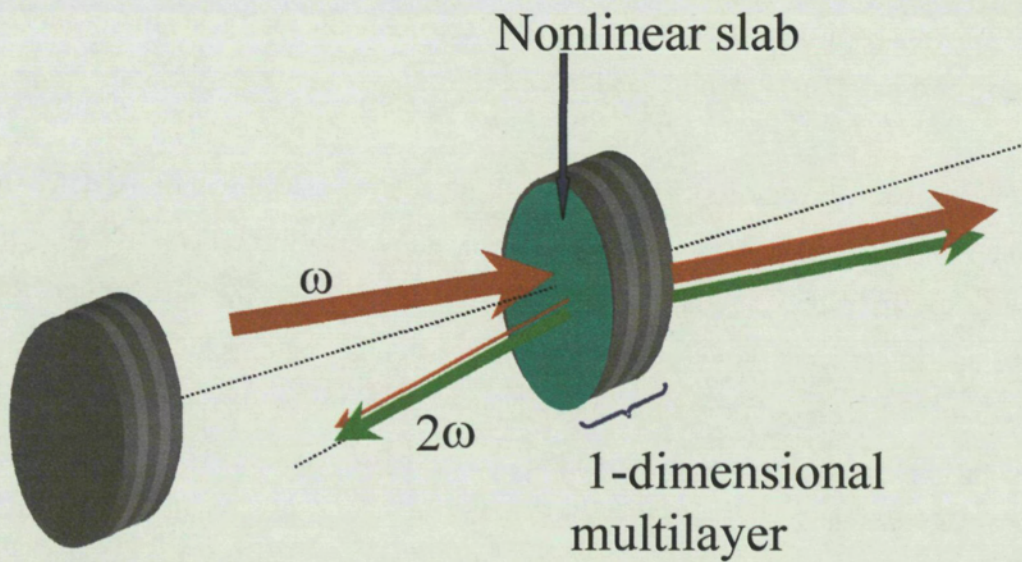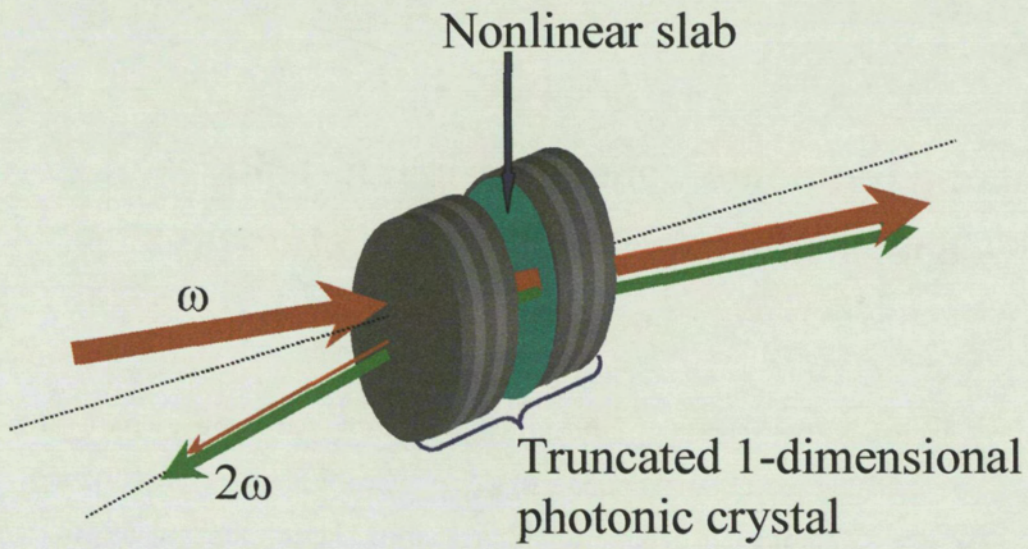
Figure 2.1 Schematic representation of the experimental configuration for the measurement of SH radiation in local modes of truncated periodic dielectric structures.

presence of the structure. This will be studied experimentally by looking at the second harmonic radiation emitted from the structure with the monolayer. In order to see the effect introduced by the periodic distribution we will also measure the SH radiation emitted by the same monolayer when placed out of the truncated 1-D photonic crystal, and will make a comparison between both results. We will give also a comparison of the experimental results with a theoretical modelization of the process. The analysis of the nonlinear interaction at the monolayer will consider a nonlinear slab of thickness approaching zero [Blo62] and the use of the transfer matrix technique [Yariv][Beth89] to account for the periodicity of the medium.

A schematic diagram of the experiment may be seen in Figure 2.1(a). The nonlinear interaction between the beam at the fundamental frequency ω (1064 nm) incident at the structure and the monolayer placed within the defect results in a generation of second-harmonic radiation, 2ω, which is measured in reflection out of the structure. Excitation of the molecules at the monolayer placed within the structure is possible since the fundamental frequency is far from the Bragg reflection bands of the periodic structure, and thus is highly transmitted through the structure.On the other hand, additional measurements of the second harmonic generated by the same monolayer when it is not placed within the defect of the truncated periodic structure will be performed according to the diagram shown in Figure 2.1(b)

A brief review of the main aspects of the wave propagation in 1-d periodic structures will be derived in sections 1 and 2 of the chapter. Section 3 will be devoted to the study of localized states appearing when defects are included within such structures. The theoretical description of the generation of second harmonic radiation by a monolayer placed within such defects will be studied in section 4 and in section 5 the experimental results obtained will be presented.

1. Wave propagation in 1- D periodic structures

The most general 1-D dielectric periodic structure can be characterized by the knowledge of its dielectric constant profile over one period. The periodicity of the structure translates into a periodicity of the dielectric constant of the medium $\varepsilon(x)=\varepsilon(x+R)$, where R denotes any vector of the periodic lattice of the structure. These

structures may be studied by direct application of the formalism seen in chapter 1 [Yariv] by solving the eigenvalue problem, Eq. 1.3 for this particular case. Nevertheless, for the particular structures used, an exact solution of the wave equation can be obtained by means of a second approach based on matrix calculations and this second approach is the one we will adopt in this work.

The particular structures we are concerned with consists of a set of layers of dielectric material with alternating refractive indices n_h and n_l and thickness l_h and l_l respectively. The dielectric medium in each layer is considered to be homogeneous and lossless and is supposed to extend in all directions in the plane transverse to the periodicity direction. Figure 2.2 represents a schematic diagram of such structures with the notation used for the axes and the geometrical and optical parameters of the structure.

The refractive index profile for these structures can be written as:

$$n(z) = \begin{cases} n_h, & 0 < z < l_h \\ n_l, & l_h < z < \Lambda \end{cases} \qquad \text{2.1.}$$

with

$$n(z) = n(z + \Lambda) \qquad \text{2.2.}$$

where the direction z is the axis normal to the layer interfaces and $\Lambda = l_h + l_l$ is the period.
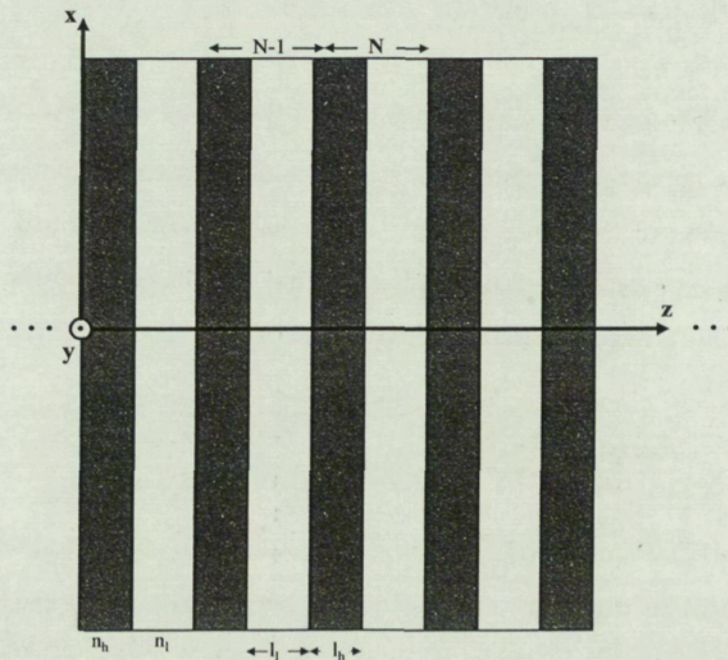
Figure 2.2 Schematic representation of a 1-dimensional periodic structure made of homogeneous and lossless dielectric layers.

Let's consider an infinite monochromatic plane wave of frequency ω propagating in the -XZ plane in a direction forming an angle θ_o with respect to the Z axis. At each interface it will be partially reflected and transmitted giving as a result a final stationary electric field distribution within the structure that can be written as a superposition of a forward propagating and a backward propagating wave in each layer (Figure 2.3).

In particular, the expression for the electric field in the nth period of the structure at the layer with index n_i (i=l,h) is written in the form:

$$\mathbf{E}(z,t) = \frac{1}{2}\left[\hat{\mathbf{e}}_+^i E_+^i(n)\exp i\left(k_{iz}(z-(n-1)\Lambda)\right) + \hat{\mathbf{e}}_-^i E_-^i(n)\exp -i\left(k_{iz}(z-(n-1)\Lambda)\right)\right]\exp\left(ik_x x - i\omega t\right)$$
$$+ c.c$$

$$2.3.$$

where $\hat{\mathbf{e}}_+^i$ and $\hat{\mathbf{e}}_-^i$ are unit vectors in the directions of the forward propagating (+) and backward propagating (-) components of the electric field in layer i. Their particular expression depends on the polarization state of the beam. E_+^i and E_-^i are the complex amplitudes of the field in the forward and backward direction and k_{iz} and k_x are the components of the wavevector in layer i. They are related through the expression:

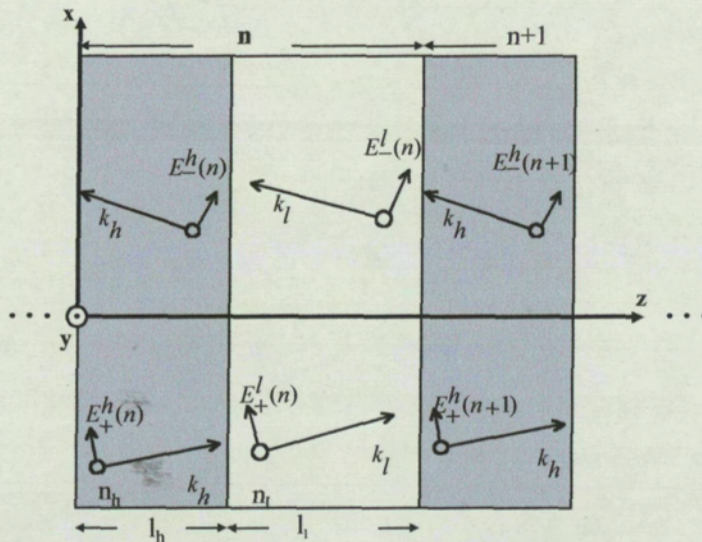$$k_{iz} = \left[\left(\frac{n_i\omega}{c}\right)^2 - k_x^2\right]^{1/2}$$

$$2.4.$$

Figure 2.3 Schematic representation of the fields in the structure.

The fields in different layers are not independent of each other, since they are related through the boundary conditions at the interfaces and as a consequence only one field can be determined arbitrarily. The knowledge of the boundary conditions for the whole structure will allow us to find the solution for each particular mode.

In the case of waves with TE polarization (electric field perpendicular to the plane of incidence) the tangential components of the fields (E_y and $H_x \propto \dfrac{\partial E_y}{\partial z}$) must be continuous at each interface (see Appendix A). By applying these conditions at the interfaces $z=(n-1)\Lambda+l_h$ and $z=n\Lambda$ (Fig 2.2) we obtain the following equations:

$z=(n-1)\Lambda+l_h$

$$E_+^h(n)\exp ik_{hz}l_h + E_-^h(n)\exp-ik_{hz}l_h = E_+^l(n)\exp ik_{lz}l_h + E_-^l(n)\exp-ik_{lz}l_h$$

$$k_{hz}\left(E_+^h(n)\exp ik_{hz}l_h - E_-^h(n)\exp-ik_{hz}l_h\right) = k_{lz}\left(E_+^h(n)\exp ik_{lz}l_h - E_-^h(n)\exp-ik_{lz}l_h\right)$$

$z = n\Lambda$ 2.5.

$$E_+^l(n)\exp ik_{lz}\Lambda + E_-^l(n)\exp-ik_{lz}\Lambda = E_+^h(n+1) + E_-^h(n+1)$$

$$k_{lz}\left(E_+^l(n)\exp ik_{lz}\Lambda - E_-^l\exp-ik_{lz}\Lambda\right) = k_{hz}\left(E_+^h(n+1) - E_-^h(n+1)\right)$$

These four equations can be written in matrix form as:

$$\begin{pmatrix} \exp ik_{hz}l_h & \exp-ik_{hz}l_h \\ \exp ik_{hz}l_h & -\exp-ik_{hz}l_h \end{pmatrix}\begin{pmatrix} E_+^h(n) \\ E_-^h(n) \end{pmatrix} = \begin{pmatrix} \exp ik_{lz}l_h & \exp-ik_{lz}l_h \\ \dfrac{k_{lz}}{k_{hz}}\exp ik_{lz}l_h & -\dfrac{k_{lz}}{k_{hz}}\exp-ik_{lz}l_h \end{pmatrix}\begin{pmatrix} E_+^l(n) \\ E_-^l(n) \end{pmatrix}$$

$$\begin{pmatrix} \exp ik_{lz}\Lambda & \exp-ik_{lz}\Lambda \\ \exp ik_{lz}\Lambda & -\exp-ik_{lz}\Lambda \end{pmatrix}\begin{pmatrix} E_+^l(n) \\ E_-^l(n) \end{pmatrix} = \begin{pmatrix} 1 & 1 \\ \dfrac{k_{hz}}{k_{lz}} & -\dfrac{k_{hz}}{k_{lz}} \end{pmatrix}\begin{pmatrix} E_+^h(n+1) \\ E_-^h(n+1) \end{pmatrix}$$ 2.6.

After some algebraic manipulation we obtain an expression relating the fields in the layer h of the nth period and the field in the layer h of the nth+1 period:

$$\begin{pmatrix} E_+^h(n+1) \\ E_-^h(n+1) \end{pmatrix} = \begin{pmatrix} A_{TE} & B_{TE} \\ C_{TE} & D_{TE} \end{pmatrix}\begin{pmatrix} E_+^h(n) \\ E_-^h(n) \end{pmatrix}$$ 2.7.

where the matrix elements are given by:

$$A_{TE} = \exp ik_{hz}l_h \left[\cos(k_{lz}l_l) + \frac{i}{2}\left(\frac{n_l \cos\theta_l}{n_h \cos\theta_h} + \frac{n_h \cos\theta_h}{n_l \cos\theta_l} \right) \sin(k_{lz}l_l) \right]$$

$$B_{TE} = \exp - ik_{hz}l_h \left[\frac{i}{2}\left(\frac{n_l \cos\theta_l}{n_h \cos\theta_h} - \frac{n_h \cos\theta_h}{n_l \cos\theta_l} \right) \sin(k_{lz}l_l) \right]$$

$$C_{TE} = \exp ik_{hz}l_h \left[-\frac{i}{2}\left(\frac{n_l \cos\theta_l}{n_h \cos\theta_h} - \frac{n_h \cos\theta_h}{n_l \cos\theta_l} \right) \sin(k_{lz}l_l) \right]$$

$$D_{TE} = \exp - ik_{hz}l_h \left[\cos(k_{lz}l_l) - \frac{i}{2}\left(\frac{n_l \cos\theta_l}{n_h \cos\theta_h} + \frac{n_h \cos\theta_h}{n_l \cos\theta_l} \right) \sin(k_{lz}l_l) \right]$$

where the relation $k_{iz} = \dfrac{n_i\omega}{c}\cos\theta_i$ has been used. The fields at each layer $n_l, E_\pm^l(n)$, may be related to the fields $E_\pm^h(n)$ from Eq.2.6.

For the case of waves with TM polarization, we can proceed in an analogue way to obtain the relation between fields in consecutive layers. By applying the boundary conditions at the tangential components of the field E_x and H_y (see Appendix A) we obtain the equations:

$$z = (n-1)\Lambda + l_h$$

$$\cos\theta_h \left(E_+^h(n)\exp ik_{hz}l_h + E_-^h(n)\exp - ik_{hz}l_h \right) = \cos\theta_l \left(E_+^l(n)\exp ik_{lz}l_h + E_-^l(n)\exp - ik_{lz}l_h \right)$$

$$k_h \left(E_+^h(n)\exp ik_{hz}l_h - E_-^h(n)\exp - ik_{hz}l_h \right) = k_l \left(E_+^h(n)\exp ik_{lz}l_h - E_-^h(n)\exp - ik_{lz}l_h \right)$$

$$z = n\Lambda \qquad\qquad\qquad\qquad\qquad\qquad\qquad\qquad\qquad 2.8.$$

$$\cos\theta_l \left(E_+^l(n)\exp ik_{lz}\Lambda + E_-^l(n)\exp - ik_{lz}\Lambda \right) = \cos\theta_h (E_+^h(n+1) + E_-^h(n+1))$$

$$k_l \left(E_+^l(n)\exp ik_{lz}\Lambda - E_-^l\exp - ik_{lz}\Lambda \right) = k_h \left(E_+^h(n+1) - E_-^h(n+1) \right)$$

Rewriting these equations in matrix form and operating on them we get

$$\begin{pmatrix} E_+^h(n+1) \\ E_-^h(n+1) \end{pmatrix} = \begin{pmatrix} A_{TM} & B_{TM} \\ C_{TM} & D_{TM} \end{pmatrix} \begin{pmatrix} E_+^h(n) \\ E_-^h(n) \end{pmatrix} \qquad\qquad 2.9.$$

with

$$A_{TM} = \exp ik_{hz}l_h \left[\cos(k_{lz}l_l) + \frac{i}{2} \left(\frac{n_l \cos\theta_h}{n_h \cos\theta_l} + \frac{n_h \cos\theta_l}{n_l \cos\theta_h} \right) sin(k_{lz}l_l) \right]$$

$$B_{TM} = \exp- ik_{hz}l_h \left[\frac{i}{2} \left(\frac{n_l \cos\theta_h}{n_h \cos\theta_l} - \frac{n_h \cos\theta_l}{n_l \cos\theta_h} \right) sin(k_{lz}l_l) \right]$$

$$C_{TM} = \exp ik_{hz}l_h \left[-\frac{i}{2} \left(\frac{n_l \cos\theta_h}{n_h \cos\theta_l} - \frac{n_h \cos\theta_l}{n_l \cos\theta_h} \right) sin(k_{lz}l_l) \right]$$

$$D_{TM} = \exp- ik_{hz}l_h \left[\cos(k_{lz}l_l) - \frac{i}{2} \left(\frac{n_l \cos\theta_h}{n_h \cos\theta_l} + \frac{n_h \cos\theta_l}{n_l \cos\theta_h} \right) sin(k_{lz}l_l) \right]$$

Equations (2.7) and (2.9.) are the matrix representation of the translation operator for the given structure. From these relations the expressions for the fields at each layer and the dispersion relation for the structure can be obtained. Note that the particular choice of the phases made in Eq. 2.3. results in a translation matrix independent of the particular period of the structure.

The expression of the dispersion relation may be obtained by applying the symmetry conditions imposed by the periodicity of the structure on the fields. From Eq. 1.6. we obtain the condition:

$$E(x + \Lambda) = \exp(iK\Lambda)\, E(x) \qquad\qquad 2.10.$$

where K is the Bloch wavevector. Applying this relation to our particular structure:

$$\begin{pmatrix} E_+^h(n+1) \\ E_-^h(n+1) \end{pmatrix} = \begin{pmatrix} A & B \\ C & D \end{pmatrix} \begin{pmatrix} E_+^h(n) \\ E_-^h(n) \end{pmatrix} = \exp(iK\Lambda) \begin{pmatrix} 1 & 0 \\ 0 & 1 \end{pmatrix} \begin{pmatrix} E_+^h(n) \\ E_-^h(n) \end{pmatrix} \qquad 2.11.$$

By solving this eigenvalue equation we obtain the eigenvalue solution:

$$K(\omega, k_x) = \frac{1}{\Lambda} \cos^{-1}\left(\frac{1}{2}(A + D) \right) \qquad\qquad 2.12.$$

The dispersion relation obtained can be demonstrated to be valid for a generic periodic media of period Λ with a translational operator expressed in matrix form[Yariv]. In the

present case, where propagation of the beam in the XZ plane is considered, we note that this dispersion relation gives a surface in the K-k_x-ω space. Within this space there exist two differentiated regions:

Those regions with $\frac{1}{2}(A+D) < 1$, give a real value for K and correspond to propagating modes of the structure , whereas for those regions where $\frac{1}{2}(A+D) > 1$, K is complex giving raise to evanescent modes with amplitude decaying exponentially as they are propagated through the structure (band gaps). The electromagnetic modes with frequency values falling within these regions will be strongly reflected.

The explicit expression for the dispersion relation in the particular structures considered may be found by substituting the values of the matrix elements in 2.12.:

TE polarization

$$4\cos K\Lambda = \frac{(k_{hz}+k_{lz})^2}{k_{hz}k_{lz}}\cos(k_{hz}l_h + k_{lz}l_l) - \frac{(k_{hz}-k_{lz})^2}{k_{hz}k_{lz}}\cos(k_{hz}l_h - k_{lz}l_l)$$

TM polarization   2.13.

$$4\cos K\Lambda = \frac{(n_l^2 k_{hz}+n_h^2 k_{lz})^2}{n_l^2 n_h^2 k_{hz}k_{lz}}\cos(k_{hz}l_h + k_{lz}l_l) - \frac{(n_l^2 k_{hz}-n_h^2 k_{lz})^2}{n_l^2 n_h^2 k_{hz}k_{lz}}\cos(k_{hz}l_h - k_{lz}l_l)$$

For the particular case of wave propagation in the direction perpendicular to the layer interfaces (k_x=0), the dispersion relation for both polarizations reduces to the same expression:

$$\cos K\Lambda = \frac{\Delta+1}{2}\cos\left(\frac{\bar{n}\omega\Lambda}{c}\right) - \frac{\Delta-1}{2}\cos\left(\frac{\bar{v}\omega\Lambda}{c}\right)$$ 2.14.

where the different terms are defined as:

$$\Delta = \frac{1}{2}\left(\frac{n_l^2 + n_h^2}{n_h n_l}\right), \bar{n} = \frac{n_h l_h + n_l l_l}{l_h + l_l} \text{ and } \bar{v} = \frac{n_h l_h - n_l l_l}{l_h + l_l}.$$
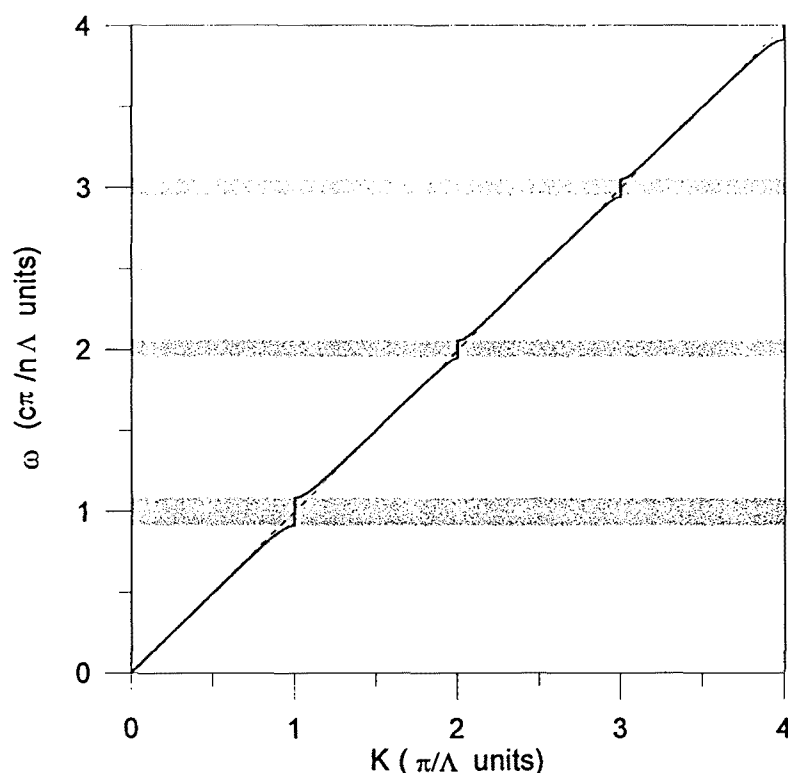
Figure 2.4 Dispersion relation for a periodic structure with $\bar{n} = 1.72, \Delta = 1.04$ and

$\bar{V} = 0.34$.

A plot of the dispersion relation given by this equation is shown in Figure 2.4. As can be seen from this Figure, band gaps appear when the Bloch wavevector reaches the values K=mπ/Λ centered at the frequency values given by the expression:

$$\omega_m = \frac{mc\pi}{\bar{n}\Lambda}$$
                                                                                                    2.15..

Note that in those regions out of the gaps the dispersion relation is close to the dispersion relation for an homogeneous medium with index of refraction $\bar{n}$: $\omega = \frac{cK}{\bar{n}}$.

A more detailed analysis of these relations shows that the relative gap width of each band is proportional to the corresponding component of the Fourier expansion of the dielectric constant at that frequency [Yariv].
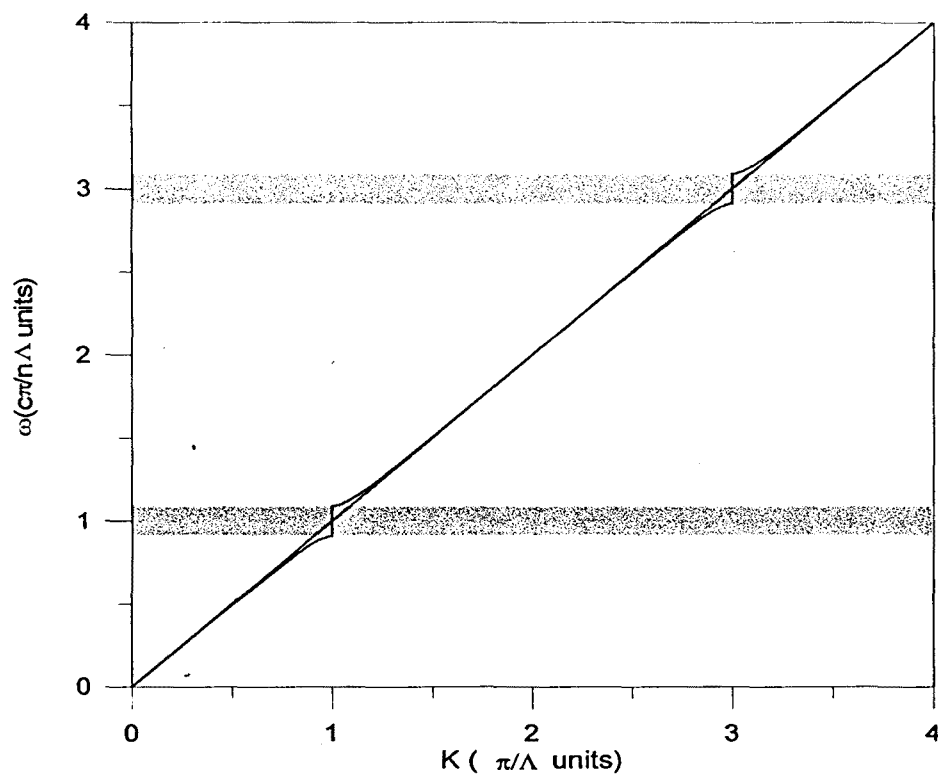
Figure 2.5 Dispersion relation for quarter wavelength Bragg reflectors.

The particular structure having each one of its layers of equal optical length, known as quarter wavelength Bragg reflector (QWBR), will be the structure we will use in our experimental work. For these structures, the even orders in the Fourier expansion of the dielectric constant vanish, thus giving no gaps at the frequencies with an even value of m. Figure 2.5 shows a typical plot of a dispersion relation for such structures. Some special properties for such QWBR are outlined in Appendix B.

The periodicity inherent to these structures has very important consequences in the propagating properties of the radiation with frequency values falling within or close to the photonic band gap [Yar76]. Several effects, reported in the literature during the last years and including both basic aspects of the interaction and potential practical applications, demonstrate the importance of photonic crystals even in the case where not full photonic band gaps are present. The bending of the dispersion relation curve at the band edges causes a reduction of the wave group velocity thus increasing the effective path length within the structure (such effect has been proposed to be the basis of the

gain enhancement for photonic band edge laser [Dow94]) and, at the same time, giving rise to an alteration in the density of states which cause the appearance of resonant states at these frequencies leading to an enhancement of radiation. This fact has been used to obtain an enhancement of SH radiation at the band edges (as will be demonstrated experimentally later in this chapter), or to the study of spontaneous emission enhancement [Toc96]. The change in the effective refractive index of the structure giving an anomalous dispersion regime in the low frequency band edges opens the possibility of obtaining phase-matching in nonlinear processes (this will be studied in further detail in chapter 4). The combination of pulse propagation through these structures together with nonlinearities in the medium has shown to be of potential use in the achievement of new optical devices such as optical limiters or the photonic band edge optical diode [Sca94]. The effects of this periodicity on the propagation properties of optical pulses, energy flow or momentum has also been object of study [Sca95][Sca96].

2. Reflection and Transmission in periodic structures

In the preceding section, we have given a brief review of the properties of infinite 1-dimensional periodic structures. Any real multilayer structure must be finite and as a consequence no real Bloch modes may formally exist as modes for the structure. The effects caused by the finite number of layers of the structure, results in the appearance of subsidiary maxima between high reflection bands, a lowering of the reflectivity of such structures at the band gap frequencies when the number of periods is very low, and broadening of the localized states when defects are present, among other effects. Nevertheless, many of the results of the preceding section may be used even in finite structures. i.e. the Bloch wavevector is useful to calculate the density of modes in a periodic structure of this kind [Ben96].

In this section we will review the transfer matrix method for the calculation of the reflectance and transmittance of such structures and will extend the concept of band gap to the angular domain. From now, we will limit our results to quarter-wavelength Bragg reflectors, since those structures will be the ones which will be used in the experimental measurements. As it is usual in such structures, the first and last layers are considered to

be of high refractive index n_h in order to have a higher reflectivity, and we consider that the multilayer structure is deposited on a substrate with index n_s. We can represent an N period structure of this kind as an g[HL]^{N}Ha structure where a represents the substrate and g the incident medium[Hecht].

In order to calculate the reflectance and transmission of such N period structures we need to relate the fields at both sides of the structure. This can be done by relating the tangential components of the electric and magnetic fields at each interface of the structure. As seen in the previous section, the fields in consecutive layers with index n_h, are related through the translational matrix given by Eqs. 2.7 and 2.9. In order to calculate the reflectance and transmittance of the medium we need to relate the fields incident at the structure with the fields at the first layer, and the fields in the last layer with the fields out of the structure. We write the fields incident and transmitted as:

Field incident at the structure

$$\mathbf{E}(z,t) = \frac{1}{2}\left[\hat{e}_+^{inc} E_+^{inc} \exp i(k_{oz}z) + \hat{e}_-^{inc} E_-^{inc} \exp - i(k_{oz}z)\right]\exp(ik_x x - i\omega t) + c.c \qquad 2.16.$$

Field transmitted by the structure:

$$\mathbf{E}(z,t) = \frac{1}{2}\left[\hat{e}_+^{tr} E_+^{tr} \exp i(k_{oz}(z - (N-1)\Lambda)) + \hat{e}_-^{tr} E_-^{tr} \exp - i(k_{oz}(z - (N-1)\Lambda))\right]\exp(ik_x x - i\omega t)$$
$$+ c.c$$

where $k_{oz} = \dfrac{\omega \cos\theta_o}{c}$ is the propagation wavevector in the medium surrounding the structure which will be considered to be air and θ_o is the incidence angle with respect to the z axis. Once the boundary conditions at the interfaces are considered the relation between fields in consecutive layers is written as:

$$\begin{pmatrix} E_+^h(1) \\ E_-^h(1) \end{pmatrix} = [AM]\begin{pmatrix} E_+^{inc} \\ E_-^{inc} \end{pmatrix}$$

$$\begin{pmatrix} E^h_+(N+1) \\ E^h_-(N+1) \end{pmatrix} = [T]^N \begin{pmatrix} E^h_+(1) \\ E^h_-(1) \end{pmatrix}$$

and

$$\begin{pmatrix} E^{tr}_+ \\ E^{tr}_- \end{pmatrix} = [MA] \begin{pmatrix} E^h_+(N+1) \\ E^h_-(N+1) \end{pmatrix}$$

where the terms between brackets [T], [AM] and [MA] denote the matrices that relate the corresponding field components. The elements of the [T] matrix are those given in Eqs. 2.7 and 2.9. The particular values of the other matrices can be found in Appendix C. The choice of the phases in 2.16 results in a [T] matrix independent of the particular period of the structure. With the values for the matrices found we can relate the incident and transmitted fields at the structure through the expression :

$$\begin{pmatrix} E^{tr}_+ \\ E^{tr}_- \end{pmatrix} = \begin{pmatrix} A & B \\ C & D \end{pmatrix} \begin{pmatrix} E^{inc}_+ \\ E^{inc}_- \end{pmatrix} \tag{2.17}$$

where the resulting matrix is obtained by multiplication of the previous ones:

$$\begin{pmatrix} A & B \\ C & D \end{pmatrix} = [MA][T]^N[AM]$$

We will consider that there is no field incident at the right of the structure ($E^{tr}_- = 0$), and that we know the field incident at the left (E^{inc}_+). After applying these boundary conditions for the whole structure, the reflection and transmission coefficients for the structure are found immediately from Eq. 2.17:

$$r = \frac{E^{inc}_-}{E^{inc}_+} = \frac{-C}{D} \qquad \text{and} \qquad t = \frac{E^{tr}_+}{E^{inc}_+} = \frac{AD - BC}{D}$$

the reflectance and transmittance of the structure are given by:
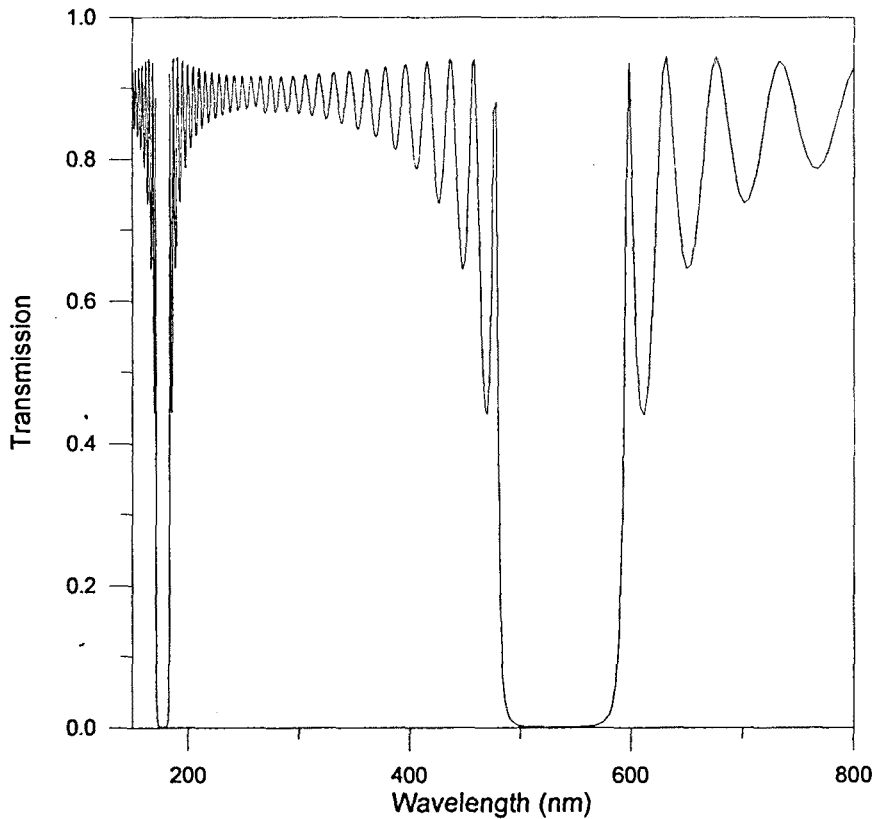
Figure 2.6 Transmission of a periodic QWBR consisting of 29 layers with indices n_h=1.95, n_f=1.46, and lengths l_h=68 nm, l_f=91 nm. The index of the substrate is 1.52.

$$R = |r|^2 \quad \text{and} \quad T = |t|^2 \qquad\qquad 2.18.$$

Figure 2.6 shows a typical transmittance curve for a QWBR structure as a function of the incident wavelength for normal incidence calculated by means of Eq. 2.18. As can be seen from this figure, high reflection bands appear in the spectrum. Electromagnetic radiation with wavelength values falling within these regions will be completely reflected by the structure. With the aid of Eq. 2.15 and considering that for our particular case all layers have equal optical thickness (L), the wavelengths at the center of these high reflection bands are given by:

$$\lambda_m = \frac{4L}{2m+1} \quad \text{with } m = 0,1,2,... \qquad\qquad 2.19.$$

As stated in previous section, the dispersion relation for radiation propagating in the XZ plane, is a surface in the $K-k_x-\omega$ plane. According to this, if we fix the incident wavelength to a given value, we will have a dispersion relation between K and k_x, that is between K and the incidence angle θ_o. For later convenience in our work, we will not be interested in the reflectance as a function of wavelength since the wavelength will be a fixed parameter in our experiments. Instead, we will change the angle of incidence of the radiation in order to reach different regions of the dispersion relation. The reflectance curves for the structure as a function of the angle of incidence can be obtained with the same equations already derived. Figure 2.7 shows the transmittance spectrum for the same structure as in Fig 2.6 for the fixed wavelength 532 nm. When the incident radiation on the structure is TM polarized, the observed gap appears between 0 and 40 degrees (that means that radiation at the given frequency and polarization will be reflected by the structure when incident at angles lower than 40 degrees). Polarization of the incident wave is important in the angular measurements
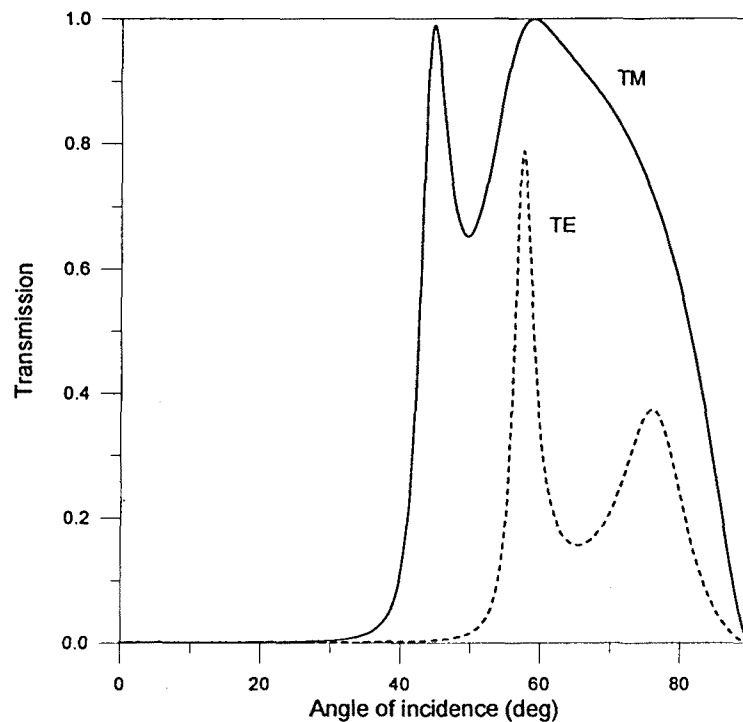
Figure 2.7   Transmission as a function of the angle of incidence for the same structure of Figure 2.6, for light incident at 532 nm.

since different polarizations give different gaps, due to the fact that the Fresnel laws depend on the polarization state of the incident wave. The transmittance for the same structure of Fig 2.6 with TE polarization is also shown in Fig. 2.7. One can see immediately that the gap width is higher in the TE case, with the band edge appearing at higher angles. This fact may be important in different applications. For our present work, we will have waves with TM polarization, the reason will be better understood in the following sections.

3. Defects in 1-dimensional photonic crystals

In chapter 1 was seen that the introduction of a defect in a periodic structure results in the appearance of localized states within the gap of the structure, with transmission values different from zero. These localized states are characterized by a high energy density of the electric field at the defect site, which falls off exponentially as we move away from the defect. For an infinite structure, light generated inside the defect should be confined within the structure, but if the structure is finite then part of the radiation can get out of it.

The observation of such defect states in QWBR is possible if one introduces some alteration in the periodicity of the structure. We will introduce the defect by changing the optical length of the layer at the middle of the structure. Increasing the optical length corresponds to the case of increasing the dielectric material in the structure, so donor modes will appear from the lower angle band edge. If instead, the optical length is diminished then defect states appear from the higher angles band edge into the gap giving rise to acceptor modes. The position and number of such localized modes within the gap depend upon the values of the length and index of refraction of the defect, whereas the localized state width and maximum transmittance depend on the number of layers of the structure. The introduction of a defect in these periodic structures may be obtained by means of a change in the refractive index or the length (or both) of one of the layers of the structure. Figure 2.8 shows the transmission of a periodic structure possessing a gap between 20 and 60 degrees. The effect of introducing a defect in the central layer (with index n_f=1.46 and length l_f=101 nm) of the structure is seen in Figures 2.9 and 2.10. Figure 2.9 shows the effect of introducing a variation in the

refractive index of the layer while keeping the length of the layer to its initial value. As the refractive index is decreased from its initial value (1.46), acceptor modes come from the higher angular band edge of the structure moving within the gap as the optical length is being reduced. On the contrary, if the optical length is increased by setting a higher refractive index, donor modes appear from the low angular band edge into the gap. In Figure 2.10 the effect of introducing a variation in the length of the structure, keeping the refractive index constant to its initial value is shown to produce acceptor and donor modes in the same way as in Figure 2.9.

As stated previously in chapter 1, the presence of the defect within the structure results in a strong localization of the electromagnetic field at the defect site and a modification of the density of states. The existence of this localized state may be used in order to enhance different phenomena and in particular nonlinear phenomena, such as SHG.
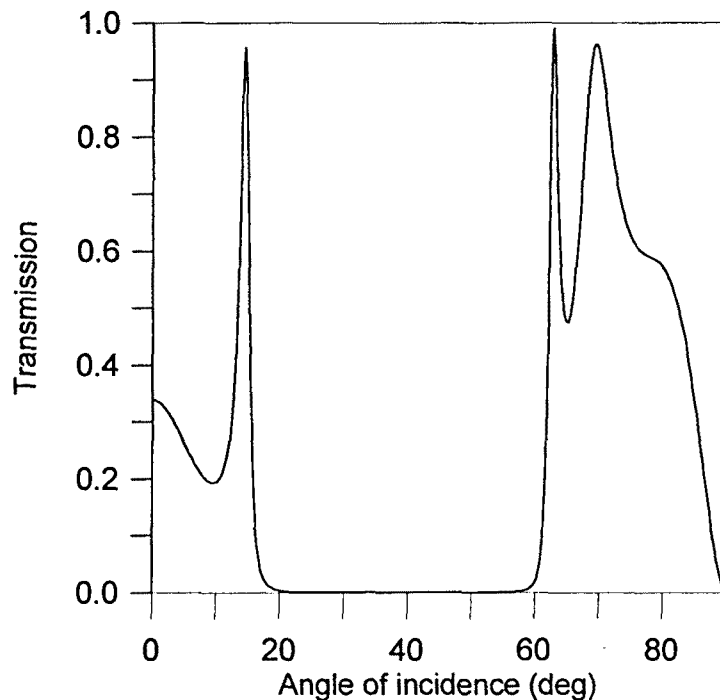
Figure 2.8 Transmission for a periodic structure consisting of 57 layers with n_h=1.95, n_l=1.46, l_h=75.5 nm and l_l=101 nm, for incident light TM polarized at 532 nm.

Acceptor
modes

Donor
modes
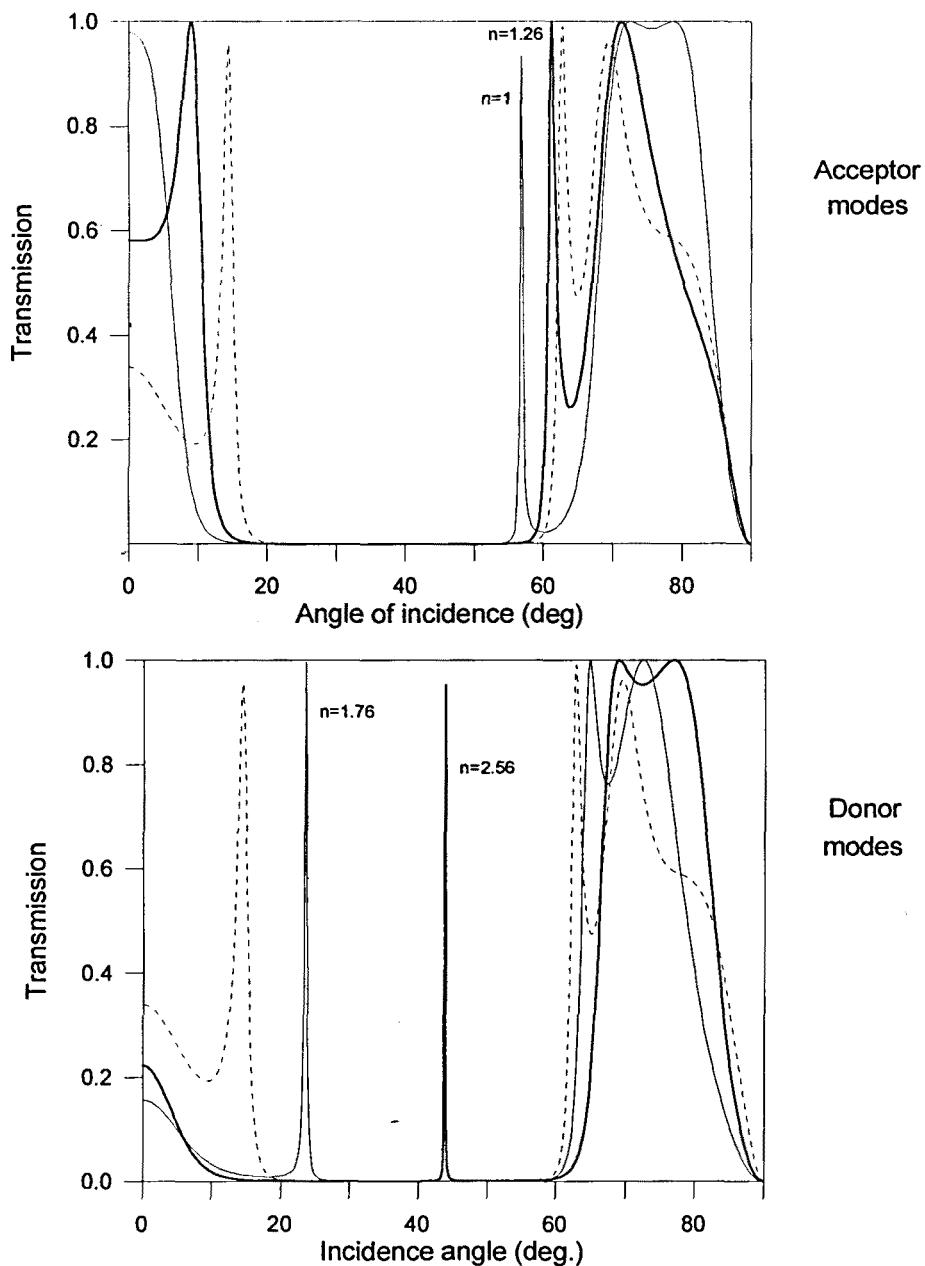
Figure 2.9 Appearance of defects in the periodic structure of Fig 2.8 when the refraction index is changed at the central layer. The dashed line corresponds to the periodic structure with no defects (Figure2.8).
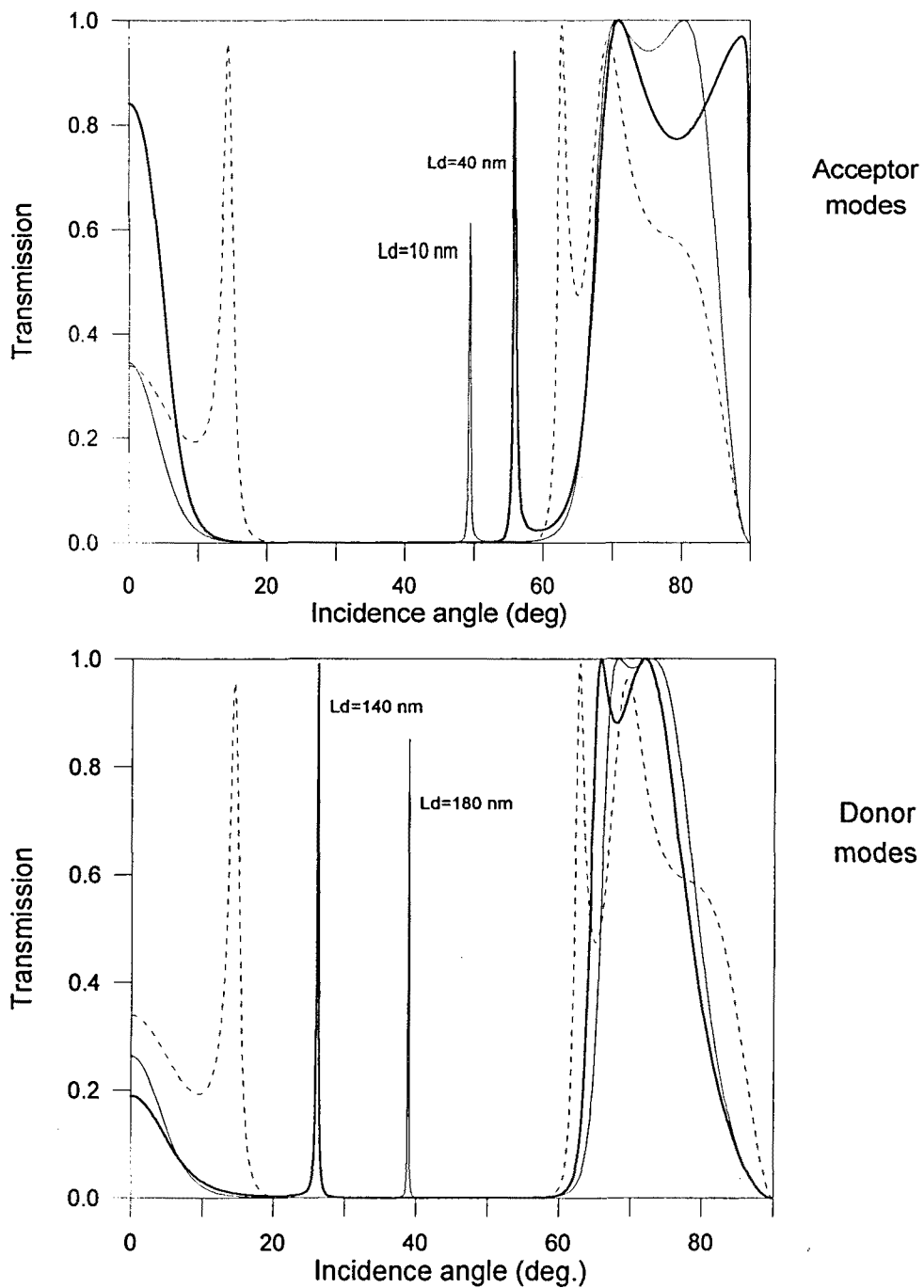
Figure 2.10 Appearance of defects in the periodic structure of Figure 2.8 when the thickness of the central layer is changed. The dashed line corresponds to the periodic structure with no defects (Figure2.8).

4. Second harmonic generation in periodic structures

The process of second harmonic generation in a bulk material in which a strong pumping field at frequency ω acts as a nonlinear driving source generating light at the doubled frequency, 2ω, has been a subject of major interest since the early work of nonlinear optics. As seen in chapter 1, phase-matching between the corresponding wavevectors $k_{2\omega}$ and $2k_{\omega}$ was necessary in a bulk material in order to achieve the necessary condition for growth of the SH field in the direction of propagation of the fields inside the material and this bulk generation is commonly used in many laser systems for efficient frequency light conversion. On the other hand, harmonic generation by monolayers has proven to be a field of great interest in the characterization of surfaces and determination of susceptibility tensors. It is known that a beam of frequency ω, incident on a surface separating two homogeneous media gives rise to a reflected SH wave, even in the case of inversion symmetry in each medium. This is possible due to the intrinsic symmetry breaking at the surface. The reflected wave, appearing as a consequence of the boundary separating two media, is generated due to electric dipole contributions to $\chi^{(2)}$ from the layers of the two media closest to each side of the surface. The contribution of other layers is very low due to the absence of phase-matching. These effects may be highly enhanced if a monolayer of nonlinear molecules is adsorbed at the surface separating both media [Che73][Che81][Hei82].

We will consider in this section the generation of second harmonic light by a monolayer of molecules with a nonzero nonlinear susceptibility second-order coefficient adsorbed at the surface separating two homogeneous media when a beam at frequency ω is incident at the surface. In section 4.1 we will derive the equations for the SHG process at the nonlinear slab when it is adsorbed on an homogeneous substrate. In section 4.2, the effect of introducing such monolayer within the defect present in a QWBR will be studied, in order to see how the process of SHG is influenced by the presence of the structure. We will see that due to the presence of the periodic structure with the defect, generation of SH is enhanced at angles for which there is a resonance with the localized state of the structure, while SH radiation at other angles (for which the frequency falls within the bandgap) is strongly inhibited.

4.1 Second harmonic generation by a nonlinear monolayer

The equations governing the evolution of the fields in a nonlinear interaction were described in the introductory chapter and will be developed here in more detail for the particular case we want to study. For the case of SHG, the wave equations describing the evolution of the fields at the fundamental frequency, ω, and at the SH frequency, 2ω are :

$$\nabla \times (\nabla \times \mathbf{E}_{2\omega}) - \frac{n_{2\omega}^2 (2\omega)^2}{c^2} \mathbf{E}_{2\omega} = \mu_o (2\omega)^2 \mathbf{P}_{NL}^{2\omega} \qquad 2.20.$$

$$\nabla \times (\nabla \times \mathbf{E}_{\omega}) - \frac{n_{\omega}^2 (\omega)^2}{c^2} \mathbf{E}_{\omega} = \mu_o (\omega)^2 \mathbf{P}_{NL}^{\omega} \qquad 2.21.$$

where μ_o is the magnetic permeability of vacuum, n_ω and $n_{2\omega}$ are the refractive indices of the medium at the corresponding frequencies, and $\mathbf{P}^{NL}$ represent the nonlinear polarization of the source terms for the fundamental and second harmonic fields, which are given by the contraction of the nonlinear susceptibility tensor $\chi^{(2)}$ with the corresponding field in each case. Preserving the second-order derivatives of the field in the double cross product term implies that propagation is allowed in both directions and that all reflections are properly accounted for at any boundaries.

The conditions that will hold in our experiment allow us to introduce the following approximations:

i) First, since the amount of SH light generated at a monolayer slab will be small, even in the assumption of a medium possessing a high nonlinear coefficient (the interaction length is much lower than the wavelength) we will assume the intensity of the fundamental wave remains undepleted. This fact is plausible in our case, since the nonlinear polarization term which governs the change in the fundamental beam due to the nonlinear interaction, scales proportional to the product of the fundamental and SH fields, and since this SH field will be very small, the contribution of this term will be negligible.

ii) Second, we will consider the generation of SH light only from the fundamental field that propagates in the forward direction. That means that we neglect the contribution of the reflected fundamental wave inside the slab in the SHG process. For the cases of low

reflection of the fundamental wave this point is justified since the SH wave is driven by a term proportional to the square of the fundamental field and consequently the contribution from the reflected component will be much lower than that from the forward component.

iii) Third, since the slab is considered to be very thin, we will consider that the general solution to the wave equation with the driving term inside the slab may be written as a superposition of the homogeneous plane wave solution and a particular solution assuming constant amplitudes for these solutions along the interaction length [Blo62].

Suppose we have a nonlinear slab of thickness δ (considered much thiner than the wavelength), adsorbed at the interface between two homogeneous materials with refractive indices n_i and n_t.(Figure 2.11). We will assume the field in each homogeneous medium to be a superposition of a forward propagating and a backward propagating plane wave, solutions of the homogeneous part of the wave equations 2.20 and 2.21.
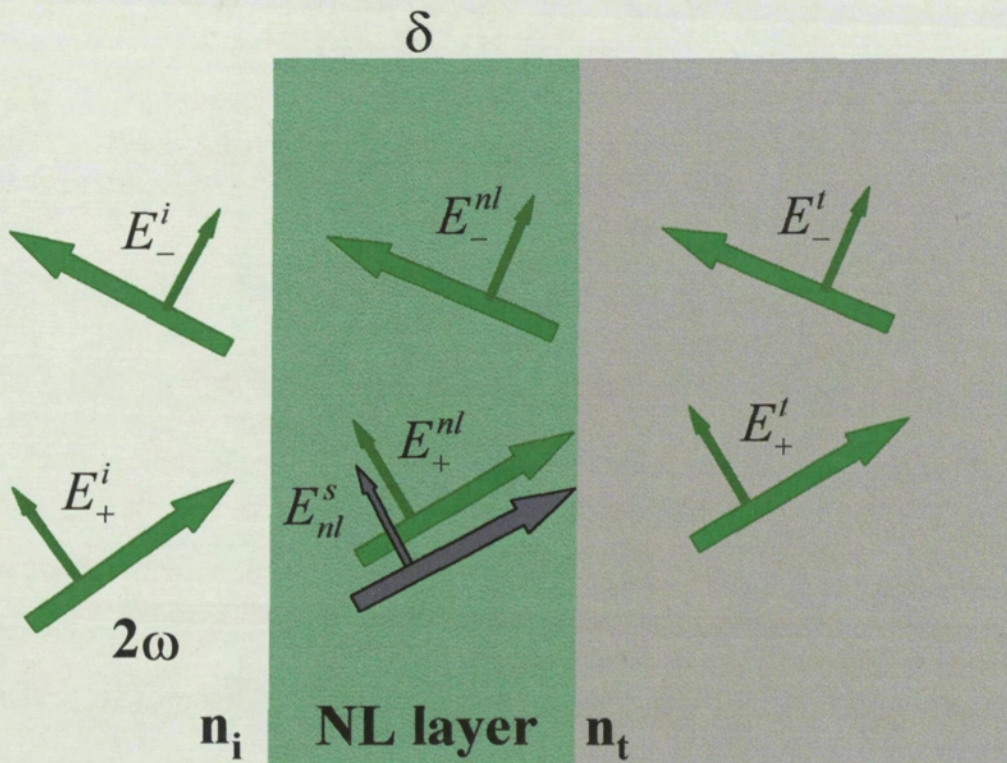
Figure 2.11 SHG by a monolayer. Schematic representation of the fields present at the monolayer and in each homogeneous medium

The field at the NL slab will be considered to be a superposition of two terms, one corresponding to the homogeneous solution of the wave equation, and a second term corresponding to the particular solution of the wave equation which accounts for the SH process. As explained in the previous paragraph, our assumptions allow us to neglect the nonlinear driving term at the fundamental frequency (no particular solution is written for the fundamental field). Within this approximation the propagation of the fundamental may be calculated by means of the transfer method outlined in section 2. We may obtain in this way the fundamental field at each layer of the structure.

The forward propagating component of the field at the fundamental frequency inside the slab will be considered to be the only field that generates light at the SH frequency according to ii) in the preceding paragraph. The fields for the field at frequency 2ω in each layer are written as:

Incident layer (i):

$$\mathbf{E}_i^{2\omega}(z,t) = \frac{1}{2}\left[\hat{e}_+^i E_+^i \exp ik_{iz}z + \hat{e}_-^i E_-^i \exp(-ik_{iz}z)\right]\exp\left(ik_{ix}x - i2\omega t\right) + c.c$$

Nonlinear slab:

$$\mathbf{E}_{nl}^{2\omega}(z,t) = \frac{1}{2}\left[\left[\hat{e}_+^{nl} E_+^{nl} \exp ik_{nl}z + \hat{e}_-^{nl} E_-^{nl} \exp(-ik_{nlz}z)\right]\exp\left(ik_{nlx}x - i2\omega t\right) + \mathbf{E}_{nl}^s \exp i\left(k_{sz}z + k_{sx}x - 2\omega t\right)\right] +$$
$$+ c.c$$

Transmitted layer:

$$\mathbf{E}_t^{2\omega}(z,t) = \frac{1}{2}\left[\hat{e}_+^t E_+^t \exp ik_{tz}z + \hat{e}_-^t E_-^t \exp(-ik_{tz}z)\right]\exp\left(ik_{tx}x - i2\omega t\right) + c.c$$

where the $\hat{e}_+^j\left(\hat{e}_-^j\right)$ terms are the unit vectors for the forward (backward) propagating homogeneous waves in layers j=i,nl and t, and $E_+^j \left(E_-^j\right)$ are the corresponding complex amplitudes at each layer and $\mathbf{E}_{nl}^s$ is the field corresponding to the particular solution of the wave equation which is driven by the nonlinear polarization term. The different wavevectors are defined through the relations:

$$k_j = \frac{n_j^{2\omega} 2\omega}{c}, \quad k_{jz} = k_j \cos\theta_j, \quad k_{jx} = k_j \sin\theta_j \quad j = i, nl, t$$

and

$$k_s = \frac{n_{nl}^{\omega} 2\omega}{c}, \quad k_{sz} = k_s \cos\theta_s, \quad k_{sx} = k_s \sin\theta_s$$

each wave component is considered to be propagating within the XZ plane and forming an angle θ_j with respect to the z direction. Note that the particular and homogeneous solutions inside the nonlinear medium propagate in different directions. Between these defined parameters the following relations hold [Blo62]:

$$k_{ix} = k_{nlx} = k_{sx} = k_{tx}^{\cdot}$$

$$n_i^{2\omega} \sin\theta_i = n_{nl}^{2\omega} \sin\theta_{nl} = n_t^{2\omega} \sin\theta_t$$

$$n_i^{\omega} \sin\theta_i(\omega) = n_{nl}^{\omega} \sin\theta_s = n_t^{\omega} \sin\theta_t(\omega)$$

2.22.

The direction of the particular solution is then, the direction of the propagating fundamental field within the slab which is different from the propagating direction of the SH beam due to the material dispersion. These relations allow us to find the fields incident and transmitted at the nonlinear slab by applying the boundary conditions at each interface. The nonlinear interaction for this case is all included in the field E_+^s, and it will modify the reflection and transmission of the wave with respect to the linear case.

In order to go on with our calculation, we should consider a particular polarization state of the fields. The particular expression for the $\chi^{(2)}$ matrix we will have, corresponding to a rotationally invariant system with respect to the z axis, gives a resulting SH field TM polarized for incident fundamental wave with either TE or TM polarization. We will assume an incident fundamental field with TM polarization for reasons which will be explained afterwards. By applying the boundary conditions in the TM case (see Appendix A) at the nonlinear slab interfaces, $z=d$ and $z=d+\delta$ (see Figure 2.11) we obtain the following set of equations:

At z=d:

$$\cos\theta_i \left[E_+^i \exp ik_{iz}d + E_-^i \exp - ik_{iz}d \right] = \cos\theta_{nl} \left[E_+^{nl} \exp ik_{nlz}d + E_-^{nl} \exp - ik_{nlz}d \right] + E_{nlx}^s \exp ik_{sz}d$$

$$k_i \left[E_+^i \exp ik_{iz}d - E_-^i \exp - ik_{iz}d \right] = k_{nl} \left[E_+^{nl} \exp ik_{nlz}d - E_-^{nl} \exp - ik_{nlz}d \right] + \frac{2\omega}{c^2 \varepsilon_o} H_{nly}^s \exp ik_{sz}d$$

At z=d+δ   2.23.

$$\cos\theta_{nl}\left[E_+^{nl}\exp ik_{nlz}(d+\delta)+E_-^{nl}\exp-ik_{nlz}(d+\delta)\right]+E_{nlx}^s\exp ik_{sz}(d+\delta)=$$

$$=\cos\theta_t\left[E_+^t\exp ik_{tz}(d+\delta)+E_-^t\exp-ik_{tz}(d+\delta)\right]$$

$$k_{nl}\left[E_+^{nl}\exp ik_{nlz}(d+\delta)-E_-^{nl}\exp-ik_{nlz}(d+\delta)\right]+\frac{2\omega}{c^2\varepsilon_o}H_{nly}^s\exp ik_{sz}(d+\delta)=$$

$$=k_t\left[E_+^t\exp ik_{tz}(d+\delta)-E_-^t\exp-ik_{tz}(d+\delta)\right]$$

Once the boundary conditions have been established, we want to relate the fields at the right of the NL slab with those to the left. As a first approximation, we will assume as usual in surface SHG that the index of the nonlinear slab is matched to that of the medium where it is adsorbed, $(n_{nl}=n_t)$ [Shen]. Taking this into account, we obtain from the first two equations:

$$E_+^t\exp ik_{tz}d=\frac{1}{2}\left[\left(\frac{\cos\theta_t}{\cos\theta_i}+\frac{k_t}{k_i}\right)E_+^{nl}\exp ik_{tz}d+\left(\frac{\cos\theta_t}{\cos\theta_i}-\frac{k_t}{k_i}\right)E_-^{nl}\exp-ik_{tz}d\right]+$$

$$+\frac{1}{2}\left(\frac{E_{nlx}^s}{\cos\theta_i}+\frac{2\omega H_{nly}^s}{c^2\varepsilon_o k_i}\right)\exp ik_{sz}d$$ 2.24.

$$E_-^t\exp-ik_{tz}d=\frac{1}{2}\left[\left(\frac{\cos\theta_t}{\cos\theta_i}-\frac{k_t}{k_i}\right)E_+^{nl}\exp ik_{tz}d+\left(\frac{\cos\theta_t}{\cos\theta_i}+\frac{k_t}{k_i}\right)E_-^{nl}\exp-ik_{tz}d\right]+$$

$$+\frac{1}{2}\left(\frac{E_{nlx}^s}{\cos\theta_i}-\frac{2\omega H_{nly}^s}{c^2\varepsilon_o k_i}\right)\exp ik_{sz}d$$

and from the second pair of Eq. 2.23:

$$E_+^{nl}\exp ik_{tz}(d+\delta)=E_+^t\exp ik_{tz}(d+\delta)-\frac{1}{2}\left(\frac{E_{nlx}^s}{\cos\theta_t}+\frac{2\omega H_{nly}^s}{c^2\varepsilon_o k_t}\right)\exp ik_{sz}(d+\delta)$$ 2.25.

$$E_-^{nl}\exp-ik_{tz}(d+\delta)=E_-^t\exp-ik_{tz}(d+\delta)-\frac{1}{2}\left(\frac{E_{nlx}^s}{\cos\theta_t}-\frac{2\omega H_{nly}^s}{c^2\varepsilon_o k_t}\right)\exp ik_{sz}(d+\delta)$$

Since we are considering the nonlinear slab length to be much lower than the wavelength, we can assume $k_{sz}\delta\ll1$ and write the terms $\exp ik_{sz}(d+\delta)\approx(1+ik_{sz}\delta)\exp ik_{sz}d$. By making these substitutions in 2.25 and using 2.24, we can get after some straightforward algebra:

$$E_+^i \exp ik_{iz}d = \frac{1}{2}\left[\left(\frac{\cos\theta_t}{\cos\theta_i} + \frac{k_t}{k_i}\right)E_+^t \exp ik_{tz}d + \left(\frac{\cos\theta_t}{\cos\theta_i} - \frac{k_t}{k_i}\right)E_-^t \exp -ik_{tz}d\right] - \frac{i\delta}{2\cos\theta_i k_i}$$

$$\left(k_s k_i \cos\theta_s - k_t^2 \cos\theta_i\right)E_{nlx}^s \exp ik_{sz}d + \frac{i\delta}{2\cos\theta_i k_i}\left(k_i \cos\theta_t^2 - k_s \cos\theta_s \cos\theta_i\right)\frac{2\omega H_{nly}^s}{c^2 \varepsilon_o}\exp ik_{sz}d$$

And   2.26.

$$E_-^i \exp -ik_{iz}d = \frac{1}{2}\left[\left(\frac{\cos\theta_t}{\cos\theta_i} - \frac{k_t}{k_i}\right)E_+^t \exp ik_{tz}d + \left(\frac{\cos\theta_t}{\cos\theta_i} + \frac{k_t}{k_i}\right)E_-^t \exp -ik_{tz}d\right] - \frac{i\delta}{2\cos\theta_i k_i}$$

$$\left(k_s k_i \cos\theta_s + k_t^2 \cos\theta_i\right)E_{nlx}^s \exp ik_{sz}d + \frac{i\delta}{2\cos\theta_i k_i}\left(k_i \cos\theta_t^2 + k_s \cos\theta_s \cos\theta_i\right)\frac{2\omega H_{nly}^s}{c^2 \varepsilon_o}\exp ik_{sz}d$$

Now, in order to get further we need to find the expressions for the fields E_{nlx}^s and H_{nly}^s

The particular solution to the wave equation can be written[Blo62]:

$$\mathbf{E}_{nl}^s = -\frac{P_{NL}(2\omega)^2}{c^2\varepsilon_o\left(k_t^2 - k_s^2\right)}\left(\hat{\mathbf{p}} - \frac{\mathbf{k}_s(\mathbf{k}_s \cdot \hat{\mathbf{p}})}{k_t^2}\right)$$ 2.27.

where $\mathbf{P}_{NL} = P_{NL}\hat{\mathbf{p}}$ is the nonlinear polarization vector at the frequency 2ω in the nonlinear slab obtained by contracting the nonlinear susceptibility tensor $\chi^{(2)}$ with the square of the forward propagating fundamental field at the nonlinear slab $P_{NLi} = \chi_{ijk}^{(2)} : E_j(\omega)E_k(\omega)$. From Maxwell equations and eq. 2.27, the expression for the magnetic induction vector can be obtained:

$$\mathbf{H}_{nl}^s = -\frac{P_{NL}(2\omega)}{\left(k_t^2 - k_s^2\right)}(\mathbf{k}_s \times \hat{\mathbf{p}})$$ 2.28.

Inserting the value for the wavevector $\mathbf{k}_s = k_s\left(\sin\theta_s\hat{\mathbf{i}} + \cos\theta_s\hat{\mathbf{k}}\right)$, into eqs. 2.27 and 2.28 we obtain the expressions for the fields:

$$E_{nlx}^s = -\frac{1}{\varepsilon_o\left(n_t^2 - n_s^2\right)}\left[P_{NLx}\left(1 - \frac{n_s^2}{n_t^2}\sin^2\theta_s\right) - P_{NLz}\frac{n_s^2}{n_t^2}\sin\theta_s\cos\theta_s\right]$$

and

$$H_{nly}^{s} = -\frac{cn_{s}}{n_{t}^{2} - n_{s}^{2}}\left[P_{NLx}\cos\theta_{s} - P_{NLz}\sin\theta_{s}\right]$$

These fields may be substituted in Eqs. 2.26 to give, after some straightforward algebra and using 2.22 :

$$E_{+}^{i}\exp ik_{iz}d = \frac{1}{2}\left[\left(\frac{\cos\theta_{t}}{\cos\theta_{i}} + \frac{k_{t}}{k_{i}}\right)E_{+}^{t}\exp ik_{tz}d + \left(\frac{\cos\theta_{t}}{\cos\theta_{i}} - \frac{k_{t}}{k_{i}}\right)E_{-}^{t}\exp - ik_{tz}d\right] +$$

$$+\frac{i2\omega}{2\varepsilon_{o}c}\left(\frac{-\delta P_{NLx}}{n_{i}} + \frac{\delta P_{NLz}n_{s}\sin\theta_{s}}{n_{t}^{2}\cos\theta_{i}}\right)\exp ik_{sz}d$$

2.29.

$$E_{-}^{i}\exp - ik_{iz}d = \frac{1}{2}\left[\left(\frac{\cos\theta_{t}}{\cos\theta_{i}} - \frac{k_{t}}{k_{i}}\right)E_{+}^{t}\exp ik_{tz}d + \left(\frac{\cos\theta_{t}}{\cos\theta_{i}} + \frac{k_{t}}{k_{i}}\right)E_{-}^{t}\exp - ik_{tz}d\right] +$$

$$+\frac{i2\omega}{2\varepsilon_{o}c}\left(\frac{\delta P_{NLx}}{n_{i}} + \frac{\delta P_{NLz}n_{s}\sin\theta_{s}}{n_{t}^{2}\cos\theta_{i}}\right)\exp ik_{sz}d$$

We can write this result in matrix form:

$$\begin{pmatrix} E_{+}^{i} \\ E_{-}^{i} \end{pmatrix} = \begin{pmatrix} A_{S} & B_{S} \\ C_{S} & D_{S} \end{pmatrix}\begin{pmatrix} E_{+}^{t} \\ E_{-}^{t} \end{pmatrix} + \begin{pmatrix} E_{nlS}^{+} \\ E_{nlS}^{-} \end{pmatrix}$$

2.30.

with

$$A_{S} = D_{S}^{*} = \frac{1}{2}\left(\frac{n_{i}k_{tz}}{n_{t}k_{iz}} + \frac{n_{t}}{n_{i}}\right)\exp i(k_{tz} - k_{iz})d$$

$$B_{S} = C_{S}^{*} = \frac{1}{2}\left(\frac{n_{i}k_{tz}}{n_{t}k_{iz}} - \frac{n_{t}}{n_{i}}\right)\exp - i(k_{tz} + k_{iz})d$$

$$E_{nlS}^{\pm} = \frac{i2\omega}{2\varepsilon_{o}c}\left(\mp\frac{\delta P_{NLx}}{n_{i}} + \frac{\delta P_{NLz}n_{s}\sin\theta_{s}}{n_{t}^{2}\cos\theta_{i}}\right)\exp i(k_{sz} \mp k_{iz})d$$

These equations are the main results of this section, giving the relation between the fields at both sides of the nonlinear slab. The generation of SH radiation by the structure is given by the last term and is seen to scale proportional to the layer thickness. This result is expected since we are considering the field amplitudes as constant at the nonlinear slab. We can obtain now the SH field generated from the nonlinear thin slab by setting the boundary conditions. Let's consider that we don't have any field at the second harmonic frequency incident at the slab. In this case we have $E_{+}^{i} = 0$ and $E_{-}^{t} = 0$ and the reflected and transmitted SH coefficients are given by:

$$r_{SH} = -\frac{C_S E_{nlS}^{+}}{A_S} + E_{nlS}^{-} \quad \text{and} \quad t_{SH} = -\frac{E_{nlS}^{+}}{A_S} \qquad 2.31.$$

These expressions give the reflected and transmitted SH field by the slab. In order to determine these fields we should calculate first the nonlinear polarization driving terms P_{NLx} and P_{NLz}. Surface molecular layers may be considered in many cases to be rotationally symmetric about an axis normal to the plane of the layer. By symmetry considerations we may see that in this case there are only three nonvanishing tensor elements in the nonlinear susceptibility tensor [Dick85]. The nonlinear terms are obtained by the contraction of the susceptibility tensor $\chi^{(2)}$ with the fundamental field.

$$\begin{pmatrix} P_{NLx} \\ P_{NLy} \\ P_{NLz} \end{pmatrix} = \begin{pmatrix} 0 & 0 & 0 & 0 & \chi_{15} & 0 \\ 0 & 0 & 0 & \chi_{15} & 0 & 0 \\ \chi_{31} & \chi_{31} & \chi_{33} & 0 & 0 & 0 \end{pmatrix} \begin{pmatrix} E_x^\omega E_x^\omega \\ E_y^\omega E_y^\omega \\ E_z^\omega E_z^\omega \\ 2E_y^\omega E_z^\omega \\ 2E_x^\omega E_z^\omega \\ 2E_x^\omega E_y^\omega \end{pmatrix} \qquad 2.32.$$

where the field at the fundamental frequency is supposed to be, as stated previously, the forward propagating field at the slab. With this form of the susceptibility tensor matrix it can be immediately seen that when the incident polarization field is incident with TM or TE polarization, the resulting generated SH field will be always TM polarized since for both cases the component P_{NLy} vanishes. In the more general case in which the incident field its a superposition of both polarizations will appear SH radiation in the TE polarization direction. These result is well known in surface SHG
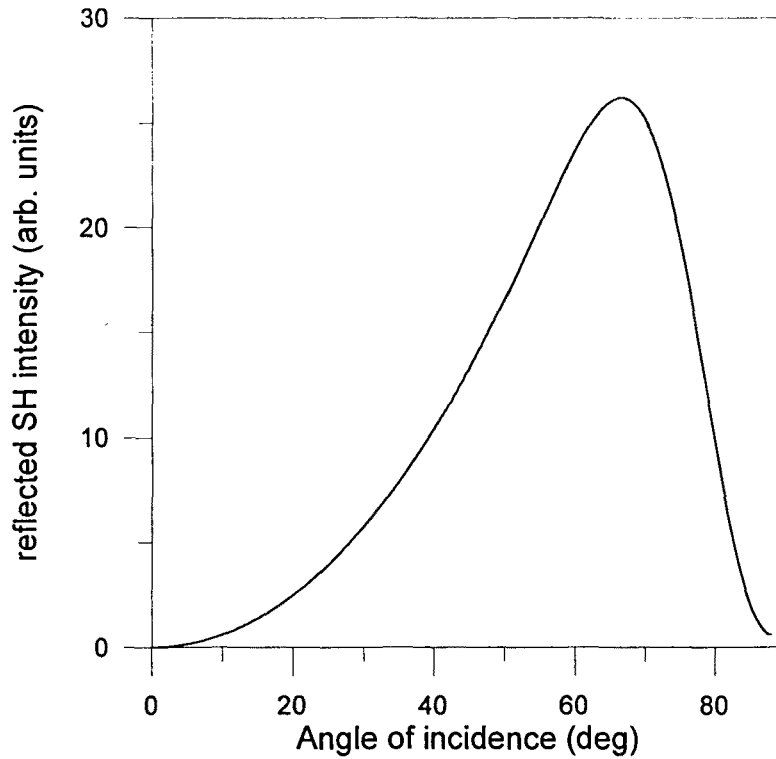
Figure 2.12 Reflected SH from a monolayer adsorbed on an homogeneous substrate.

and can be stated as a 'selection rule' for the SHG process. For our particular case, in which TM polarization is considered, the particular expressions to be considered for the nonlinear polarization terms is written explicitly as:

$$P_{NLx} = 2\chi_{15}E_x^\omega E_z^\omega$$
$$P_{NLz} = \chi_{31}E_x^\omega E_x^\omega + \chi_{33}E_z^\omega E_z^\omega$$

2.33.

Since the monolayer thickness is not known, we will consider its effect included in the nonlinear polarization by considering the actual nonlinear polarization times the layer thickness as an effective surface nonlinear polarization. This parameter will give us a corresponding scale of the interaction strength of the nonlinear process.

By substituting the expressions given above into Equation 2.29, the reflected and transmitted radiation by the nonlinear slab can be calculated. Figure 2.12 shows a typical reflectance curve at the SH frequency for a nonlinear slab. As can be seen the figure shows the typical bell-shaped form characterizing the surface SHG process.

Measurements of such curves have been proven to be useful in determining the elements of the second order susceptibility tensor, characterization of molecular adsorbates at surfaces and others [Shen94].

4.2 Second harmonic generation in periodic structures

We want to consider now the observable effects on the SHG process, when the nonlinear slab is placed at the defect located within a periodic structure. We will assume our structure to be a QWBR, that is, a structure in which every layer has equal optical thickness (Appendix B) since these particular structures will be the ones used in the experimental configuration. Nevertheless, the method outlined in this section may be immediately used to characterize other kind of structures in a straightforward manner.

Let's assume we have a $g(HL)^N Ha$ structure (as defined in section 2 of the present chapter), and suppose we change the optical length of the central layer in order to introduce a defect at the central period of the structure. Our main purpose is to study how the presence of the cavity may influence the emission of radiation by the nonlinear oscillating dipoles at the monolayer. The periodic structure will be supposed to have a band gap at the second harmonic frequency but not for the fundamental. Since the fundamental wave will be highly transmitted through the structure, it will be able to reach the monolayer placed inside the cavity and force the dipoles of the nonlinear layer to oscillate, generating a SH wave as studied in section 4.1. The radiated SH light by the monolayer will be reflected at each layer of the periodic structure (since its frequency lies within the band gap of the structure), reacting on the oscillating dipoles. The coherent superposition of the multiply scattered waves within the structure should have observable effects on the SH radiated.

The calculation of the SH radiated by the nonlinear slab at the defect will be based on a transfer matrix method in the same way as explained in section 2. The structure to be considered here has N periods before the defect and N' periods after the defect (in our contracted notation is represented as $gH(LH)^N D(HL)^{N'} Ha$, where D denotes the defect layer). The expression for the fields, which will be considered to be TM polarized as

usual is the following, where the election of the phase factors in each case has been selected for later convenience:

Field incident at the structure:

$$\mathbf{E}_i^{2\omega}(z,t) = \frac{1}{2}\left[\hat{\mathbf{e}}_+^i E_+^i \exp ik_{iz}z + \hat{\mathbf{e}}_-^i E_-^i \exp-ik_{iz}z\right]\exp\left(ik_{ix}x - i2\omega t\right) + c.c$$

Field at layer with index n_j in the nth period before the defect:

$$\mathbf{E}_{jn}^{2\omega}(z,t) = \frac{1}{2}\left[\hat{\mathbf{e}}_+^j E_+^j(n)\exp i\left(k_{jz}\left(z-(n-1)\Lambda\right)\right) + \hat{\mathbf{e}}_-^j E_-^j(n)\exp- i\left(k_{jz}\left(z-(n-1)\Lambda\right)\right)\right]\exp\left(ik_x x - i2\omega t\right)$$
$$+ c.c$$

Field at the defect:

$$\mathbf{E}_d^{2\omega}(z,t) = \frac{1}{2}\left[\hat{\mathbf{e}}_+^d E_+^{di} \exp ik_{dz}(z-(N-1)\Lambda) + \hat{\mathbf{e}}_-^d E_-^d \exp- ik_{dz}(z-(N-1)\Lambda)\right]\exp\left(ik_x x - i2\omega t\right) + c.c$$

Field at the nonlinear slab

$$\mathbf{E}_{nl}^{2\omega}(z,t) = \frac{1}{2}\left\{\left[\hat{\mathbf{e}}_+^{nl} E_+^{nli} \exp ik_{nliz}(z-(N-1)\Lambda) + \hat{\mathbf{e}}_-^{nli} E_-^{nli} \exp- ik_{nliz}(z-(N-1)\Lambda)\right]\exp\left(ik_{nlx}x - i2\omega t\right)\right\}+$$
$$+ \frac{1}{2}\mathbf{E}_+^s \exp i\left(k_{sz}(z-(N-1)\Lambda) + k_{sx}x - 2\omega t\right) + c.c$$

Field at layer with index n_j in the mth period behind the nonlinear slab:

$$\mathbf{E}_{jm}^{2\omega}(z,t) = \frac{1}{2}\left[\hat{\mathbf{e}}_+^j E_+^j(m)\exp i\left(k_{jz}\left(z-\phi\right)\right) + \hat{\mathbf{e}}_-^j E_-^j(m)\exp- i\left(k_{jz}\left(z-\phi\right)\right)\right]\exp\left(ik_x x - i2\omega t\right) + c.c$$

Field transmitted by the structure:

$$\mathbf{E}_{ti}^{2\omega}(z,t) = \frac{1}{2}\left[\hat{\mathbf{e}}_+^t E_+^{ti} \exp ik_{tz}(z-\phi') + \hat{\mathbf{e}}_-^t E_-^t \exp- ik_{tz}(z-\phi')\right]\exp\left(ik_x x - i2\omega t\right) + c.c$$

The length and refractive index of the defect are l_d and n_d respectively, the parameters ϕ are defined as $\phi = (N-1)\Lambda + l_h + l_d + (m-1)\Lambda$ and $\phi' = (N-1)\Lambda + l_h + l_d + (N'-1)\Lambda$, and the other factors have been already defined.

These fields will be related through the boundary conditions at each interface. As in preceding sections, we write these relations in matrix form:

$$\begin{pmatrix} E'_+ \\ E'_- \end{pmatrix} = \begin{pmatrix} A_F & B_F \\ C_F & D_F \end{pmatrix} \begin{pmatrix} E^i_+ \\ E^i_- \end{pmatrix} - \begin{pmatrix} A_{nl} & B_{nl} \\ C_{nl} & D_{nl} \end{pmatrix} \begin{pmatrix} E^+_{nlS} \\ E^-_{nlS} \end{pmatrix} \qquad \text{2.34.}$$

where the resulting matrices are obtained by multiplication of the following ones:

$$\begin{pmatrix} A_F & B_F \\ D_F & C_F \end{pmatrix} = [MA][T']^N [F][U][T]^N [AM] \quad \text{and} \quad \begin{pmatrix} A_{nl} & B_{nl} \\ D_{nl} & C_{nl} \end{pmatrix} = [MA][T']^N [F]$$

The particular expression for each of the matrices is given in Appendix C. Once the matrix coefficients are known we can obtain the reflection and transmission coefficients for the structure. Since we suppose that the only field incident on the structure is just the fundamental field at frequency ω, the boundary conditions for the whole structure are given by $E^i_+ = E^i_- = 0$. Applying these conditions to eq. 2.32 we find

$$r_{SH} = \frac{C_{nl}E^+_{nlS} + D_{nl}E^-_{nlS}}{D_F} \quad \text{and} \quad t_{SH} = \frac{B_F\left(C_{nl}E^+_{nlS} + D_{nl}E^-_{nlS}\right) - \left(A_{nl}E^+_{nlS} + B_{nl}E^-_{nlS}\right)}{D_F} \qquad \text{2.35.}$$

The reflectance and transmittance of the structure at the SH frequency are given by:

$$R_{SH} = |r_{SH}|^2 \quad \text{and} \quad T_{SH} = |t_{SH}|^2 \qquad \text{2.36.}$$

Figure 2.13 (a) shows the reflected SH intensity of a truncated periodic structure with the nonlinear layer adsorbed at the surface between the defect and the first layer at the right. As can be seen from the figure, sharp resonances of reflected SH intensity appear at certain angles separated by regions for which the SH intensity radiated is very low. If we compare this result with that of Figure 2.12 it is immediately observed that there exists a clear influence of the periodic structure on the radiated pattern. While in the case of no structure present, the SH intensity radiated presents the bell shaped form, characteristic of surface SHG, the SH radiated when the structure is present shows that now the SH generation is enhanced at those angles corresponding to local modes of the structure, as can be seen from Figure 2.13 (b) in which the transmittance for incident radiation at the SH frequency is plotted. In contrast, it is seen that SHG is strongly inhibited at other angles within the gap. This fact may be explained in two

complementary ways, either by the alteration of the density of modes introduced by the structure, or by the resulting interference effects arising from the coherent superposition of the multiply reflected waves within the structure. Both effects, enhancement and inhibition, are due to the environmental effect imposed by the presence of the structure.

In our case this fact is demonstrated in a very clear way. The radiation at the fundamental frequency forces the dipoles to oscillate at all incident angles and thus, with no structure present SH is radiated at all angles (Figure 2.12). The presence of the periodic structure, however, makes the emitted field at the second-harmonic frequency to react back on the dipoles upon reflection on the structure. The coherent superposition of the SH radiation gives rise to the observed effects. The enhancement of the SH field at the localized modes within the gap corresponds to the excitation of the SH oscillation in a local mode of the structure. In contrast, the nonlinear interaction in modes lying within the forbidden zone other than the defect mode is inhibited by a destructive interference among the multiply scattered waves at each layer of the structure and the dipoles oscillating at the SH frequency. More details about the interpretation of SHG enhancement and inhibition in such 1D photonic crystals will be given in next chapter.

Near the band edge the bending of the electromagnetic wave dispersion curve (Figure 2.5) slightly above and below the forbidden zone indicates that the group velocity approaches zero, giving raise to an increased path length and a Van Hove-type singularity in the photon density of states for the 1-dimensional lattice. This effect, arising as a consequence of the periodicity in the material and independent of the size of the defect, may be observed in Figure 2.13 (a) for angles corresponding to the high angular band edge.

If we look now to the reflected SH intensity for the same periodic structure of Figure 2.13 but with a longer defect length, as shown in Figure 2.14, we found a higher number of resonances within the gap. By inspection of the corresponding transmittance of the structure for incident radiation at the SH frequency, we can explain the resonances appearing in Figure 2.14 (a) in the same way as it was done in Figure 2.13. Notice that the resonance close to 60 degrees, at the band edge stands at the same position, since as previously commented it is independent of the size of the defect.
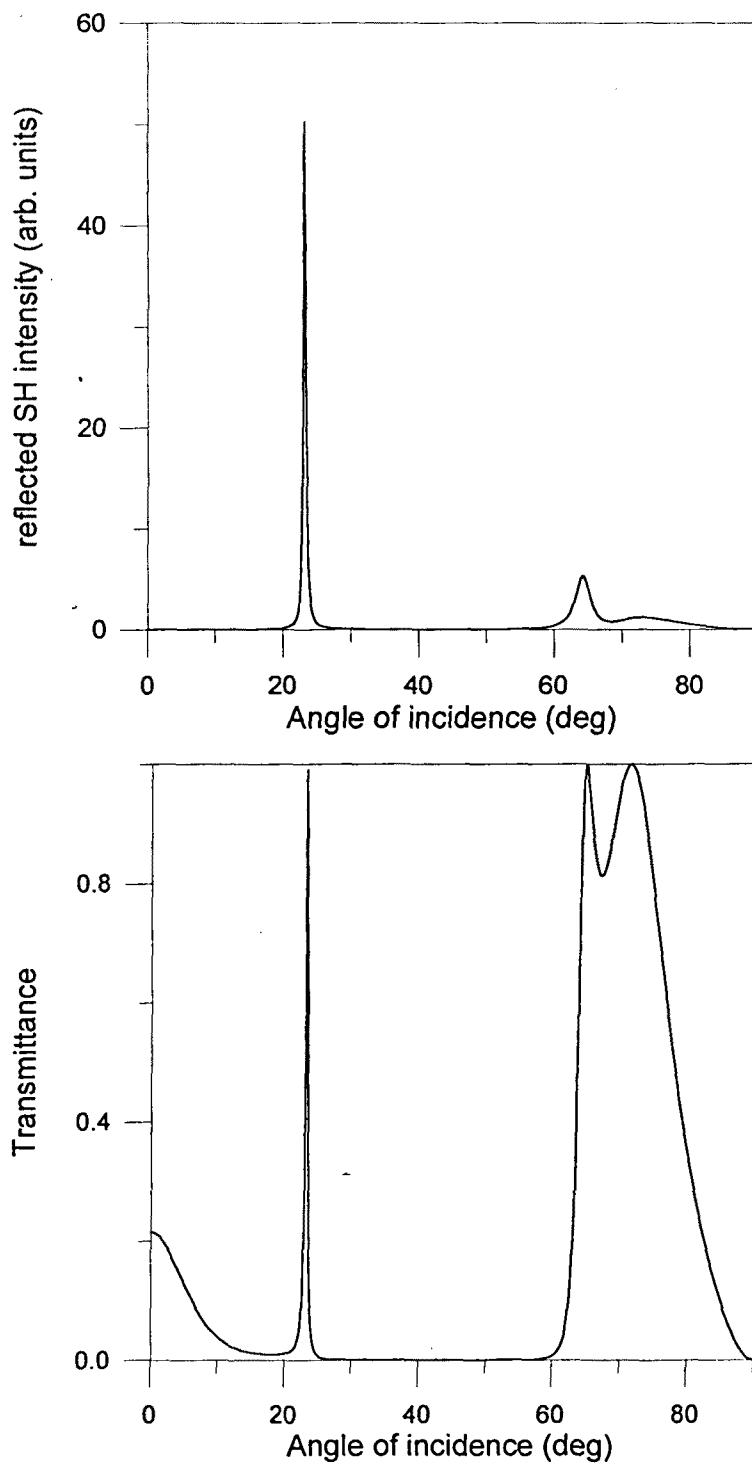
Figure 2.13 (a) Reflected SH intensity and (b) transmittance of the structure for incident radiation at 532 nm as a function of the angle of incidence.
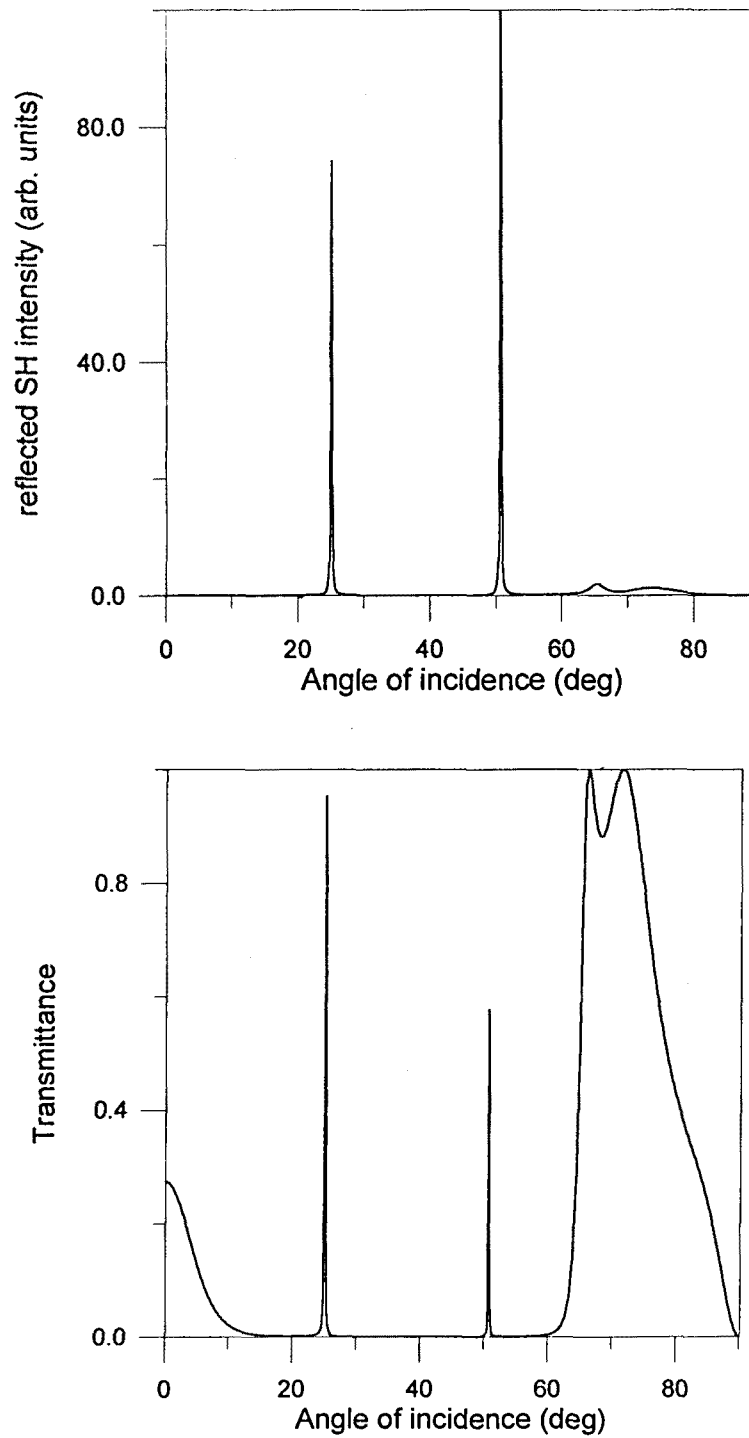
Figure 2.14 Same as in Figure 2.13 with a different defect thickness.

5. Experimental measurement of SH enhancement and inhibition in a truncated 1-D photonic crystal

In this section we present the experimental study of the SH radiation of a slab of nonlinear material embedded in a truncated multilayer stack of dielectric material. As shown in the previous section, the environmental effect of the structure should lead to the appearance of sharp resonances in the reflectance and transmittance spectra. In the first part of the section we will give a characterization of the truncated periodic structure used. The experimental setup characteristics and the method used to obtain the nonlinear monolayer slab at the defect will be outlined in the second part of the section and the experimental results will be given in the last part of the section. General aspects of the measurements have already been pointed out in the introduction of this chapter.

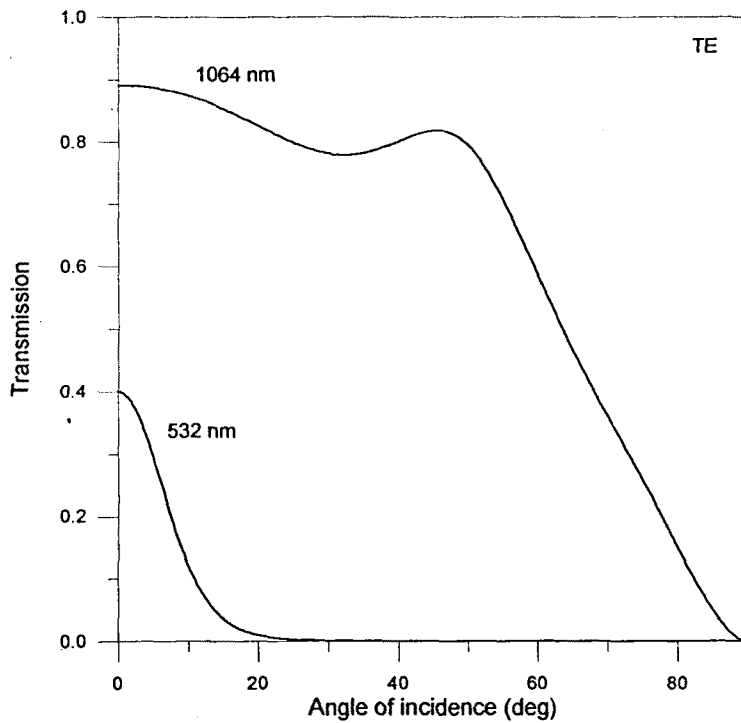## 5.1 Characterization of the truncated periodic structure

The truncated periodic structure necessary to perform the experiments is formed by two identical multilayer dielectric mirrors separated by a small air gap acting as the defect. The first step in the characterization of the structure should be the measurement of the optical and geometrical parameters of each mirror. Several measurements were performed to determine all the parameters needed for a complete characterization of the commercial high-quality dielectric mirrors used as the multilayers. The determination of the refractive indices and lengths of the layers was obtained through a method developed by us based on a measurement of the reflectance of the structure as a function of the incident wavelength for normal incidence and as a function of the incident angle for a fixed wavelength. The details of this method are given in Appendix B.

An experiment to observe the environmental effects on the SH generation may be performed in the frequency domain with a tunable laser source, but since in our case the laser is a Nd:YAG laser with fixed frequency at 1064 nm we have carried out the measurements in the angular domain. (In view of this fact the results presented in previous sections were obtained in the angular domain). In order to avoid interference with the SH field generated at the substrate, a reflection geometry for the experiment will be required. This fact makes preferable to have structures where the reflection at normal incidence is avoided. Due to this fact the chosen dielectric structures for the

experiment are dielectric mirrors reflecting the light at the SH frequency, that is at 532
nm, at 45 degrees and not at normal incidence. The parameters for these mirrors,
obtained experimentally as explained in Appendix B, are the following. Each dielectric
stack is made of two identical QWBR made of 27 layers $(g(HL)^{13}Ha)$ with high index
$n_h=1.97$ and low index $n_f=1.47$ and corresponding thicknesses $l_h=74.6$ nm and $l_f=100.4$
nm deposited upon a glass substrate. Figures 2.15 and 2.16 show the transmittance
curves for such structure as a function of the angle of incidence for both polarizations
and for incident radiation at 532 nm and at 1064 nm. As can be seen, a gap region of
almost zero transmittance (high reflection) appears for radiation at 532 nm, while
radiation at the fundamental frequency is highly transmitted through the structure since
this frequency is not within the band gaps of the structure. The gap for the TE
polarization is much wider than the gap for TM polarization. Although this fact may be
of potential interest for some applications [Winn98], in our present case we will be
interested in observing the SH radiation at the TM polarization (see the comments on
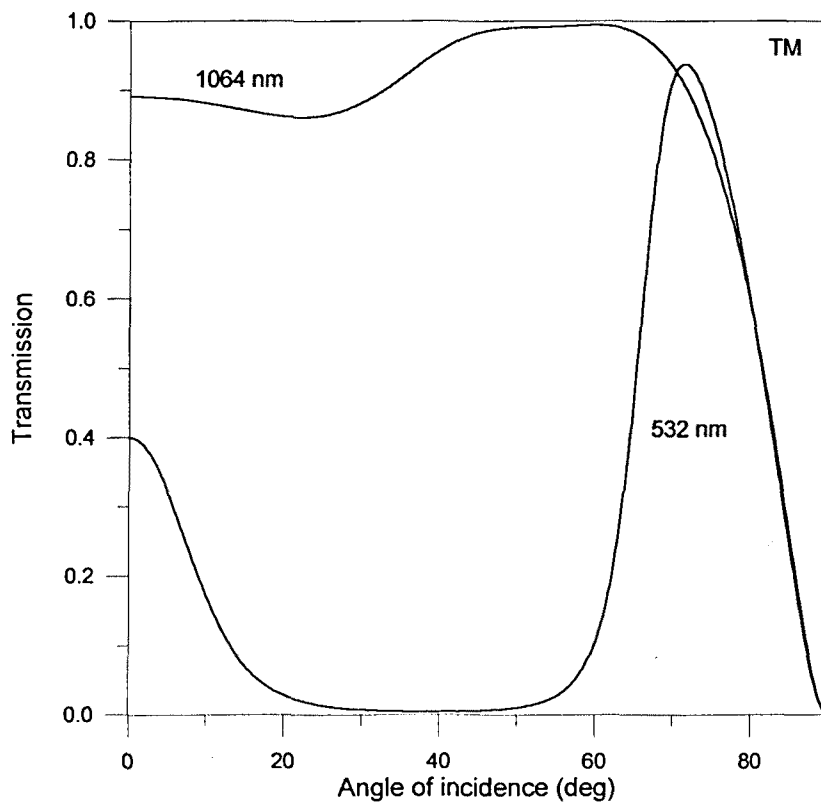
Figure 2.15 Transmittance of the multilayer structure for incident radiation at 532 nm
and 1064 nm and with TM polarization.

Figure 2.16 Transmittance of the multilayer structure for incident radiation at

532 nm and 1064 nm and with TE polarization.

section 4.1) for which the effects due to the band edge should be present. The TM polarization is selected for the fundamental field since its transmission values are higher.

Once the dielectric mirrors to be used have been characterized we can assemble them
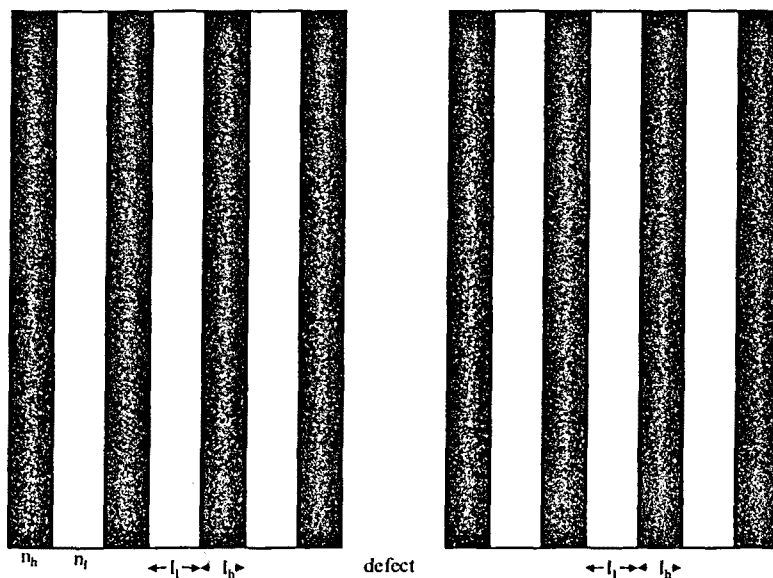
Figure 2.17 Two 1-dimensional dielectric mirrors separated by an air-gap or defect

together, leaving a small air gap between them, in order to obtain the truncated periodic structure we will use in the experiments. Figure 2.17 shows a schematic representation of the structure.

The reflectance and transmittance of such structure, calculated by means of the formalism given in section 3 of this chapter, shows the appearance of defect modes. The position and number of defect modes within the gap is related to the thickness of the defect. Figures 2.18 and 2.19 show two transmittance curves obtained for the structure
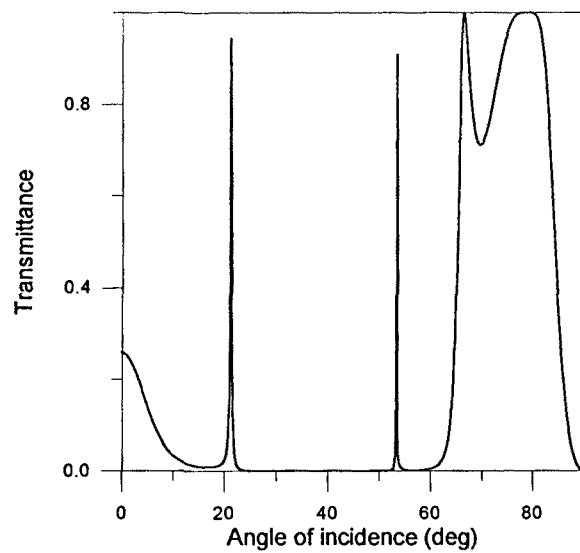
Figure 2.18 Transmittance of the periodic structure with a defect thickness of 500 nm for incident radiation at 532 nm.
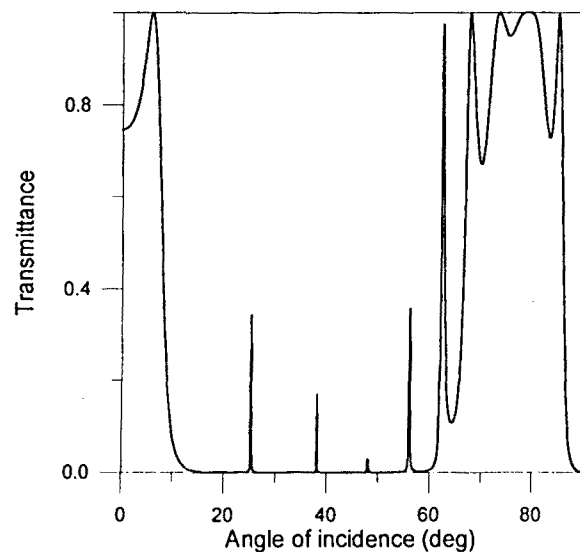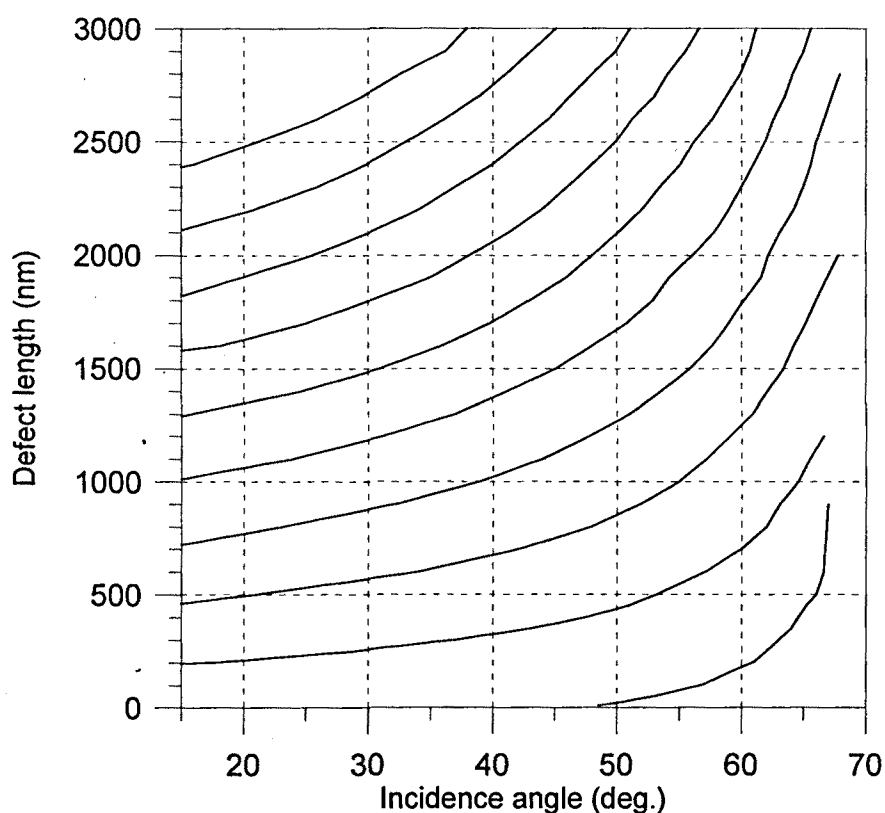
Figure 2.19 Transmittance of the periodic structure with a defect thickness of 2000 nm for incident radiation at 532 nm.

Figure 2.20 Angular position of the defect modes as a function of the defect length of the structure of Figure 2.16

considered with defect thicknesses of 500 nm and 2000 nm.

The angular position of the defects of the 1-D photonic crystal of Figures 2.18-19 as a function of the defect length is shown in Figure 2.20. It can be seen from this figure the appearance of acceptor modes, from the high angular band edge, when the length of the defect is lower than 150 nm and of donor modes, appearing from the low angular band edge of the structure, for higher values of the defect length. Measuring the angular position of the SH resonances, the defect length can be obtained from these curves.

5.2 Experimental measurement of SHG within the 1D photonic crystal

Once we have characterized the periodic structures which will be used in the experiment, next we should include the nonlinear slab within the structure. This is done by adsorbing the monolayer at the surface of one of the dielectric mirrors using the dipping technique [Gar82]. The nonlinear slab adsorbed at the surface consists of molecules of Malaquite Green (MG) oxalate, which have been reported to be efficient

in surface SHG at the desired wavelength [Mee90]. In order to obtain the monolayer, a 5×10^{-4} M solution of MG in 1-propanol was prepared. The deposition is obtained by inserting the mirror in the dye solution and then slowly withdrawn it (typical velocity is of the order of 5mm/min). As the surface slides off the solution, the dye is adsorbed. These molecules are shown to present a $C_{\infty vm}$ symmetry, rotationally symmetric about the z-axis.

Measurements were performed by using the experimental setup shown in Figure 2.21. The fundamental field incident on the dye molecules is provided by a 35 ps Nd:YAG laser, with active-passive mode-locking operating at a repetition rate of 10 Hz. The average energy of each pulse is about 5 mJ and its coherence length is approximately 1 centimeter. The incident beam is focused to a beam diameter of 2 mm onto the truncated periodic structure which is mounted upon a rotating stage with an angular precision of 0.017 deg. In order to achieve high stability for the structure both dielectric mirrors are mounted on a micrometric translation stage. By moving one of the mirrors keeping the other fixed, the separation between them (which is the defect length) may be varied. From Figure 2.20 we see that if we want to have few defects within the gap, the defect length should be lower than 1 micron, which makes the obtention of the desired structure a difficult task. In order to align the mirrors as parallel as possible, a He-Ne laser was used in order to observe the interference fringes formed. The interference pattern formed by the structure is very sensitive to a misalignment of one of the mirrors with respect to the other.

The SH light reflected from the structure is measured with an R212 Hamamatsu photomultiplier preceded by heat absorbing and interference filters in order to eliminate the fundamental signal. The photomultiplier is connected to an oscilloscope Tektronix DSA602A (Figure 2.21). Each measurement was performed by averaging over 100 pulses in order to overcome possible fluctuations in the output laser energy, which was monitored as a reference signal measured with the aid of a photodiode (PD). The average fluctuation of each experimental point considered is of the order of 10 %.

In order to avoid saturation at the photomultiplier, neutral density filters are used at the fundamental path before being incident on the structure. The desired polarization of the beam at the fundamental frequency, is controlled by using a Glann-laser polarizer and a
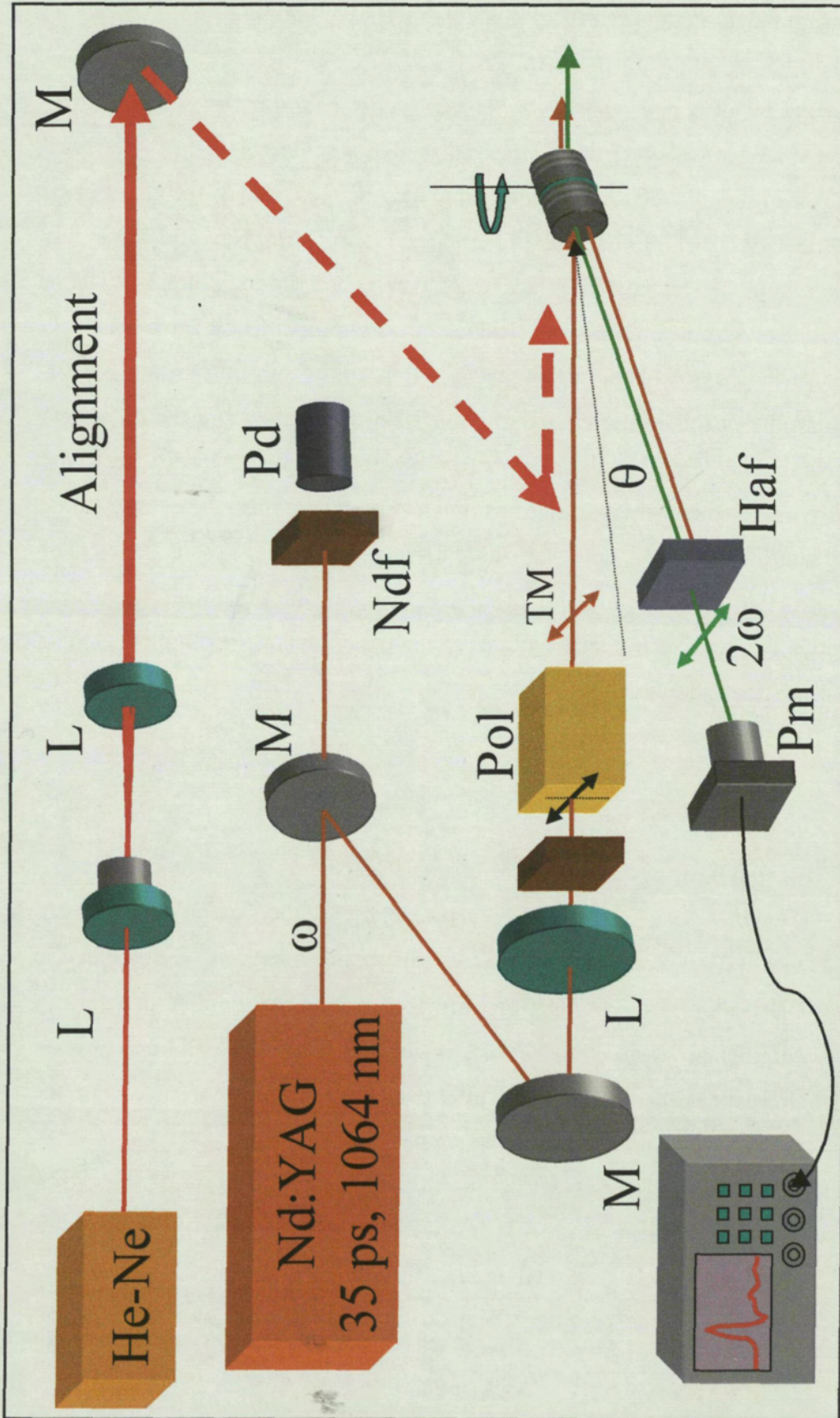
Figure 2.21 Experimental setup for the measurement of the SHG from the truncated periodic structure. The different elements are: M-mirror, L-converging lens, Pol-Glann-laser polarizer, Ndf- neutral density filters, Pm-photomultiplier, Pd-photodiode. The polarization state of the beams is TM. The alignment setup(dashed) is used to adjust the cavity and is not present in the measurements.

half-wavelength plate. For the case of TM polarization, the half-wavelength plate is not necessary, since the laser output is TM polarized. Even in this case the polarizer is used in order to ensure the desired polarization incident at the structure.

The experimental results obtained for the SH light reflected from the slab when the mirrors are separated a distance much longer than the coherence length of the laser (1cm) are shown in Figure 2.22. As it can be seen, the reflected SH has the bell shaped form characteristic of a surface nonlinear process (see Figure 2.12). Nevertheless in this case a local minimum appears at 68 degrees which is not observed in Figure 2.12 where the monolayer was assumed to be adsorbed on an homogeneous substrate. This is related to the periodicity of the structure that is acting as the substrate in the present case, which introduces some interference effects. When the curve from the numerical calculation (continuous line), based on the matrix transfer formalism, is adjusted to the experimental values, the only variable parameters to be adjusted are the three nonvanishing coefficients of the nonlinear susceptibility tensor, since the parameters of the periodic structure were obtained previously. By varying these parameters, we can obtain the ratios between such coefficients from the experimental measurements. The obtained ratios are the following

$$\frac{\chi_{33}}{\chi_{15}} = -30 \quad \text{and} \quad \frac{\chi_{33}}{\chi_{31}} = 2 \qquad\qquad 2.37.$$

With our experimental setup an absolute determination of the coefficients was not possible, and since the unknown parameter δ (monolayer thickness) will we included in the effective polarization term (as discussed previously) an absolute determination of the outgoing energy is not given. Nevertheless, since the same values will be used in all the results, the relative variations will be totally comparable in order to determine the effect of the structure on the generated SH radiation.

Additional measurements were made of the SH radiation emitted by the periodic structure when no layer was adsorbed at the surface, in order to detect possible influence of the mirror in the resulting SH intensity. The SH radiation in this case, arising from the quadrupolar contributions at the surfaces or at the substrate, is also
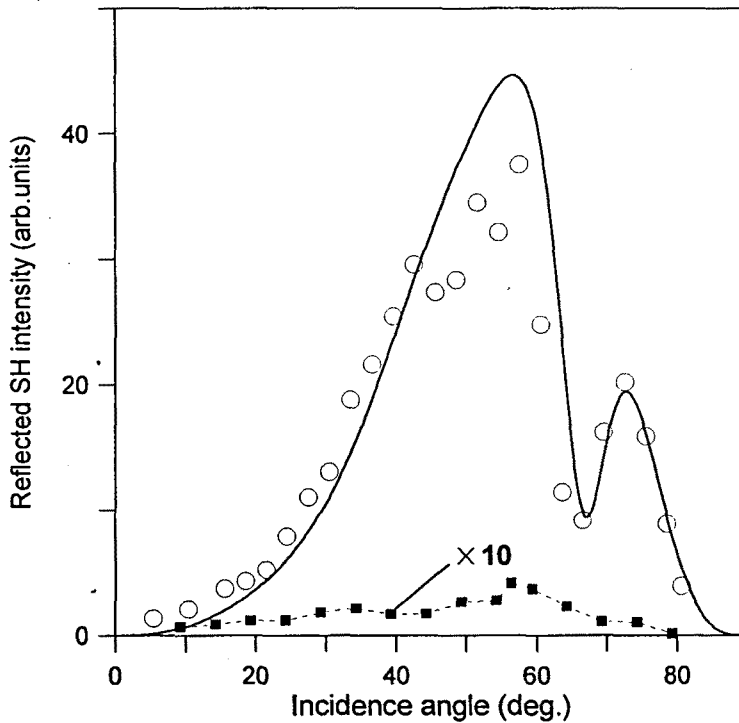
Figure 2.22 Reflected SH intensity when the separation among the multilayer stacks is larger than the coherence length of the laser pulse. The open circles indicate the experimental data when the nonlinear layer is adsorbed. The square data are obtained when no layer is adsorbed (the scale for this case has been multiplied by a factor of 10). The continuous line shows the result of the theoretical model.

represented in Fig. 2.22 as squares and is seen to be negligible in comparison to the dipolar contribution when the nonlinear layer is adsorbed.

In order to check the correctness of the values obtained for the nonlinear coefficient ratios for the nonlinear layer we performed additional measurements with the same monolayer adsorbed at the surface of a different dielectric mirror. In this case we used a dielectric mirror reflecting light at 532 nm at an angle of zero degrees, which was characterized in the same way as the other mirrors (as explained in Appendix B). The SH reflectivity measured for this mirror (open circles) is shown in Figure 2.23 together with the theoretical curve obtained using the mirror parameters and the values of the nonlinear coefficients given by Eq. 2.37. As can be seen, although the nonlinear slab is the same, the reflectivity minima fall at different angles since the periodic structure
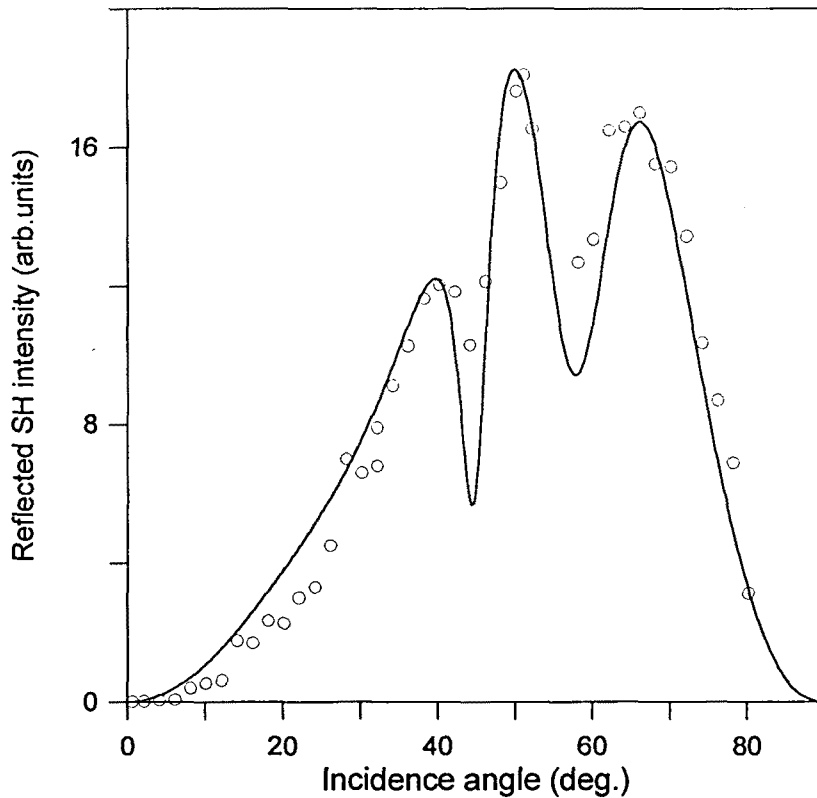
Figure 2.23 Reflected SH intensity for the same situation as in Figure 2.21 when the nonlinear slab is adsorbed on a different periodic structure.

acting as the substrate has been changed. The agreement between the experimental and numerical simulation is also very good in this case.

In a subsequent step we will consider the configuration where the two mirrors are in closer contact in order to obtain the truncated structure. The length of the defect is a parameter that in the experimental setup cannot be accurately controlled (since the defect thickness we seek is below the accuracy given by the micrometer), so the experimental procedure is to align the mirrors, put them into contact (or almost contact) and then measure the reflected SH as a function of the angle of incidence. The obtained defect thickness for each case may be determined, since we have seen that the sharp resonances in reflected SH appear at those angles for which local modes exist (Figure 2.13). Figure 2.20 gives us the defect length from the position of the reflected SH resonances. Figure 2.24 shows the reflected SH intensity measured when the slab is within the truncated periodic structure. As may be seen, a sharp resonance is obtained at
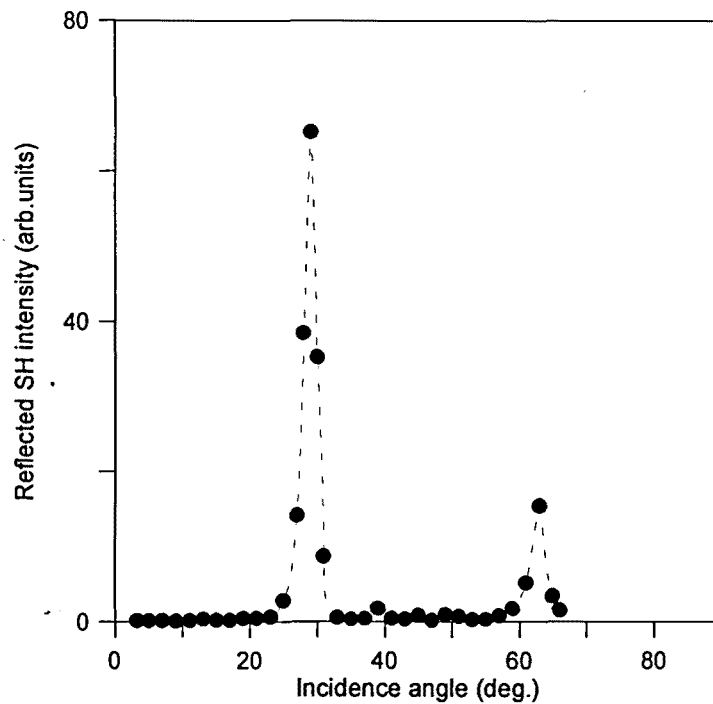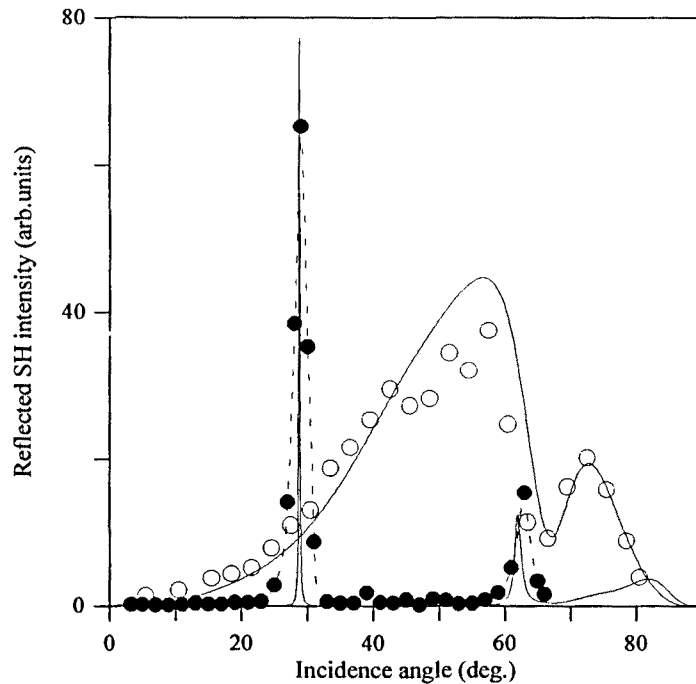
Figure 2.24 Reflected SH intensity as a function of the angle of incidence, from the multilayer stack described in the text. The angle is given relative to the normal of the multilayer stacks. The filled circles indicate the experimental data while the dashed curve is a guide for the eye.

28.7 degrees and a smaller one is seen at 63 degrees, while no SH radiation appears at other angles within the gap. The defect length we have in this case is 250 nm, as can be obtained from Figure 2.20.

In order to correlate the results obtained in both cases, when the nonlinear slab is within the defect and when one of the mirrors is separated a distance much higher than the coherence length, measurements of both curves were taken in the same experimental conditions, since an absolute value of the emitted radiation was not measured. The mirror with no layer, was not simply taken away in order to maintain the amount of fundamental radiation upon the monolayer in both cases as equal as possible. The effect introduced by the structure may be seen in Figure 2.25 in which both results are shown together. A comparison of both curves indicates that at an angle of 28.7 deg., corresponding to a defect mode within the forbidden band, the generated SH intensity is six times larger when the nonlinear interaction occurs in a mode of the microresonator

Figure 2.25 Reflected SH intensity as a function of the angle of incidence measured for the truncated periodic structure (full circles) and when the separation among the multilayer stacks is larger than the coherence length of the laser pulse (open circles). The continuous ciurves corresponds to the theonumerical prediction of the theoretical analysis.The scales for the experimental data are the same. The scale of the theoretical curve for the first case is reduced by a factor of 10 relative to the scale of the other theoretical curve.

formed by the two multilayer stacks. The high energy density of this local mode is responsible for the enhancement of several times of the nonlinear interaction in the vicinity of the defect.

Near the band edge, the bending of the electromagnetic wave dispersion curve slightly above or below the forbidden zone indicates that the group velocity approaches zero, giving rise to an increased effective path length and a Van-Hove-type singularity in the photon density of states for the one-dimensional lattice. The relevance of the effects introduced by this change in group velocity and refractive index at the band edge has been already discussed previously in this chapter. In our experiment, this leads to an enhancement of the SH radiation at the angle of 63 deg. as shown. This enhancement, predicted by Bloembergen and Sievers [Blo70] is a result of the periodicity built into

the material, and its location in the angular spectrum is essentially independent of the size and position of the defect. Our experimental measurement gives additional confirmation to the existence of such effects in these kind of multilayered structures.

The nonlinear interaction in modes lying within the forbidden zone other than the defect mode is inhibited by a destructive interference among the forward-generated wave, the backward-reflected wave, and the dipoles oscillating at the SH frequency. As can be seen in the Figure, SHG is completely suppressed for modes other than the defect mode within the forbidden band. This suppression corresponds to the first experimental observation of the inhibition of the radiation from a classical dipole source [Dow92] (details to this respect will be given in next chapter).

A numerical simulation of the process, obtained through the expressions derived in section 4, and using the parameters for the nonlinear coefficients, defect length (obtained from the experimental measurements) and the geometrical and optical parameters of the periodic structures (obtained with the method outlined in Appendix B), is shown in Figure 2.25 as solid lines. The theoretical curves show that the relative position and relative intensity of both resonances are in close agreement with the experimental measurements. The scale for the theoretical curve in the case of the structure with the defect is reduced by a factor of 10 relative to the scale of the theoretical curve of Figure 2.22. The numerical prediction gives an enhancement of 80 times at the defect mode. This prediction is considerably larger than the enhancement observed experimentally. This discrepancy probably arises from the spreading of the laser beam, diffraction by imperfections in the multilayer stacks and imperfect parallelism of the two stacks.

In order to further confirm that the theoretical values give us a good agreement we should check that the conditions imposed in deriving the expressions in section 4 are valid in the experimental case. As explained in section 4.1 of this chapter, the driving term of the SH field is supposed to be given by the forward propagating component of the fundamental field at the NL slab. For the structure used in the experiment it is seen that the intensity of the forward propagating field is six times larger than the corresponding intensity for the backward propagating component at the angle corresponding to the defect mode. With these values, the expected error in the

theoretical curve made if the backward propagating component at the fundamental field
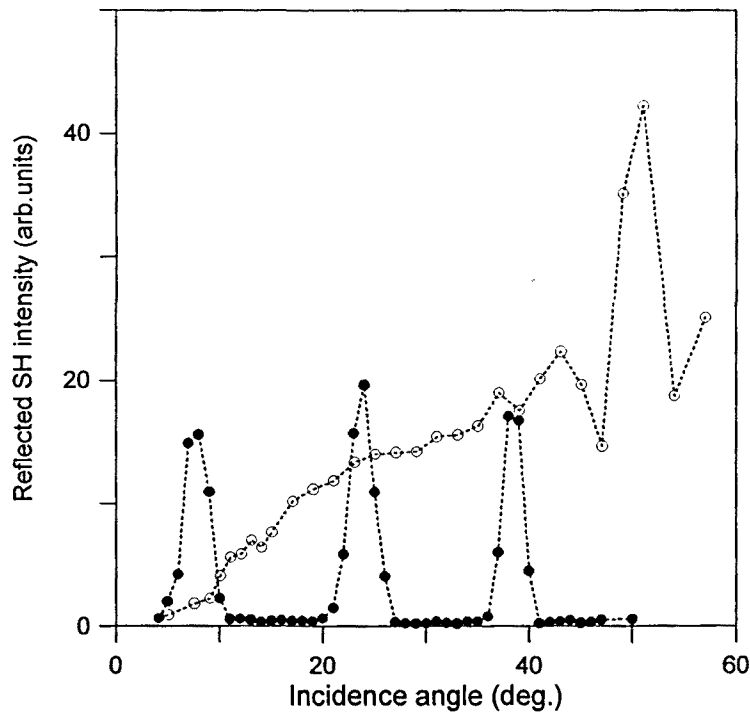
Figure 2.26 Reflected SH intensity measured for the same periodic structure of Figure 2.24 when the defect length is around 1700 nm and the incident fundamental is TE polarized.

is neglected in the SHG process, should be of the order of 15%. A more detailed calculation of the reflected SH intensity from the structure when the contribution of the SH generation by the backward propagating component of the fundamental field at the nonlinear slab is considered may be obtained by means of the same techniques explained in previous sections, These effects should become more important as the index contrast in the given structure is increased.

In order to see how the increasing of the defect length results in the appearance of an increasing number of localized states within the band gap of the structure, we show in Figure 2.26 the experimental results of the reflected SH intensity for the same periodic structure when the defect length is around 1700 nm and the incident fundamental is TE polarized instead of TM polarized as in previous cases. Here again the full circles correspond to the SH reflected when the nonlinear slab is placed within the defect and

the open circles represent the reflected SH intensity when one of the mirrors is placed at a distance much higher than the coherence length.

A detailed analysis of the process of quadratic nonlinear interaction within a 1-dimensional photonic crystal has been described including both theoretical modeling of the problem and experimental evidence of the process.

<center>Chapter 3</center>

Phase dependence of quadratic nonlinear radiation within a 1-d photonic crystal

In the previous chapter, we studied experimentally and theoretically the SHG from a sheet of nonlinear material located within an air gap (or "defect") in a 1-dimensional photonic crystal. The fact that the nonlinear layer had to be adsorbed on one of the two surfaces delimiting the air gap, prevented us from the possibility of locating the NL layer at different positions within the defect. In this chapter, we study theoretically what would occur if the NL layer could be located at different positions within the air gap. We will see that this results in a change in the amplitude and phase of the SH light generated (which accumulates around the defect at the localized state) at the slab. This fact has a very large effect on the resulting interaction between the generated SH light and the dipoles of the NL layer, enhancing or inhibiting their emission depending on the values of amplitude and phase that the SH field takes at the position of the NL layer. Further unexpected features such as emission in one direction and reabsorption in the opposite direction also occur in certain conditions.

The control of the radiative properties of oscillating dipoles has been a subject of interest during the last decades. Since the pioneering experiments performed by Drexhage [Dre70] where the radiation of a molecular dipole placed in front of a metallic or dielectric surface was considered, it has been shown in many cases that the radiation properties of the dipoles may be modified by changing the boundary conditions of the problem. Inhibition of spontaneous emission of dipoles surrounded by a 3D periodic distribution of dielectric material has been observed [Mar90][Yab89]. It is also possible to observe strong alteration of such interaction in more simple 1D systems where radiation is emitted in only one or two directions [Dow92][Sul97][Tru95].

The modification of the free space emission rate of the dipole is governed in all cases by the change in the result of the product between the electromagnetic field and the current

density vector. The SHG process described in the previous chapter constitutes a system in which such effects can be studied. In this chapter we study theoretically the behavior of the amplitude and relative phase of a field radiated at frequency 2ω through a quadratic nonlinear interaction from a thin sheet of coherent dipoles placed in between two identical dielectric multilayer mirrors separated by an air gap (defining a 1-D photonic crystal with a defect), and that is "forced" to oscillate by an incident beam at frequency ω. This interaction, explained in detail in chapter 1, will be considered as a function of the position of the sheet within the air gap, as well as a function of the orientation of the dipoles relative to the axes that define the dielectric structure.

Efficient dipole radiation not only requires a large field mode density in the material structure at the frequency of the dipole source. Enhancement or inhibition phenomena can occur even when the field-mode density is large. In some particular cases of 1-D structures, these enhancement or inhibition phenomena may be directly linked to the field intensity distribution inside the dielectric structure [Lid97][Bur97], in the sense that the dipole emission responds to the local value of the field intensity distribution. However, in general one can only establish a direct relation between this enhancement or inhibition and the energy transfer from the dipole to the field or vice versa, which is governed by the dot product of the field and the current density vectors. Thus the amount of this energy transfer can only be fully determined if both: the amplitude or intensity of the electromagnetic field, and the relative phase between this field and the oscillation of the dipole source are known.

The classical nature of this type of interaction allows for a clear establishment of the phase relation between the dipole oscillation and the phase of the radiated field. We show below that in addition to the previously reported change in the field intensity distribution inside such structure [Dow92][Lid97], there is also a strong modification of the phase difference between the field at ω, that induces a polarization oscillation at frequency 2ω, and the field radiated at such frequency. Inside a microcavity the phase of the radiated field does not lag the oscillation of the dipole source by $\pi/2$ as in free space, but it turns out to be strongly dependent on the position of the dipole sheet within the air gap and the orientation of the polarization vector relative to the axes defined by the microcavity symmetry. The value of this phase difference strongly affects the amount of energy transferred from the dipoles to the field. In particular, we will show

that, for certain dipole sheet positions, the phase of one of the counterpropagating components of the field at 2ω may even advance the phase of the radiation source, indicating that the energy radiated at frequency 2ω can be transferred back to the oscillating dipole, resulting in a strong "inhibition" of the radiation from such classical dipole source. This type of "inhibition" can also be observed from the second harmonic generation of a thin dipole sheet placed in front of a single mirror [Kau98][Ram95]. An interesting feature of these energy transfer processes from the dipole sheet to the field is that it is asymmetric with respect to the forward-backward field propagation directions, so that the energy can be radiated in one direction and then lost by the field coming in the opposite direction.

The results reported in the present chapter are not limited to the nonlinear quadratic interaction considered, and their applicability can be extended to a wider range of cases since the radiation at 2ω of a thin layer of dipoles "forced" by an incident beam at frequency ω, is formally equivalent to the radiation of a sheet of forced classical linear dipoles. It can be useful, in particular, to understand radiation emission from microcavity lasers and optically or electrically injected passive microcavities, filled with organic or semiconductor films, subjects of present large technological and scientific interest.

1. Quadratic second harmonic radiation by oscillating dipoles

We want to study in this section the dependence of the total emission of SH radiation by the structure used in chapter 1, when some parameters are changed such as the position of the nonlinear slab within the defect or the dipole orientation.

The generation of SH radiation from the slab driven by the fundamental field incident on the structure is calculated by means of the formalism introduced in section 4 of chapter 2. The general expression for the electromagnetic radiation from a plane sheet of quadratic nonlinear dipoles is found by solving Eq. 2.20 for the field $E_{2\omega}$. To obtain a complete solution that fully describes the wave transfer mechanism, one should consider the additional equation 2.21 for the field at ω. However, in the approximation of no depletion of the intense field at ω an analytical solution can be obtained from just

Eq. 2.20. as shown in chapter 2. It should be noted that even in this approximation energy may be transferred back from the field at 2ω to the oscillating dipoles. This transfer is only seen as a depletion of one (forward or backward propagating) of the components of the field at 2ω that is fully described by a general solution of Eq. 2.20. Note also that if the nonlinear polarization is substituted by an equivalent current source

$\mathbf{J}_{eq} = \dfrac{\partial \mathcal{P}^{NL}}{\partial t}$, the above equation is equivalent to the equation that describes the

radiation from a plane sheet of linear dipoles forced at frequency 2ω. In the case considered here, the oscillation amplitude and phase of these dipoles is completely determined by those of the forcing field at frequency ω.

The emission of radiation for the periodic structure with a defect described in chapter 2, will be considered now as a function of the position of the nonlinear layer within the defect and molecular dipole orientation. As seen in the previous chapter such structure provides sharp resonances with localized modes at certain angles of incidence and regions where the radiation is inhibited at other angles within the gap. We will first center in the study of the case for which the beam at the fundamental frequency is incident at the angle corresponding to the resonance and later we will extend the results to the case of incidence at any other angle within the gap. We will first take in our study the particular values for the structure obtained in the experimental results of the previous chapter so the local mode appears at the incident angle of 28.7 degrees.

Incidence at resonance

In this case the angle of incidence of the fundamental field is such that the generated SH field is resonant with the mode density peak defining the localized state shown in Figure 2.24 , where a strong enhancement of the SH radiation was observed. As pointed out in the introduction, however, resonance with the density of modes is not the only factor determining the dipole radiation efficiency. Figure 3.2 shows the total intensity radiated at the frequency 2ω out of the material structure in the forward and backward directions, calculated by means of the transfer method outlined in chapter 2 (Eq. 2.36), as a function of the position (z_o) of the nonlinear layer within the defect, when the beam at ω is incident at the angle corresponding to the localized state and for different values of the orientation of the molecular dipoles in the nonlinear layer. As can be seen in Figure 3.1, this orientation is defined by giving the angle, α, that the resulting electric
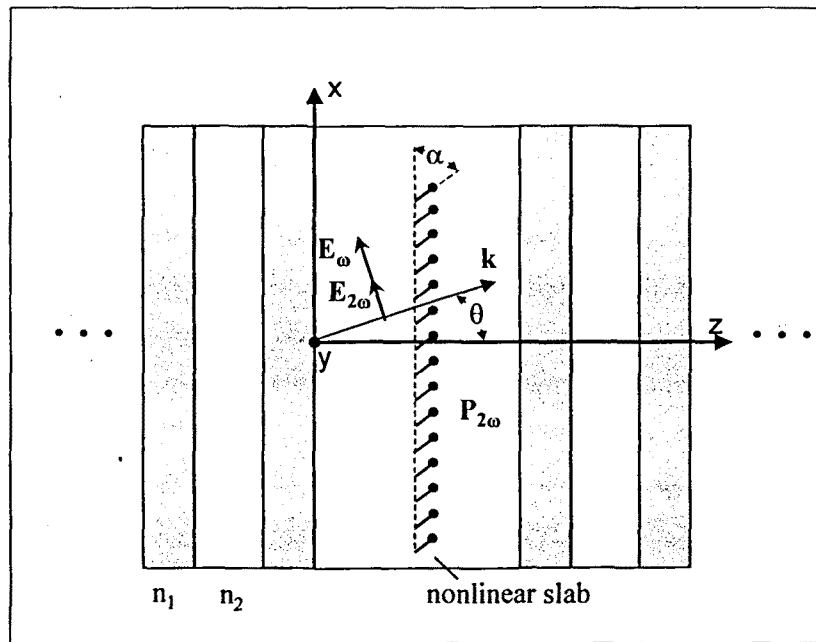
Figure 3.1 Schematic diagram of the truncated periodic structure studied. The origin of the coordinate system used is taken at the beginning of the defect. The fields at the fundamental and second-harmonic frequency propagate in the direction of the wavevector *k* determined by the angle, *θ*, with respect to the z-axis. The dipole orientation was defined through the angle *α*, as can be seen from the figure.

polarization vector forms with respect to the direction parallel to the mirror planes through the relation $tan\alpha = P_z^{NL}/P_x^{NL}$. The thin nonlinear layer of dipoles is assumed to have a $C_{\infty v}$ symmetry for all the values of the angle α=0, for which an orientation of the dipoles parallel to the X axis is assumed. With this symmetry and when the incident field is TM polarized (as it is the case assumed in the following) the component P_y^{NL} of the electric polarization vector vanishes.

The intensity curves for the field at 2ω in Figure 3.2 are normalized to the values of the total intensity for the field at 2ω radiated by the nonlinear layer in free space (i.e. when no structure is present) for each case. From this figure is observed that a strong enhancement of the intensity at 2ω is found for most of the molecular dipole orientations, except for the orientation normal to the mirror planes (α=90 deg.). For this particular case, inhibition instead of enhancement is obtained when the nonlinear layer is placed close to the center of the defect. Note that a maximum enhancement of 350
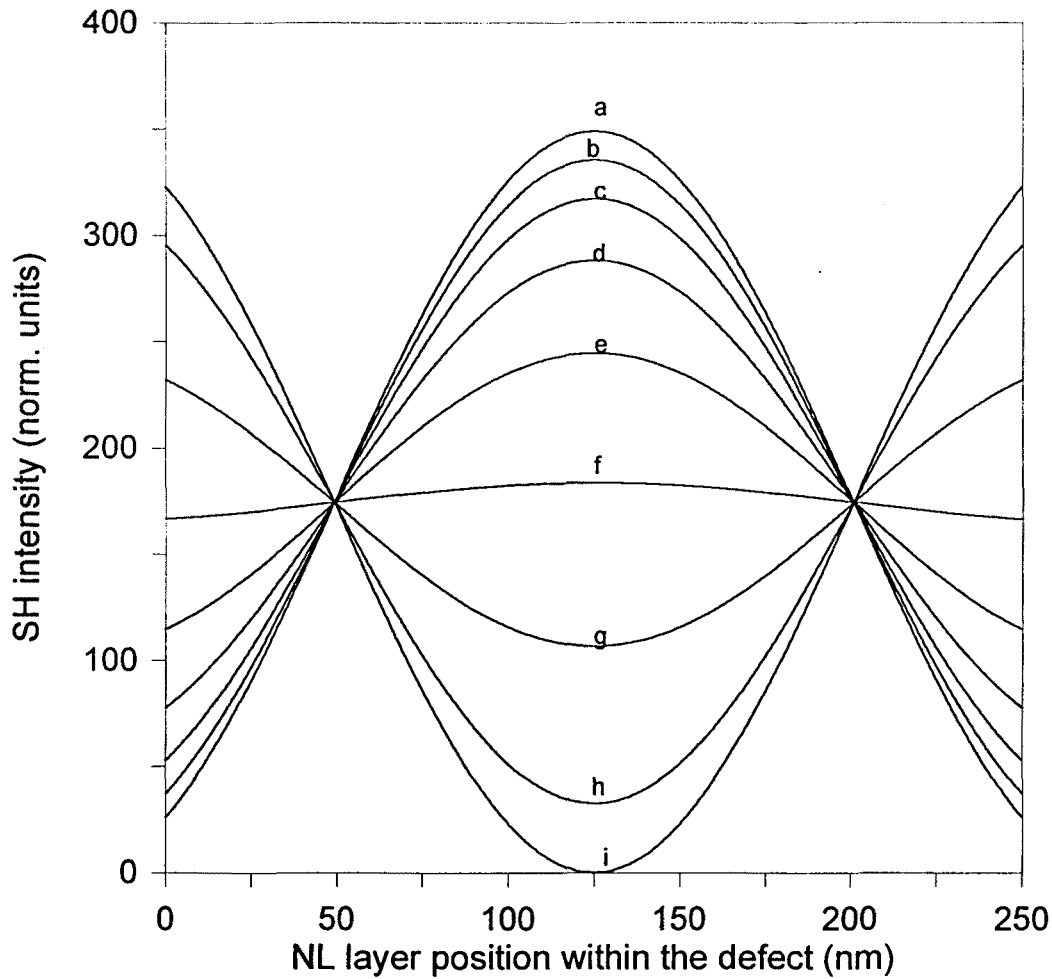
Figure 3.2 Total emission at frequency 2ω (both in the forward (transmission) and backward (reflection) directions) of the 1D truncated periodic structure when a thin layer of nonlinear material is placed within the defect region as a function of the position (z_o) of that thin layer within the defect. This emission is given for nine different dipole orientations: a, $\alpha=0°$; b, $\alpha=20°$; c, $\alpha=30°$; d, $\alpha=40°$; e, $\alpha=50°$; f, $\alpha=60°$; g, $\alpha=70°$; h, $\alpha=80°$; i, $\alpha=90°$. At the left boundary of the defect the position is 0 nm, and at the right boundary the position is 250 nm, under the assumption that the incident beam at ω propagates from left to right.

times the emission in air is found in the same position when dipoles are oriented parallel to the mirror planes ($\alpha=0$ deg.). From these results it may be immediately seen the strong dependence of the dipole radiation with the environmental conditions imposed by the structure. Varying the position of the nonlinear slab inside the defect results in a

strong variation of the enhancement factor (the radiated intensity is increased ten times for instance for the case $\alpha=0$, when the slab is moved to the center of the defect.) as can be also seen from the same Figure.

This variation of intensity with the layer position may be directly related, in some particular cases, to the field distribution within the cavity as pointed out by some authors [Lid97]. In our present case, the additional dependence with the dipole orientation is shown to be important in the resulting emitted intensity. The change in the conversion efficiency as the angle is changed may be seen in Figure 3.2, since the position of maximum enhancement changes from the center of the defect, for dipole orientation parallel to the mirror plane (Figure 3.2(a)), to the defect edge when the angle is close to the perpendicular to the mirror planes (Figure 3.2 (i)).

Let us study the possible relationship of the radiation patterns shown in Figure 3.2 with the field distribution inside the structure. The calculation of the field distribution may be taken up by the transfer matrix method. The total field in each layer is given by the expressions given in chapter 2. Once the reflectance and transmittance of the structure are calculated by means of Eq. 2.36, the complex amplitudes are obtained after multiplication of the corresponding matrices relating the fields in different layers.

The distribution for the field amplitude at the second-harmonic frequency 2ω inside the structure is shown in Figure 3.3a when the orientation of the dipoles is such that $\alpha=0$ deg. and in Figure 3.3b, when $\alpha=90$ deg., for two different positions of the nonlinear layer within the gap. The field amplitude in each case has been normalized to the value of the amplitude of the field at 2ω reflected from the nonlinear layer in free space. It is observed from these figures that the field amplitude distribution of the second harmonic field within the structure, which corresponds to the resonant mode of the structure, remains essentially the same in all the cases and has its main peak localized in the defect region. As can be seen in Figure 3.3 the total field localized within the structure, however, is strongly dependent on the dipole orientation and the nonlinear layer position within the defect.

For the case $\alpha=0°$ (Figure 3.3(a)), the total field amplitude in the structure increases 4.5 times as the nonlinear layer is moved from the edge (curve A) to the center (curve B) of the air gap, whereas for $\alpha=90°$ (Figure 3.3(b)), the field amplitude decreases 440 times in the same conditions. These variations in the field amplitude have a direct influence on the energy radiated out from the structure, since this field distribution extends up to the outer surfaces of the structure(right and left parts in Figures 3.3(a) an 3.3(b)) and propagates through the external free space, in the forward and backward directions.

These emission variations with the nonlinear layer position indicate that, in general, the intensity at 2ω radiated out of the structure as a function of the dipole layer position (Figure 3.2) is not proportional to the field amplitude distribution within the air gap or the density of modes, since as have been shown, a maximum in the amplitude distribution for the field at 2ω is always observed at the middle of the air gap (Figures 3.3(a) and 3.3(b)), while the maximum of the field radiated changes with the polarization vector orientation and, as may be seen, it reaches its maximum value at the defect edges and not at the center of the defect when the dipoles are oriented at enough high angles with respect to the normal to the layer planes. As we have seen in the preceding paragraph, as we move the monolayer inside the defect, the total field inside the cavity changes in magnitude keeping its envelope corresponding to the resonant mode for the structure. In Figure 3.4 the total field amplitude at 2ω (thick curve) *at the location of the nonlinear layer* is shown as a function of the layer position (z_o) within the air gap, for different values of the dipole orientation. The field amplitude in each case has been normalized to the value of the amplitude of the field at 2ω reflected from the nonlinear layer in free space. The variations of the intensity at 2ω radiated as a function of the nonlinear layer position (Figure 3.2) are qualitatively correlated with the variations of the field amplitude at the nonlinear layer (Figure 3.4, thick curve), but these changes are clearly not directly proportional to each other, especially for $\alpha=90°$ (Figure 3.4(d)).

The calculated field amplitudes at each layer, obtained by means of the transfer matrix method, were used to obtain the stationary radiation distribution out of the structure (Figure 3.2). Note that in the calculation of these fields, all reflections within the structure are taken into account and give us all the information necessary to fully
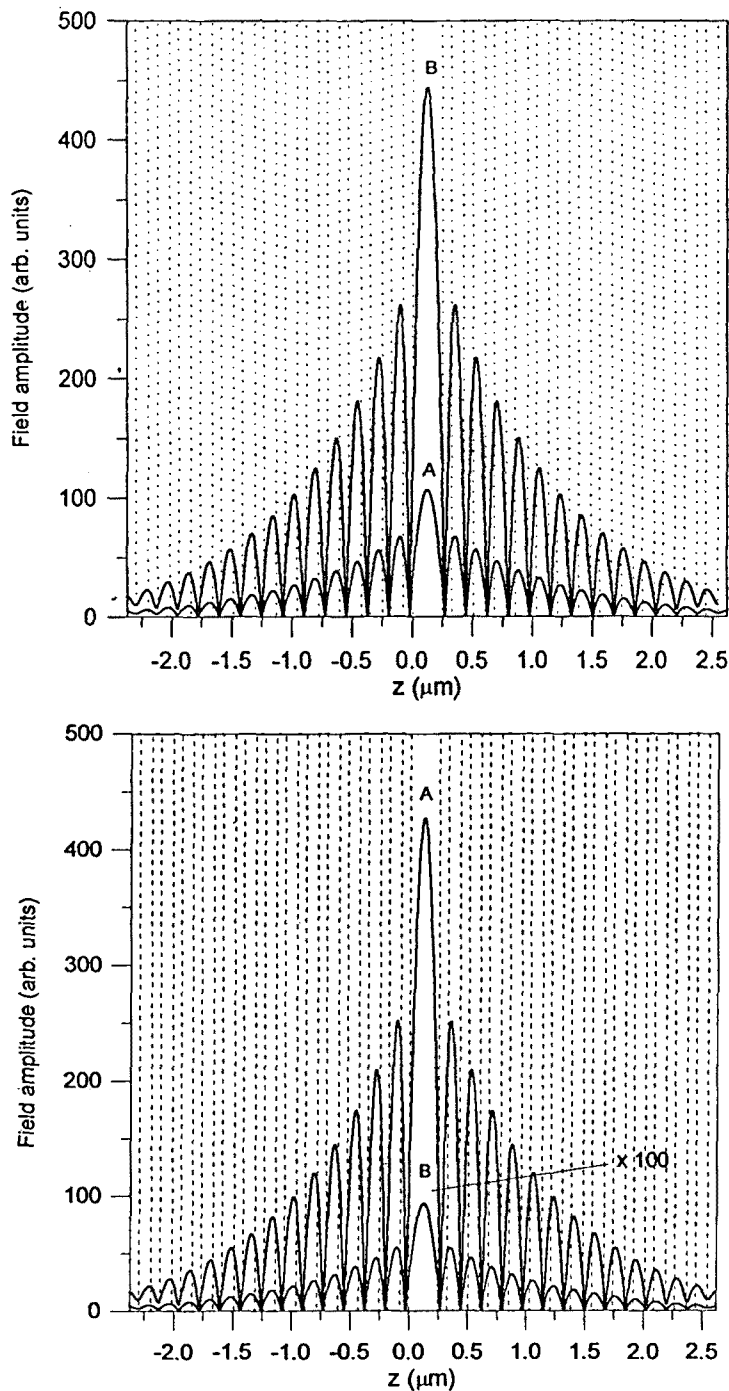
Figure 3.3 (a) Field amplitue distribution inside the 1D truncated periodic structure when the nonlinear layer is at $z_0=0$ nm (A) and $z_0=125$ nm (B), and the dipole orientation is such that $\alpha=0°$. The field at 2ω is resonant with the localized state (incidence angle equal to 28.7°). The vertical broken lines indicate the positions of the interfaces of the structure. **(b)** The same as (a), for $\alpha=90°$.
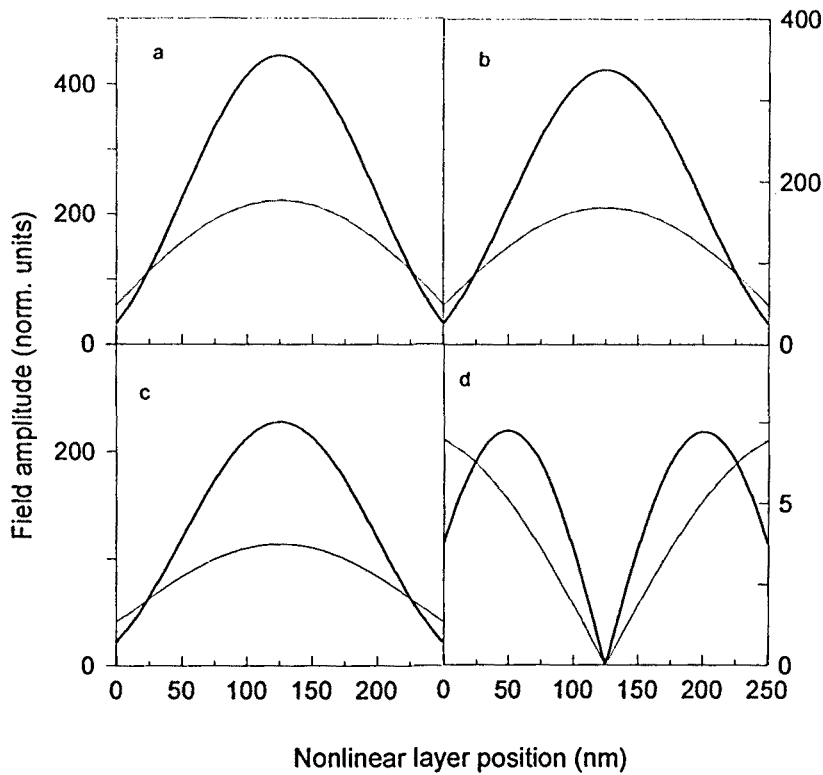
Figure 3.4 Total field amplitude (thick curve), forward propagating field amplitude (thin curve), and backward propagating field amplitude (broken curve) at the location of the nonlinear layer, as a function of the layer position (z_o) inside the defect of the 1D truncated periodic structure, for four different dipole orientations, a, $\alpha=0°$; b, $\alpha=30°$; c, $\alpha=60°$; d, $\alpha=90°$, when the incident field at ω is incident at a resonance angle of 28.7°.

calculate the intensity radiated by the structure. Nevertheless, as we have seen from the preceding paragraph, the intensity radiated by the structure is not, in the most general case, directly related to the field-amplitude distribution inside the structure as it is the case for some particular parameter settings. In these particular cases, the measure of the outgoing radiation could be used to map the field distribution within the structure [Bur97]. In the more general case, this radiated intensity should be directly related to the energy transfer between the oscillating dipoles and the fields. In order to see this point in further detail, the energy transfer mechanism from the dipoles to the field (or viceversa) will be analyzed in the next section.

2. Energy Transfer in nonlinear monolayers

In the preceding section we showed that in the case of coupling the SH radiation into a local mode of the structure, where an enhancement of SH radiation is obtained, the radiation emission rate varies strongly as we move the monolayer within the defect or change the dipole orientation. In this section we will study the energy transfer between the oscillating dipoles and the field at the frequency 2ω in order to obtain additional information about the way in which the enhancement or inhibition of radiation by the structures takes place.

It is known from dipole radiation theory that the rate at which the energy per unit volume is transferred from the nonlinear source to the field at 2ω is given by the quantity $-\mathbf{J}_{2\omega} \cdot \mathbf{E}_{2\omega}$, where $\mathbf{J}_{2\omega} = \partial \mathbf{P}_{NL}/\partial t$ is the current density vector at frequency 2ω, which is fixed in amplitude and phase by the strong fundamental field at the frequency ω, and $\mathbf{E}_{2\omega}$ is the field at frequency 2ω that exists at the position of the source. This means that not only the amplitude of the field, but also the orientation and phase (relative to those of the oscillating dipoles at 2ω) determine the energy transferred from the dipolar source to the field. The calculation of the energy transferred $-\mathbf{J}_{2\omega} \cdot \mathbf{E}_{2\omega}$ can be performed either directly, or by the use of the well known relationship

$$-\frac{1}{2} \iiint_V \mathrm{Re}\left(\mathbf{J}_{2\omega}^* \cdot \mathbf{E}_{2\omega}\right) dV = \frac{1}{2} \oiint_S \mathrm{Re}\left(\mathbf{E}_{2\omega} \times \mathbf{H}_{2\omega}^*\right) \cdot d\mathbf{s} \qquad 3.1.$$

that is based on the continuity equation for time averaged fields [Jackson]. The fields appearing in the equation are the complex representations of the electric field and magnetic induction respectively. The left-hand side of Eq. 3.1 corresponds to the work done by the dipoles on the field at 2ω in a volume V, and can be easily determined in the 1-D system considered, by performing the integral on the right-hand side on a surface S enclosing a rectangular box of volume V. In order to evaluate such integral, we should calculate first the electric and magnetic fields at both sides of the nonlinear layer. These fields, which result from the generated radiation at the slab and the effect
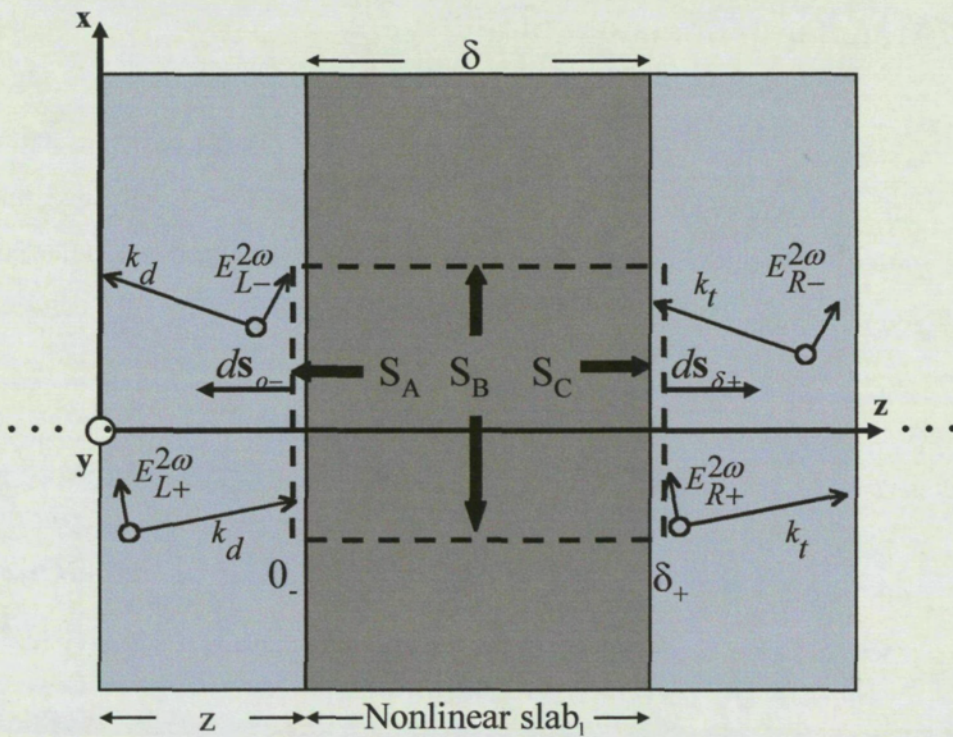
Figure 3.5 Schematic representation of the nonlinear slab and the fields present at this point of the structure. The dashed line gives the surface enclosing the integration volume. The size of the nonlinear slab doesn't scale it's real dimensions with respect to the defect length.

of the multiple reflections within the structure, were obtained previously with the transfer matrix technique and were already used to calculate the emission of SH radiation by the structure (Figure 3.2).

Figure 3.5 shows the given fields at the surfaces of the nonlinear slab and the integration surface we will use in performing the integral of Eq. 3.1. The position of the nonlinear slab surfaces will be denoted by $z_o{=}0_-$ and $z_o{=}\delta_+$. The total electric field and magnetic induction at each side of the nonlinear slab are written as:

$z_o{=}0_-$

$$\mathbf{E}_L^{2\omega} = \left[\hat{\mathbf{e}}_+ E_{L+}^{2\omega} \exp\left(ik_{dz}z_o\right) + \hat{\mathbf{e}}_- E_{L-}^{2\omega} \exp\left(-ik_{dz}z_o\right)\right]\exp(i(k_x x - \omega t))$$

and   3.2.

$$\mathbf{H}_L^{2\omega} = \left[\hat{\mathbf{h}}_- H_{L+}^{2\omega} \exp(ik_{dz}z_o) + \hat{\mathbf{h}}_- H_{L-}^{2\omega} \exp(-ik_{dz}z_o) \right] \exp(i(k_x x - \omega t))$$

The corresponding fields at the right side of the nonlinear slab are:

$z_o = \delta_+$

$$\mathbf{E}_R^{2\omega} = \left[\hat{\mathbf{e}}_+ E_{R+}^{2\omega} \exp(ik_{tz}z_o) + \hat{\mathbf{e}}_- E_{R-}^{2\omega} \exp(-ik_{tz}z_o) \right] \exp(i(k_x x - \omega t))$$

and   3.3.

$$\mathbf{H}_R^{2\omega} = \left[\hat{\mathbf{h}}_+ H_{R+}^{2\omega} \exp(ik_{tz}z_o) + \hat{\mathbf{h}}_- H_{R-}^{2\omega} \exp(-ik_{tz}z_o) \right] \exp(i(k_x x - \omega t))$$

where $E_{L+}^{2\omega}$ and $E_{L-}^{2\omega}$ are the complex amplitudes of the electric field in the forward and backward propagating directions at the outer side of the left surface of the nonlinear slab at $z_o = 0.$, and $H_{L+}^{2\omega}$ and $H_{L-}^{2\omega}$ are the corresponding complex amplitudes for the magnetic induction at the same position. The corresponding fields at the right side of the nonlinear slab, at $z_o = \delta_+$ are given by the terms $E_{R+}^{2\omega}$ and $E_{R-}^{2\omega}$ for the electric field and $H_{R+}^{2\omega}$ and $H_{R-}^{2\omega}$ for the magnetic induction respectively. The fields at the right side of the slab are related to the fields at the left through equation 2.30 in chapter 2. The magnetic induction is obtained from the electric field from Maxwell equations. The unitary vectors in the direction of each component of the electromagnetic field are given by the expressions (Appendix A gives the criterion used in this work for the direction of the fields at each boundary):

$$\hat{\mathbf{e}}_\pm = \cos\theta \hat{\mathbf{i}} \mp \sin\theta \hat{\mathbf{k}}$$

and   3.4.

$$\hat{\mathbf{h}}_\pm = \pm \hat{\mathbf{j}}$$

k_{dz} and k_{tz} are the components of the wavevector in the z direction at each side of the nonlinear slab. In our particular case we will assume the same medium at each side of the slab to be air (the use of a different medium changes the absolute values of the emitted radiation, but the qualitative aspects of the process remain unchanged) so the subindex d and t will be omitted in the remaining expressions. θ denotes the

propagation direction of the beam with respect to the normal at the surface and in this case is the angle corresponding to the localized state of the structure. By taking into account the explicit form of the unit vectors given by eq. 3.4 and using Maxwell equation we can write the expression for the electric field at each side of the monolayer as:

$z_0=0_-$

$$\mathbf{E}_L^{2\omega} = \left[\hat{\mathbf{i}}\left(E_{L+}^{2\omega}\exp(ik_zz_o)+E_{L-}^{2\omega}\exp(-ik_zz_o)\right)\cos\theta + \hat{\mathbf{k}}\left(-E_{L+}^{2\omega}\exp(ik_zz_o)+E_{L-}^{2\omega}\exp(-ik_zz_o)\right)\sin\theta\right]$$
$$\exp(i(k_xx-\omega t))$$

$z_{o=\delta_+}$ 3.5.

$$\mathbf{E}_R^{2\omega} = \left[\hat{\mathbf{i}}\left(E_{R+}^{2\omega}\exp(ik_zz_o)+E_{R-}^{2\omega}\exp(-ik_zz_o)\right)\cos\theta + \hat{\mathbf{k}}\left(-E_{R+}^{2\omega}\exp(ik_zz_o)+E_{R-}^{2\omega}\exp(-ik_zz_o)\right)\sin\theta\right]$$
$$\exp(i(k_xx-\omega t))$$

the corresponding expressions for the magnetic induction are given by:

$z_0=0_-$

$$\mathbf{H}_L^{2\omega} = \hat{\mathbf{j}}\frac{k}{\omega\mu_o}\left[E_{L+}^{2\omega}\exp(ik_zz_o)-E_{L-}^{2\omega}\exp(-ik_zz_o)\right]\exp(i(k_xx-\omega t))$$

$z_{o=\delta_+}$ 3.6.

$$\mathbf{H}_R^{2\omega} = \hat{\mathbf{j}}\frac{k}{\omega\mu_o}\left[E_{R+}^{2\omega}\exp(ik_zz_o)-E_{R-}^{2\omega}\exp(-ik_zz_o)\right]\exp(i(k_xx-\omega t))$$

Once we have the expressions for the fields at each side of the nonlinear slab, we can perform the integral that gives the energy transfer (ET) from the oscillating dipoles to the field at the frequency 2ω. By dividing the surface enclosing the chosen volume into the three parts shown in Figure 3.5, we obtain:

$$ET = \iint\limits_{S_A}\mathbf{S}_{o-}d\mathbf{s}_{o-} + \iint\limits_{S_C}\mathbf{S}_{\delta+}d\mathbf{s}_{\delta+}$$ 3.7.

where the contribution to the surface integral from the surfaces normal to the plane sheet (S_B in Figure 3.5) have been omitted since they cancel each other giving no net contribution to the energy transfer. The expression in equation 3.7 has been written in terms of the averaged Poynting vector $S = \frac{1}{2}\text{Re}(\mathbf{E} \times \mathbf{H}^*)$, and the differential surface elements appearing in the integrals are given explicitly by (Figure 3.5) $d\mathbf{s}_{o-} = -\hat{k}ds$ and $d\mathbf{s}_{\delta+} = \hat{k}ds$. By performing the dot product in S, using equations 3.5 and 3.6 we obtain:

$$
\mathbf{S}_{o-} = \frac{1}{2}\text{Re}\left[\frac{k}{\omega\mu_o}sin\theta\left(\left|E_{L+}^{2\omega}\right|^2 + \left|E_{L-}^{2\omega}\right|^2 - 2\text{Re}(E_{L+}^{2\omega}E_{L-}^{2\omega*}\exp i2k_z z_o)\right)\right]\hat{i} +
$$

$$
+\frac{1}{2}\text{Re}\left[\frac{k}{\omega\mu_o}cos\theta\left(\left|E_{L+}^{2\omega}\right|^2 - \left|E_{L-}^{2\omega}\right|^2 - 2i\text{Im}(E_{L+}^{2\omega}E_{L-}^{2\omega*}\exp i2k_z z_o)\right)\right]\hat{k}
$$

and   3.8.

$$
\mathbf{S}_{\delta+} = \frac{1}{2}\text{Re}\left[\frac{k}{\omega\mu_o}sin\theta\left(\left|E_{R+}^{2\omega}\right|^2 + \left|E_{R-}^{2\omega}\right|^2 - 2\text{Re}(E_{R+}^{2\omega}E_{R-}^{2\omega*}\exp i2k_z z_o)\right)\right]\hat{i} +
$$

$$
+\frac{1}{2}\text{Re}\left[\frac{k}{\omega\mu_o}cos\theta\left(\left|E_{R+}^{2\omega}\right|^2 - \left|E_{R-}^{2\omega}\right|^2 - 2i\text{Im}(E_{R+}^{2\omega}E_{R-}^{2\omega*}\exp i2k_z z_o)\right)\right]\hat{k}
$$

By substituting these expressions in 3.7 we obtain the final expression for the energy transfer from the dipoles to the field at 2ω to be:

$$
ET = \frac{nc\varepsilon_o cos\theta}{2}\left[\left|E_{R+}^{2\omega}\right|^2 - \left|E_{R-}^{2\omega}\right|^2 - \left|E_{L+}^{2\omega}\right|^2 + \left|E_{L-}^{2\omega}\right|^2\right]
$$ 3.9.

where n is the refraction index within the defect and θ is the angle of propagation of the field at 2ω with respect to the z direction. At this point, we recall the fact that the values of the fields needed for the calculation of the ET were previously obtained with the transfer matrix method and that these fields are related through equation 2.30 which accounts for the nonlinear quadratic interaction within the slab. The final expression for the energy transfer may be separated into two distinct contributions, one for the forward (+) and another for the backward (-) propagating components of the field.

$$ET^{(+)} = \frac{nc\varepsilon_o \cos\theta}{2}\left[\left|E_{R+}^{2\omega}\right|^2 - \left|E_{L+}^{2\omega}\right|^2\right]$$

3.10.

$$ET^{(-)} = \frac{nc\varepsilon_o \cos\theta}{2}\left[\left|E_{L-}^{2\omega}\right|^2 - \left|E_{R-}^{2\omega}\right|^2\right]$$

The total energy transfer from the dipoles to the field, calculated from Equation 3.9 is shown as the thick curves in Figure 3.6, normalized to the energy transfer of a nonlinear layer emitting in free space, for the same cases studied in Figure 3.4. As expected, the total intensity emitted by the structure (Figure 3.2) equals the energy transfer from the dipoles to the field at 2ω (Figure 3.6). As the resultant stationary field at the second-harmonic frequency within the structure can be written as a superposition of two terms corresponding to forward and backward propagating plane waves, the separation of the total energy transfer (Eq. 3.9) into these two contributions allows for the possibility of studying how each one of these components contribute to the resulting conversion efficiency. These separate energy transfers from the dipole sheet to the forward (thin line) and backward (dashed line) components of the field at the nonlinear layer position are also shown in Figure 3.6. Interestingly enough, these two energy transfers are different from each other and, in particular, it can be seen that there are certain regions that give negative energy transfer for one of these components as is, for example, the case for the forward propagating contribution when $\alpha=0°$ and the nonlinear layer is placed between 0 and 30 nm within the air gap (Figure 3.6(a)). This means that for such conditions the corresponding field at the nonlinear layer position is losing energy, in spite of the fact that the total energy transfer is always positive. Thus what occurs is that the dipoles radiate the field in one direction, this field is reflected by the mirror structure, it comes back in the opposite direction, and the energy is again transferred back, partially, to the dipoles being lost by the corresponding component of the field. Since we are calculating the emission of the structure in steady state, we do not see the contributions of the different components separately but what we observe is the resulting emission rate arising from the whole interaction. Because of this fact, it may even occur that the field radiated by the dipoles in one direction is larger than in free
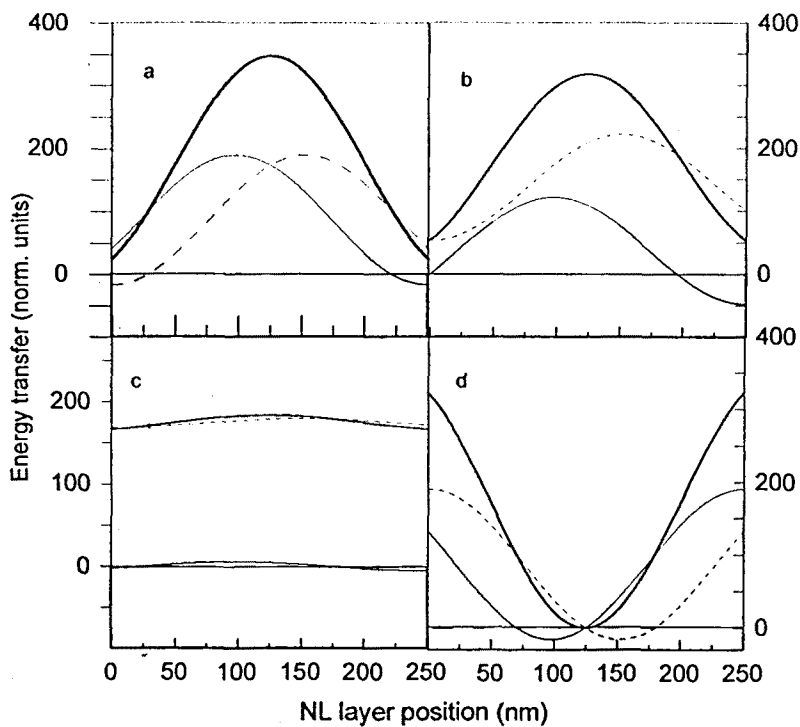
Figure 3.6 Energy transfer from the dipole sheet, to the total field at 2ω (thick full curve), to the forward propagating field at 2ω (thin full curve), and to the backward propagating field at 2ω (broken curve), as a function of the position of the nonlinear layer inside the defect of the 1D truncated periodic structure, for the same four different dipole orientations and incidence angle as in figure 3.4. The grey regions indicate the phase difference values at which the energy transfer is negative (absorption)

space, but the total energy getting out of the structure is smaller than in free space, since the net conversion efficiency is partially reduced in the opposite direction. For instance, this can be seen in Figure 3.6 (d) when the nonlinear layer position is close to (but not exactly at) the center of the air gap. At the center of the air gap, transfer of energy to the field at 2ω is completely inhibited in both directions, so that the energy radiated outside the structure is also below the energy radiated in free space. For the case $\alpha=60°$, we see that the energy transfer is provided by the backward component of the field while the forward propagating component does not give contribution. This fact is explained in this particular case, since the angle between the forward propagating field and the oscillating dipoles is approximately $90°$ in this case, and consequently no energy may be transferred in this case.

This asymmetry in the forward-backward dipole radiation as well as the previous results described above cannot be understood by looking only at the field amplitude value at the dipole layer position. In effect, Figure 3.4 shows that the field amplitude at the layer position is very similar for the forward (thin full curve) and the backward (broken curve) field components. Clearly the phase difference between the oscillation of the dipoles and the field components will play a dominant role in this process.

3. Phase dependence of quadratic nonlinear radiation in periodic structures

In this section we will study the phase difference between the generated field at the frequency 2ω at the nonlinear slab position and the oscillating dipoles, in order to see how this phase difference is modified by the presence of the structure and how this factor affects the resulting emission rate at frequency 2ω. The dependence of this quantity with the monolayer position within the defect of the microresonator and the orientation of the dipoles will be also studied showing a close relation between this phase difference and the resulting energy transfer to the field.

In order to calculate this phase difference we will write the fields at the position of the nonlinear slab, already calculated in previous sections by means of the transfer matrix method, as:

$$\mathbf{E}_j^{2\omega} = \hat{\mathbf{e}}_+ \left| E_{j+}^{2\omega} \right| \exp i(\phi_{E+} - 2\omega t) + \hat{\mathbf{e}}_- \left| E_{j-}^{2\omega} \right| \exp i(\phi_{E-} - 2\omega t) \qquad 3.11.$$

where the subindex $j=L,R$ refers to the fields at the right or left boundaries of the nonlinear slab respectively. The oscillation of the dipoles at the second harmonic frequency, driven by the field at the fundamental through the quadratic nonlinear interaction may be written in a similar form as:

$$\mathbf{P}_{NL}^{2\omega} = \hat{\mathbf{p}}_+ \left| P_{NL}^{2\omega} \right| \exp i(\phi_P - 2\omega t) \qquad 3.12.$$

where the nonlinear polarization is obtained after contraction of the second order susceptibility tensor with the square of the field at the fundamental frequency as usual. Only the forward component is considered since this is the only component for which generation of second-harmonic is considered. Once the fields are written in this form, we calculate the phase difference between each of the components of the field (forward (+) and backward propagating (-)) and the polarization vector. When the nonlinear layer is considered to emit in free space with no structure present, a phase difference of $\pi/2$ is obtained corresponding to a maximum in the energy transfer from the dipoles to the second-harmonic field. Figure 3.7 shows the phase difference between the dipole oscillation and the forward (full curve) or backward (broken curve) field oscillations at the position of the dipole layer, for the same cases of dipole orientation shown in Figures 3.4 and 3.6. It can be seen that inside the truncated periodic structure, the phase of the radiated field is strongly dependent on the position of the dipole sheet within the air gap and the orientation of the dipoles. When this dependence is studied, one finds, as expected, that when the energy transfer shown in Figure 3.6 for the corresponding forward or backward field component is positive (i.e. the energy is transferred from the oscillating dipole to the field), the phase difference ranges from $0°$ to $180°$ (Figure 3.7). In contrast, when the energy transfer for the forward or backward components of the field is negative (i.e. the energy is lost by the corresponding component of the field being transferred to the dipoles), the phase difference ranges from 0 to $-180°$ or from 180 to $360°$ (Figure 3.7). In this way, the variations in the energy transfer for each one of the components are related to a corresponding change in the phase relation between the resulting field at the nonlinear slab position and the oscillating dipoles driven by the fundamental field.

By comparing Figures 3.4 and 3.6, we can observe that the peak of maximum field amplitude for the forward or backward components of the field (for all four dipole orientations), Figure 3.4, does not coincide with the location of maximum energy transfer to the corresponding component, Figure 3.6. Inspection of Figure 3.7 indicates that the peak of maximum energy transfer is shifted away from the peak of maximum field amplitude and is pulled towards the position of the nonlinear layer where the phase difference is exactly $90°$, a phase difference that in free space leads to maximum transfer of energy from the dipole oscillation to the field at the frequency 2ω.
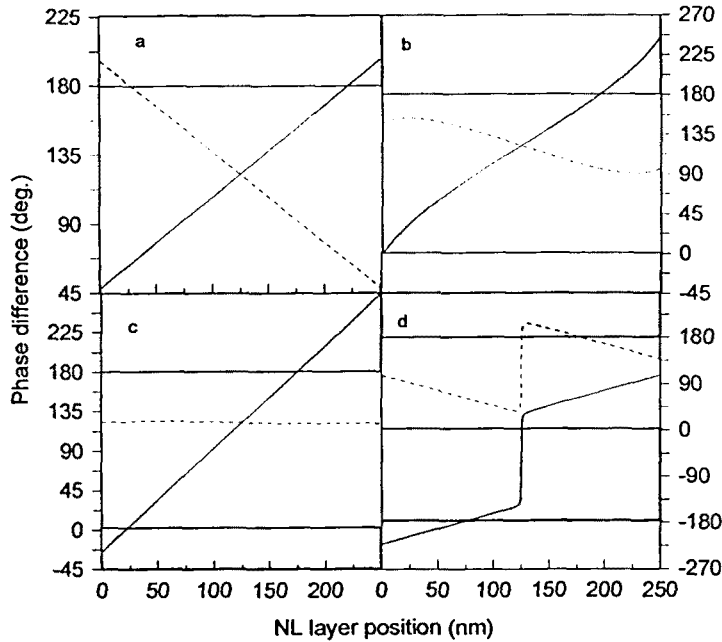
Figure 3.7 Phase difference between the dipole oscillation and the forward propagating field at 2ω (full curve), and the backward propagating field at 2ω (broken curve) as a function of the position of the nonlinear layer inside the defect of the 1D truncated periodic structure, for the same four different dipole orientations and angle of incidence shown in figure 3.4. The grey regions indicate the phase difference values at which the energy transfer is negative (absorption)

Nevertheless, this pulling from one component of the field is compensated with a pulling in the opposite direction by the corresponding counterpropagating component of the field, and for most of the dipole orientations, the total field amplitude distribution (shown in Figure 3.4) approximately mimics the total energy transfer shown in Figure 3.6, as already pointed out above. The most complex case is that with $\alpha=90°$, where the total energy transfer as a function of the layer position is strongly influenced by the fast variations of both the phase and the amplitude with the nonlinear layer position.

4. Incidence angle out of resonance

We have been studying in the previous sections how the presence of the structure affects the emission rate of the nonlinear slab, when the angle of incidence of the

fundamental field is such that the SH light is resonant with the local mode. It has been shown that the enhancement factor may be improved by changing the position of the monolayer within the defect or the dipole orientation of the slab. This behavior was shown to be correlated to the associated variation in the phase difference between the field and the oscillating dipoles. As it was shown in chapter 2, when the incidence angle does not correspond to the resonant angle for the given structure, inhibition instead of enhancement is observed for the SH emission of the structure. In this section we analyze how the ideas given for the resonant case may be equally applied in the non-resonant cases in order to explain how the inhibition process takes place.

If the incidence angle of the fundamental field is detuned from the value that makes the SH generated field to be on resonance with the localized state of the structure, the density of states decreases very quickly and thus the SH intensity also decreases fast to zero, as was experimentally demonstrated in the previous chapter. Let us consider an incidence angle not far from resonance, for which the SH intensity generated is still noticeable, and let us study the emission process as previously done for the resonant case. Figure 3.8 shows the total SH emission of the structure normalized to the emission in free space, when the fundamental field is incident at an angle of 32°, for the four dipole orientations shown in Figures 3.4, 3.6 and 3.7. From this figure it can be seen that the emission dependence as a function of the monolayer position within the defect is very similar to that found for the resonant case (Figure 3.2), but in this case the SH radiation is strongly inhibited instead of enhanced, i.e., for the case of $\alpha=0^{\circ}$ SH radiation is inhibited by a factor of 5 in the same position for which an enhancement factor of 350 is found for the resonant case. A much higher inhibition factor is found at other positions and dipole orientations as can be seen in Figure 3.8.

The calculation of the energy transfer between the field and dipoles may be performed in the same way as for the resonant case. This energy transfer is shown in Figure 3.9. It can be seen that the total energy transfer equals the total emitted intensity (Figure 3.8) also in this case. However, the total energy radiated from the dipoles (thick continuous line) is much smaller than in free space indicating that the SH radiation is inhibited in this case. When the energy transfer to each one of the components of the field is calculated in the same way as for the resonant case, it is observed that the energy
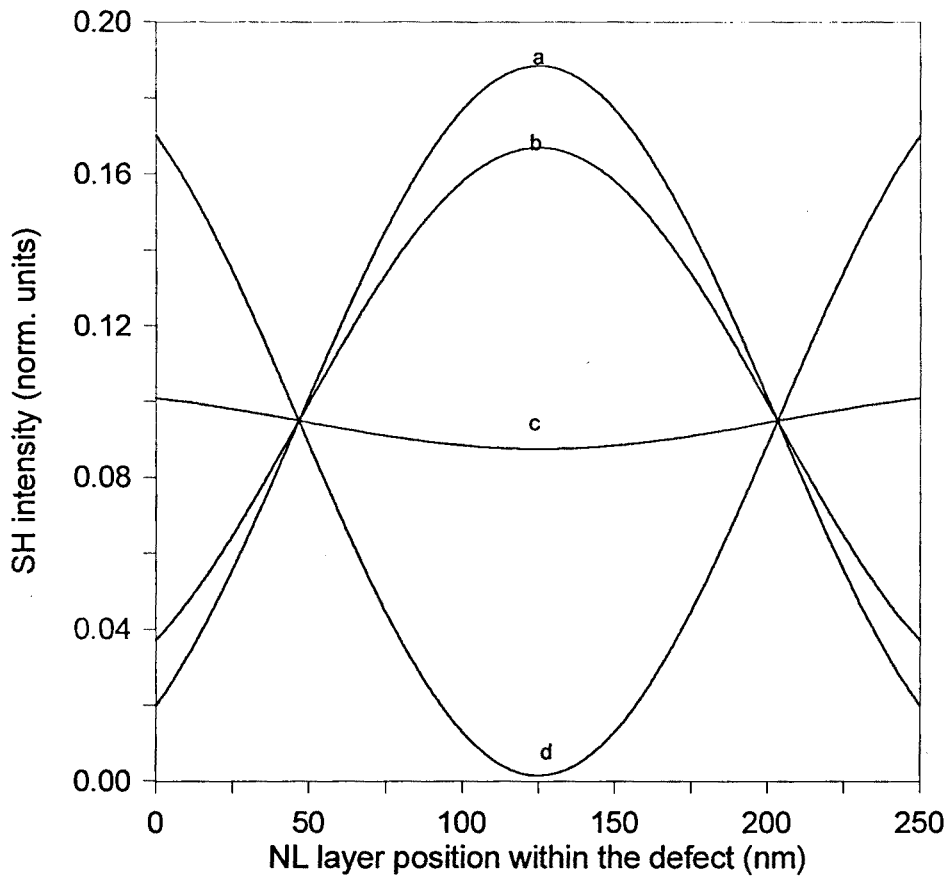
Figure 3.8 Total emission at frequency 2ω (both in the forward (transmission) and backward (reflection) directions) of the 1D truncated periodic structure when a thin layer of nonlinear material is placed within the defect region as a function of the position (z_o) of that thin layer within the defect. This emission is given for four different dipole orientations: a, $\alpha=0°$; b, $\alpha=30°$; c, $\alpha=60°$; d, $\alpha=90°$. At the left boundary of the defect the position is 0 nm, and at the right boundary the position is 250 nm, under the assumption that the incident beam at ω propagates from left to right. The incidence angle for the fundamental radiation is 32°

transfer at the nonlinear layer position can still be larger than in free space for one of the components, so a significant field can still be present within the structure (see for example that in Figure 3.9 (a) where the energy transfer to the forward propagating component of the field is enhanced 3 times with respect to the emission in free space when the slab is at the position z=200 nm within the defect). This energy transfer to the field component at the nonlinear slab position in one direction is almost completely compensated by a loss of energy from the corresponding counterpropagating field component at the same position resulting in a net reduction of the radiated energy from
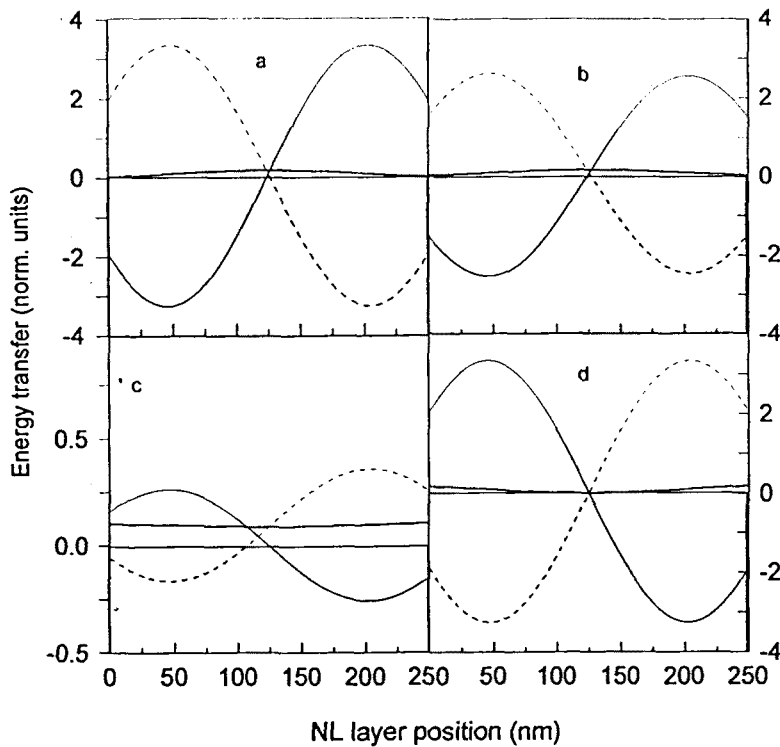
Figure 3.9 Energy transfer to the total field at 2ω (thick full curve), energy transfer to the forward propagating field at 2ω (thin full curve), and energy transfer to the backward propagating field at 2ω (broken curve) as a function of the position of the nonlinear layer inside the defect of the 1D truncated periodic structure, for the same four different dipole orientations shown in Figure 3.6, when the beam at ω is incident at an angle of 32°.

the whole structure. A similar phenomenon of radiation in one direction and absorption from the counterpropagating direction was observed by Kauranen et al. [Kau95], where a thin nonlinear layer of material was placed in front of a single mirror. Complete dipole emission inhibition, in both directions, only occurs in the very symmetric position where the nonlinear layer is exactly at the center of the air gap (which is also the center of the whole structure) (Figures 3.9(a)-3.9(d)).

The phase difference may be calculated in the same way indicated for the resonant case in order to see its variation in this case. It is found a strong variation in the phase difference at both sides of the monolayer. In Figure 3.10 it is shown the phase difference between the dipoles and the forward and backward propagating components
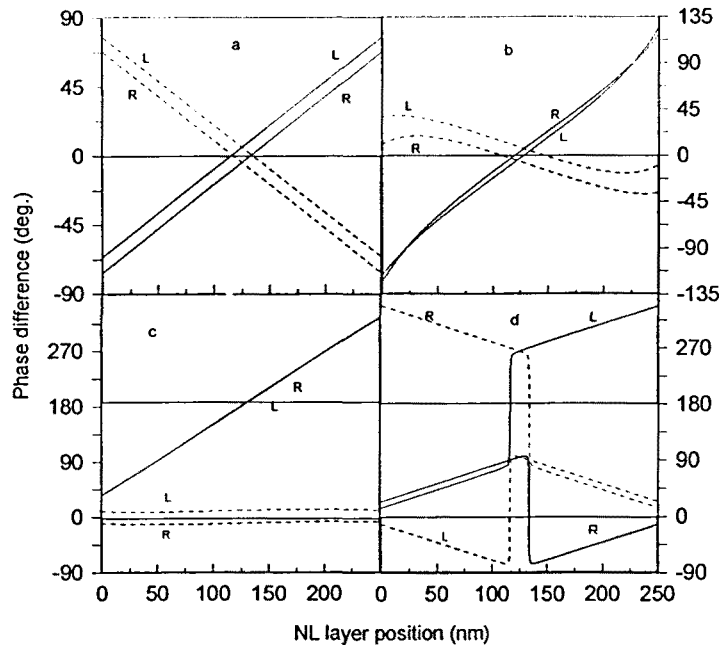
Figure 3.10 Phase difference between the dipole oscillation and the forward propagating field at 2ω (full curve) at z=0₋ (L) and at z=δ₊ (R), and the backward propagating field at 2ω (broken curve) at z=0₋ (L) and at z=δ₊ (R) as a function of the position of the nonlinear layer inside the defect of the 1D truncated periodic structure, for the same four different dipole orientations and angle of incidence shown in figure 3.9. The grey regions indicate the phase difference values at which the energy transfer is negative (absorption)

of the SH field at the slab surfaces, in the positions $z=0_-$ and $z=\delta_+$. It is seen immediately that there exists a change in phase difference when crossing the slab both in the forward and in the backward propagating directions. We can take the averaged value of the phase at each side of the slab to be the phase at the nonlinear slab position for each one of the components of the field. By looking at this averaged value we see that the corresponding regions with positive energy transfer are related to phase difference values between 0° and 180° and regions with negative energy transfer are related to values between 180° and 360° or between 0° and −180°. In this way we see that the change in phase difference is also playing a determinant role in the inhibition process.

When we study the energy transfer and phase difference at other angles within the gap we see a similar behavior to that observed at this position, with positive energy transfer to one of the components of the field which is lost by the counterpropagating component.

It has been shown by considering this quadratic nonlinear radiation of a plane of oscillating dipoles within the 1D photonic crystal that not only the field distribution but also the phase difference plays a determining role in the process of energy transfer that defines the radiative properties of the dipoles within the structure. This energy transfer mechanism has been found to be very different to that found in free space and strongly dependent on the position of the dipoles as well as on their orientation. We have also seen that one can distinguish two types of radiation inhibition: one where there is no transfer of energy to either of the counterpropagating components of the field, and another one where one of the components loses the energy that is transferred to the other counterpropagating component.